ANALYSIS OF CELLULAR SENTINELS FOR EXTRACELLULAR HEAT SHOCK PROTEIN-PEPTIDE COMPLEXES

by

Michelle Nicole Messmer

BS. Biotechnology, State University of New York at Buffalo, 2008

Submitted to the Graduate Faculty of

School of Medicine in partial fulfillment

of the requirements for the degree of

Doctor of Philosophy

University of Pittsburgh

2013

UNIVERSITY OF PITTSBURGH

SCHOOL OF MEDICINE

This dissertation was presented

by

Michelle Nicole Messmer

It was defended on

November 1st, 2013

and approved by

Walter J. Storkus, PhD, Professor, Department of Dermatology

Adrian E. Morelli, MD, PhD, Associate Professor, Department of Surgery

Claudette M. St. Croix, PhD, Assistant Professor, Department of Environmental & Occupational Health

John M. Kirkwood, MD, Professor, Department of Medicine

Kang Liu, PhD, Assistant Professor, Department of Microbiology & Immunology, Columbia University, NYC

Dissertation Advisor: Robert J. Binder, PhD, Associate Professor, Department of Immunology

Analysis of cellular sentinels for extracellular Heat Shock Protein-peptide complexes

Michelle N. Messmer, PhD

University of Pittsburgh, 2013

Since the discovery of gp96 in the 1980's as a "tumor rejection antigen," Heat Shock Proteins (HSPs) have received attention from immunologists for their ability to prime immune responses. Originally known for their important intracellular roles as chaperones to newly synthesized, misfolded, and/or recently degraded proteins, it is now understood that HSPs released into the extracellular environment can also initiate immune responses. Shown both *in vitro* and *in vivo*, HSPs act on antigen presenting cells (APC) to 1) deliver antigenic peptides for presentation by both MHC class I and class II molecules and 2) activate APC to increase expression of co-stimulatory molecules. Both of these activities contribute to productive T cell responses, which has led to current trials using HSP-peptide complexes as cancer vaccines. However, the cell populations responsible for monitoring exogenous HSPs and priming resulting immune responses have yet to be fully characterized. This study identifies the cells that incorporate HSPs *in vivo*, following either vaccination or release by tumors, and analyzes the immune response generated by these cells. A $CD11c^{+}CD11b^{+}CD4^{+}$ dendritic cell population selectively takes up HSPs, coincident with higher expression of the HSP receptor CD91 on these cells. We also show the dependence on CD91 of HSP-mediated immune responses. Increased knowledge of the process by which HSPs shape immune responses will contribute to the understanding of HSP-mediated immunity as well as assist in optimizing current tumor-vaccine strategies.

TABLE OF CONTENTS

LIST OF TABLES

LIST OF FIGURES

ACKNOWLEDGEMENTS

First, thank you to my mentor, Dr. Robert Binder, who welcomed a freshly graduated Bachelors student with limited research experience into his lab and was able to work with my high expectations for this research. Also, thanks to my entire committee for your steady guidance over these five years.

Special thanks to previous lab members Laura Kropp, always ready to talk and laugh and contributing data on the presentation of gp96-chaperoned peptides to our paper, and Sudesh Pawaria, for patient and encouraging instruction in genetic engineering ($gp96_{EGFP}$ would not have been possible without her). Yu (Jerry) Zhou has been a strong partner as we have traversed through grad school together. His contributions to Aim 2 are numerable, and I am honored to be included as a co-author on his paper. I also appreciated the efforts of undergraduates Kimberly Curtis, Lydia Popichak, and finally Josh Pasmowitz, who worked closely with me at the microscope to attain the images of gp96-peptide complexes following cellular internalization.

I owe extreme gratitude to Dewayne Faulkner, the man responsible for sorting my $A488^{+}$ cells at the flow core and who was always willing to listen when I had a new question about fluorescent antibodies. Dr. Simon Watkins and the staff at CBI also contributed valuable knowledge and skills in microscopy to my training.

Finally, thank you to my entire family and especially my fiancé, Doug Cook. You may not always understand what I'm talking about, but you've always been there to support me.

ABBREVIATIONS

Abbreviations:

APC: Antigen Presenting Cells

HSP: heat shock protein

TRA: tumor rejection antigen

α2M: alpha-2-Macroglobulin

gp96: glycoprotein 96 (also known as grp94)

CRT: calreticulin

MHC: Major histocompatibility complex

DC: dendritic cell

BMDC: bone-marrow derived DC

LN: lymph node

hrs: hours

KO: knock out

SEM: standard error of the mean

1.0 PROJECT AIMS

Heat Shock Proteins (HSPs) have been described as early precursors of innate immunity, acting as danger signals in the extracellular environment. They are also involved in adaptive immunity, delivering peptides for efficient processing and presentation on MHC. HSPs such as gp96 isolated from tumor cells elicit tumor peptide-specific immunity in mice. For this reason, the use of HSPs as tumor vaccines is currently under clinical investigation.

Though it is clear that gp96 provokes immune responses, the cellular targets of gp96 *in vivo* are not known. Exogenously added gp96 or gp96 released into the extracellular environment, due to membrane damage or active secretory mechanisms, may be taken up by cells expressing the HSP receptor CD91. Importantly, gp96 may be taken up by peripheral dendritic cells for transport to lymph nodes or it may passively drain through the lymphatics to be taken up by lymph node resident cells to prime T-cell responses. Subtypes that selectively take up gp96 may determine the type of response produced. **This study identifies cells that incorporate HSPs *in vivo*, following either vaccination or release by tumors, and analyzes the immune response generated by these cells.** Expression of the HSP receptor CD91 is assessed for each subset. The ability of these cells to prime immune responses is also analyzed. These studies improve our understanding of the immunologic role of HSPs as well as provide insight for enhanced cancer treatment strategies.

1.1 AIM 1: DETERMINE THE CELLULAR SENTINELS OF HSPS IN A VACCINE SETTING

Fluorescent labeling of gp96 allowed for tracking of this HSP to draining lymph nodes following vaccination. Cells that took up fluorescent protein were then phenotyped by flow cytometry and immunofluorescent microscopy. Sorted cell populations were analyzed for their ability to generate immune responses. This aim identifies $CD11c^{+}CD11b^{+}$ cells in the subcapsular region of the lymph node as the major endocytic cells for gp96, both due to their expression of CD91 and their prime localization.

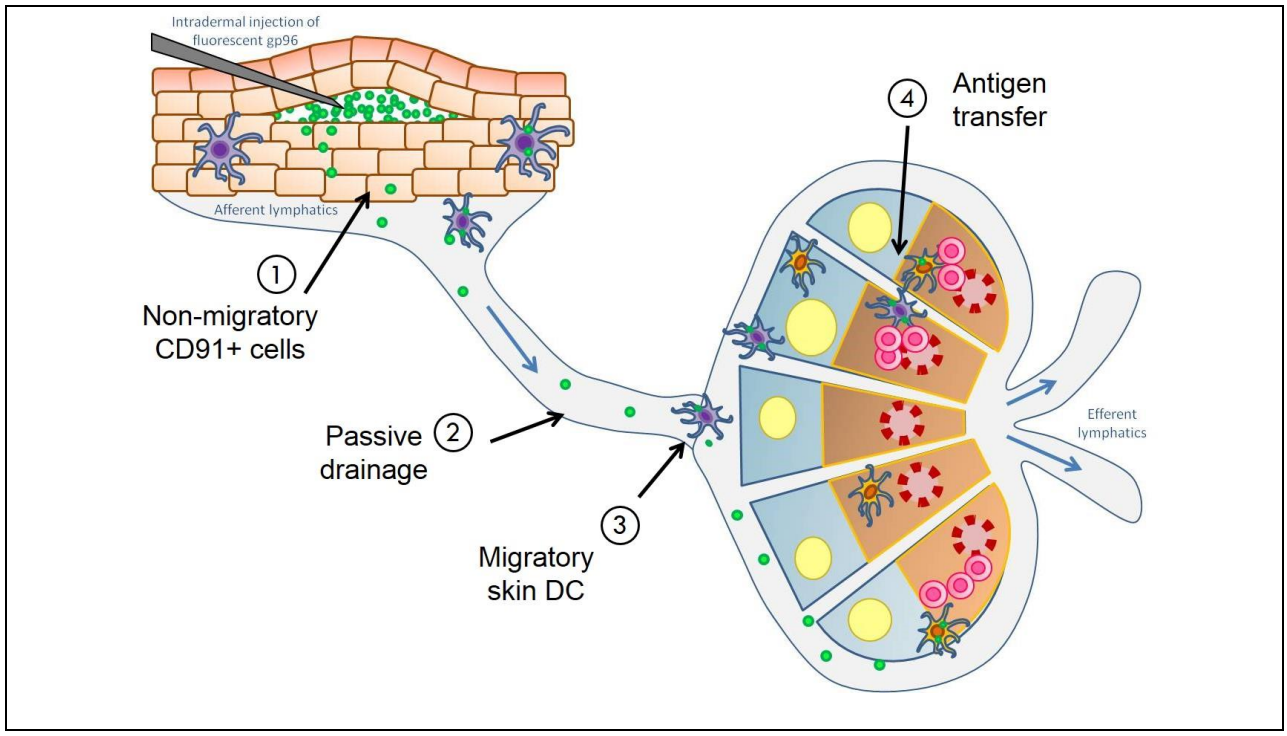

Figure 1-1. Model for HSP trafficking to LN for generation of immune responses.
There are multiple potential routes for gp96 trafficking. Following intradermal injection, gp96 may be taken up by CD91 expressing cells at the site of injection and be retained there (1). (2) However, since gp96 is a soluble molecule, gp96 may drain through the lymphatics to LNs where it may interact with LN resident cells to stimulate immune responses. Alternatively, gp96 may be internalized by skin resident dendritic cells that migrate to LN following activation (3). These migratory cells may be responsible for presenting gp96-chaperoned antigen to generate immune responses themselves or they may transfer antigen to LN resident cells for priming (4).

1.2 AIM 2: EXAMINE IMMUNE RESPONSES TO HSPS RELEASED BY TUMORS

Tumor cells expressing EGFP-tagged gp96 were generated and used to track this HSP to tumor-draining lymph nodes. This effect was blocked by introduction of a competitive endogenous inhibitor of the HSP receptor CD91. Additionally, abrogation of CD91 expression reduced immunogenicity of tumor cells. This aim demonstrates a dependence on HSPs and CD91 for induction of tumor-specific immunity.

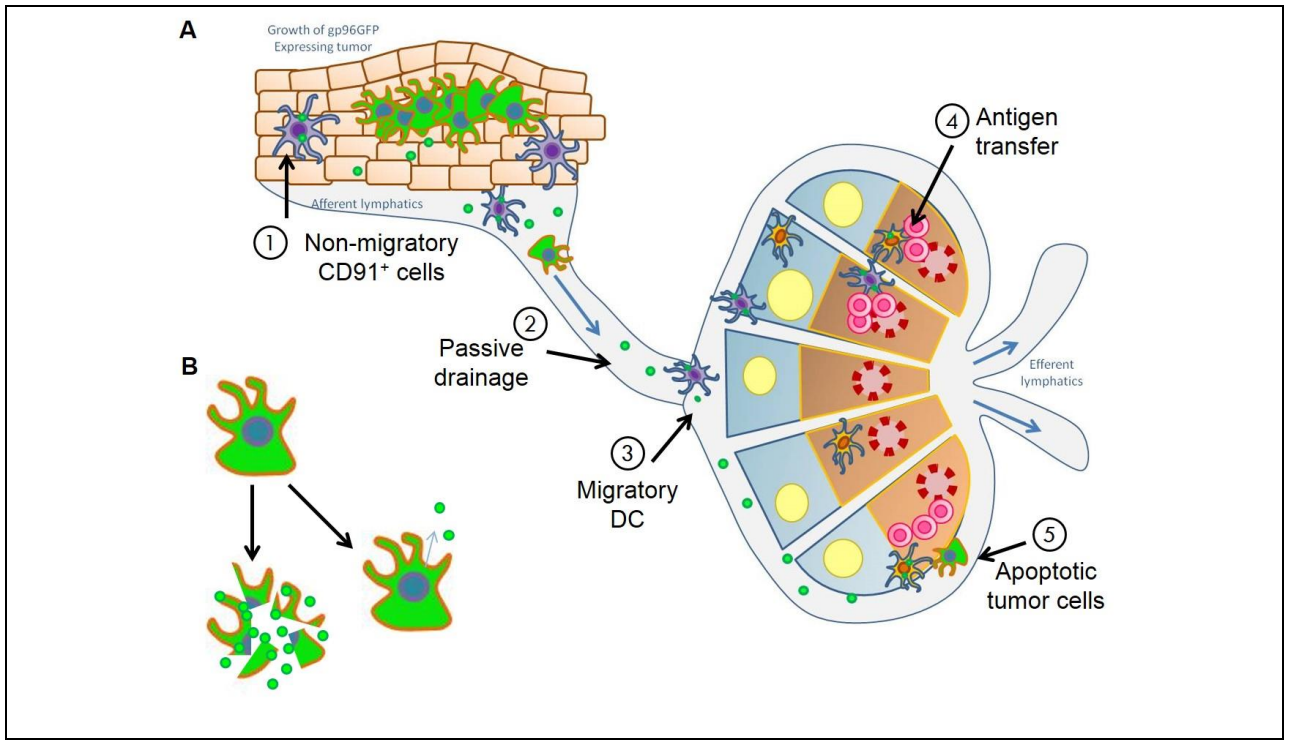

Figure 1-2. Model for HSP release from tumor to generate immune responses.
Tumor-derived extracellular gp96 may drain to LN along routes akin to those proposed in Figure 1-1. **A:** (1) Non-migratory $CD91^+$ cells within or surrounding the tumor may endocytose gp96 and retain it at that location. Excess gp96 may passively drain via the lymphatics to LN resident cells to generate anti-tumor immune responses (2). Migratory skin resident dendritic cells may also carry gp96 to draining LNs (3) where they may directly promote immune responses or undergo antigen transfer with a LN resident subset (4). An additional mechanism of tumor-derived $gp96_{EGFP}$ delivery to the lymph nodes may be in the form of drainage of apoptotic tumor cell fragments or exosomes containing HSPs (5). **B:** Studies have suggested at least two mechanisms for tumor release of HSPs into the extracellular environment: either through tumor cell necrosis or via active secretion.

1.3 AIM 3: IDENTIFY ANTIGEN-PROCESSING PATHWAYS FOLLOWING HSP:CD91 INTERACTION

Bone marrow derived dendritic cells are used to analyze the endocytosis of HSP:peptide complexes. Intracellular localization shows peptide translocation into the cytosol and a lack of interaction between gp96 containing endosomes and the lysosomal compartment. Additionally, levels of the HSP receptor CD91 are examined on these cells following activation with LPS. This aim defines important intracellular processes that give rise to HSP-mediated immunity.

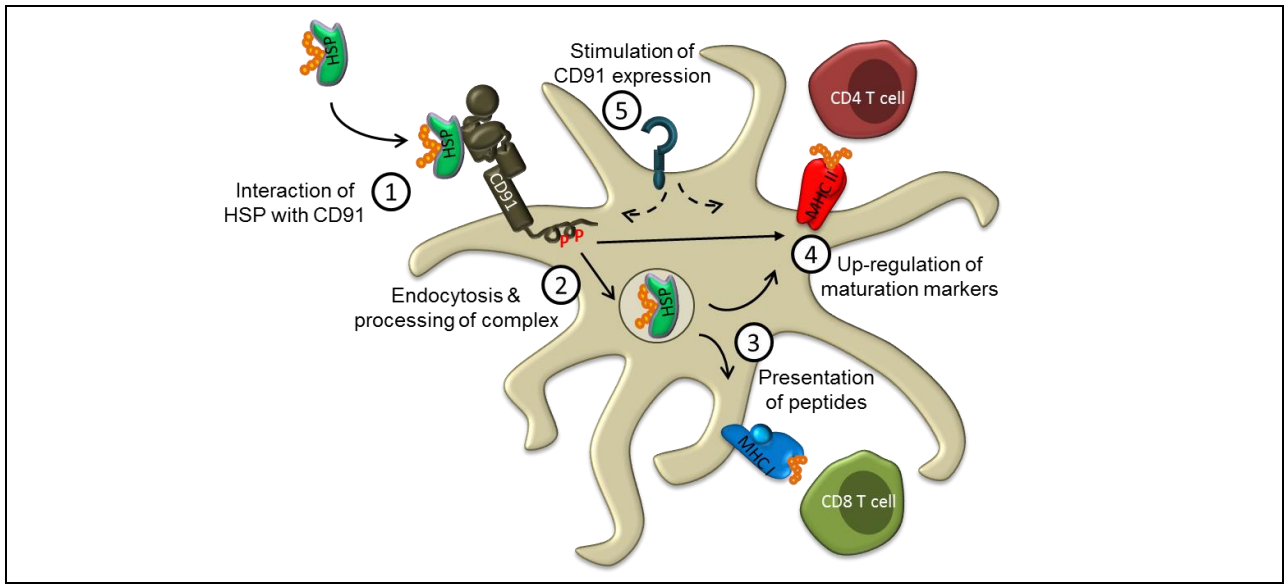

Figure 1-3. Model for the cellular effects of HSP:CD91 interaction.
A number of downstream effects of HSP:CD91 interaction remain to be elucidated. (1) HSP:peptide complexes engage with the surface receptor CD91 and are then internalized. (2) Endocytosis of this complex has previously been visualized but the fate of gp96 or the chaperoned peptide, including their localization with major cellular organelles, is still unclear. (3) Extended length peptides chaperoned by gp96 can ultimately be presented by both MHC class I and MHC class II, despite theoretically separate processing pathways. (4) In addition to delivery of peptides for processing, HSP:CD91 interaction stimulates increased expression of maturation markers such as MHC class II on APC. (5) Stimulation of TLRs with LPS also matures APC to increase expression of MHC class II. The effects of APC maturation on CD91 expression are unknown, but we can use LPS signaling as a non-specific stimulator of DC to investigate this.

2.0 BACKGROUND

Heat shock proteins (HSPs) are ubiquitously expressed in eukaryotic and prokaryotic cells. They play pivotal roles in protein folding and cell cycle regulation, and several members show high evolutionary conservation [1,2]. Uniquely, a subset of these proteins have been observed to generate highly effective and specific immune responses, earning them the title "immunogenic." This chapter covers what is known regarding the major immunogenic HSPs and mechanisms of HSP-mediated immune responses, including direct effects of HSPs on various cells of the immune system and dependence on the HSP receptor CD91. It will establish roles for HSPs in several aspects of immunity. Finally, data from recent clinical trials of HSP-based vaccines will be reviewed to highlight the need for expanded understanding of the cells acting to generate HSP-mediated immunity.

2.1 DISCOVERY OF THE IMMUNOGENIC HSPS

For over three decades, scientists have appreciated that heat shock proteins generate immune responses. This section details the original discoveries defining immunogenic HSPs as a special class of proteins.

2.1.1 Identification of "Tumor Rejection Antigen" gp96, a prototypic immunogenic HSP

The middle of the 20th century witnessed great debate over whether the immune system was capable of recognizing and defending against tumor cells. Some believed tumors did not contain the requisite antigens to stimulate immune cells. However, a series of elegant experiments in the 1940's and '50's showed that tumors, particularly chemically induced sarcomas, do possess unique antigens that can produce anti-tumor immunity [3-6]. A slew of "tumor rejection antigens" were identified in the following decades, often in the form of mutated, over-expressed, or aberrantly expressed normal proteins.

TRAs seemed to be highly unique, such that inoculation with one tumor rarely protects against challenge with even closely related tumors. To efficiently isolate new TRAs for study, researchers purified TRAs using column chromatography, monitoring the antigenicity of each fraction. In this way, Srivastava et al. discovered an apparently common TRA isolated from two distinct methylcholanthrene induced sarcomas [7]. Despite having undergone identical isolation procedures, this 96 kDa TRA retains specificity for the tumor of origin. TRA isolated from Meth A was

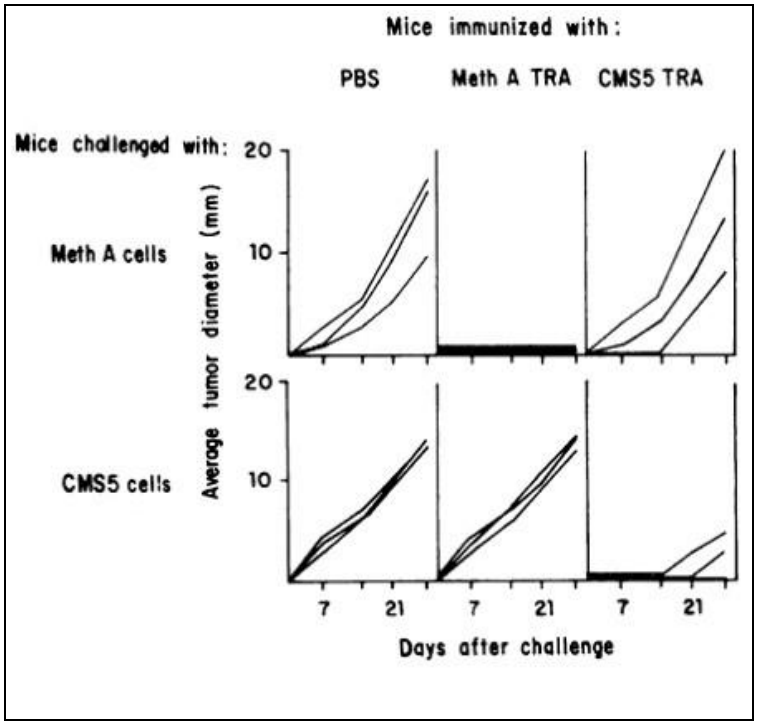

Figure 2-1. "Tumor Rejection Antigen" promotes tumor-specific immunity.
Isolation of a 96 kDa protein from two distinct methylcholanthrene-induced sarcoma cell lines induces tumor specific protection in vaccinated mice. Original publication: Figure 4 [7]. Copyright 1986 Srivastava.

protective against Meth A fibrosarcoma but not protective against the closely related tumor, CMS5, and vice versa (Figure 2-1). This tumor rejection antigen was called gp96. Structural and biochemical similarities between the TRAs reported in this first paper, combined with intensive comparisons between various gp96 isolates as well as genetic mapping of the gp96 gene from normal and tumor tissue as well as between mouse and human, failed to uncover the source of tumor specificity [8-14]. However, these studies did identify gp96 as a ubiquitously expressed stress-induced heat shock protein.

2.1.2 Additional immunogenic HSPs

In addition to gp96, other immunogenic HSPs, as defined by their ability to elicit tumor/peptide specific immune responses, include the following structurally diverse proteins: hsp90 [15,16], hsp70 [16-18], calreticulin [19], hsp110 [20,21] and grp170 [20]. The major receptor for four of these HSPs (hsp90, hsp70, gp96, and calreticulin) has been confirmed to be CD91 [22,23], discussed at length in the section "Discovery of the HSP Receptor CD91" (Chapter 2.3, page 13). Other potential receptors for immunogenic HSPs will not be discussed at length, but will be mentioned where appropriate.

Even for HSPs sharing the same receptor, functional differences have been reported. A direct comparison of the immunogenicities of hsp90, hsp70 and gp96 within a single tumor vaccine model found molar equivalents of hsp70 and gp96 outperformed hsp90 in tumor rejection assays [16]. At the time, this was attributed to potential differences in peptide chaperoning ability (discussed below), but we have also shown that treatment with hsp70, calreticulin or gp96 elicits different cytokine profiles both *in vitro* and *in vivo*, independent of specific peptide binding [24]. These functional differences remain an intriguing area of research.

2.1.3 The specific nature of HSP immunogenicity

A number of the immunogenic HSPs were implicated as TRAs around the time gp96 was identified [15,17,21], coincident with observations that HSPs function by binding peptides to assist in protein folding [25]. Since no intrinsic differences in tumor vs. normal HSPs could be found, this led to the theory that the peptide-binding ability of HSPs was also the source of their antigenicity [11]. It was soon shown that gp96 has measurable ATPase activity, akin to other heat shock proteins, and peptides can be stripped from the purified protein [26]. These peptides associate with HSPs such as gp96 within the cell and are not contaminates from the purification process [27]. Stripping peptides from HSPs abrogates tumor-specific immunity [17]. Further, it was found that peptides can be exogenously complexed to hsp70 and gp96, albeit under different experimental conditions, and that it is only after direct association, rather than simply being mixed, that these HSPs enhance peptide specific immunity [28].

As reviewed elsewhere [29], multiple antigenic systems have been used to test HSP-mediated immunity. Defined epitopes from bacteria, viruses, tumors, and model antigens have been shown to associate with HSPs (Table 2-1). In comparison to the relatively strict peptide-binding requirements for MHC molecules, peptides stripped from HSPs are a heterogeneous pool with limited length restrictions and loose sequence requirements [26,30-35]. Comparing the peptides isolated from HSP70, HSP90, and gp96 identified differences in the endogenous peptide repertoire chaperoned by these HSPs [36]. This may be due to differences in cellular localization (hsp90, hsp70, hsp110 are primarily located in the cytosol whereas gp96, calreticulin, and grp170 are usually retained in the endoplasmic reticulum), or they may be shaped by a natural directional pathway for peptide processing that delineates sequential interactions with each HSP family member [37,38]. Given the structural diversity of the immunogenic HSPs, differences in

the identified peptide binding sites may also account for their peptide selectivity [39-41]. The full crystal structure for gp96 has been solved [42], and it is believed that immuno-relevant peptide binding occurs on the N-terminal domain [30,43-46], although the chaperoning functions of gp96 depend on the C-terminal domain [43,46-48].

Table 2-1. Examples of peptide epitopes associated with immunogenic HSPs

CTL epitope	*MHC I Restriction*	*Reference*
PRL1a	L^d	Ishii et al. 1999 [36]
MART1, gp100 melanoma ags	A2	Castelli et al. 2001 [49]
HPV16 E7 Ag	D^b, A2	Ren et al. 2010 [50], Ding et al. 2013 [51]
Pokemon		Yuan et al. 2012[52]
RCC Ags		[35]
Vesicular stomatitis virus	K^b	Suto & Srivastava 1995 [53], Nieland et al. 1996 [54]
Simian virus 40	D^b, K^b	Blachere et al. 1993 [55], 1997 [28]
Influenza	K^b	Blachere et al. 1997 [28], Heikema et al. 1997 [56]
Herpes simplex virus-2	d, A2	Navaratnam et al. 2001 [57], Mo et al. 2011 [58]
Hepatitis B		Meng et al. 2001 [59]
M. tuberculosis	d	Zugel et al. 2001 [60]
Listeria	d	Sponaas et al. 2001 [61]
Ovalbumin	K^b	Breloer et al. 1998 [62], Blachere et al. 1997 [28], Kropp et al. 2010 [37]
Beta-galactosidase	L^d	Arnold et al. 1995 [63], 1997 [64], Binder et al. 2007 [65]
Minor Histocompatibility Antigens	K^b, K^d	Arnold et al. 1995 [63], 1997 [64]

This table was adapted from the review by Binder in 2006 [29]. Examples include peptides derived from human cancers, viral antigens, bacterial antigens, model antigens, and minor histocompatibility antigens.

Thus, immunogenic HSPs derive their tumor specific antigenicity from the peptides they are endogenously or exogenously associated with, but this does not explain the enhanced

immune responses observed for HSP-peptide complexes compared to non-HSP associated antigens. The targeting of HSPs to professional APCs combined with stimulation of innate effects will be explored in detail in the next two sections, 2.2 Factors associated with HSP-mediated immunity and 2.3 Discovery of the HSP Receptor CD91.

2.2 FACTORS ASSOCIATED WITH HSP-MEDIATED IMMUNITY

This section details the cellular players in HSP-mediated immunity as well as the innate effects HSPs have on cells of the immune system.

2.2.1 Cellular requirements for HSP-mediated immunity

Upon observing the effective anti-tumor immune responses elicited by immunogenic HSPs, researchers began to dissect the cellular mediators of this response. Treating mice with carrageenan, a polyanionic polysacharride ligand for a number of scavenger receptors, to ablate phagocytic cells during the priming phase diminished anti-tumor protection in response to purified gp96 but not whole

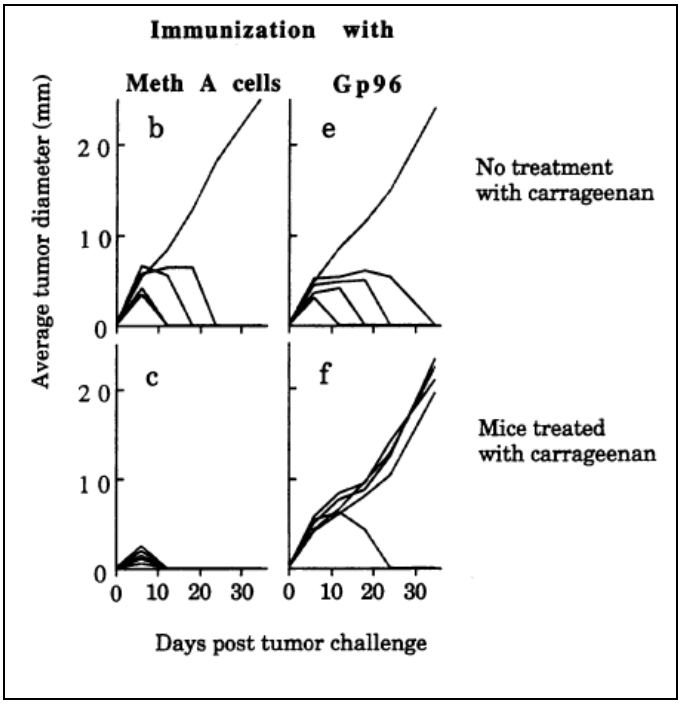

Figure 2-2. Requirement for phagocytic cells for HSP-mediated immunity.
Vaccination of mice with either whole cell lysate of Meth A or gp96 purified from Meth A cells was protective against challenge with Meth A (top row). Treatment of mice with carrageenan to ablate phagocytic cells abrogated gp96-mediated protection, but not lysate-mediated protection, demonstrating a differential requirement for APCs. Original publication: [66], Figure 5. Copyright (1994) National Academy of Sciences, U.S.A.

cell lysates (Figure 2-2, [66]). Additionally, it was found that immune responses to purified gp96 were highly dependent on $CD8^+$ cells during priming, such that antibody depletion of $CD8^+$ cells at the time of vaccination ablated the observed protection [66]. These cells, however, were dispensable during the priming phase following whole cell vaccination. It was hypothesized that the phagocytic cells played a major role as acceptors of HSP-peptide complexes for cross-presentation of antigen on MHC class I to stimulate strong CTL responses [38]. The mechanism for this targeted up-take for effective processing and presentation of peptide will be discussed in Section 2.3. However, we also know that, beyond peptide presentation, additional support from mature APCs is required for effective immune responses [67]. Cells required during the effector phase of gp96-mediated immunity include $CD4^+$, $CD8^+$ and NK cells [18,66]. Innate effects of HSPs include stimulating the production of cytokines and co-stimulatory molecules by APC to shape these downstream effector phase responses.

2.2.2 Innate effects of HSPs

In addition to delivering peptides for efficient processing and presentation, immunogenic HSPs stimulate non-specific, innate immune responses. Treatment of APCs *in vitro* with immunogenic HSPs has a number of effects, as summarized in Table 2-2 (adapted from [23]). This includes translocation of NF-κB, stimulation of cytokine and chemokine production (ex. TNFα, IL-12p40, IL-1β, IL-6, RANTES), up-regulation of activation and co-stimulatory markers (ex. MHC class II, CD80, CD86, CD83, CD40), as well as production of nitric oxide. The observed effects are independent of any bound peptide and vary depending on the target cell as well as the identity of the HSP used.

Table 2-2. Selected reports showing activation of APCs by HSPs

Type of HSPs	*Targeted cells*	*Markers of Activation*	*Inflammatory mediators*	*Year*	*Ref.*
gp96, HSP70, HSP90	DC	NF-κB translocation, ↑MHC II and CD86	TNF-α, IL-12, IL-1β	2000	[68]
gp96, HSP70, CRT	*RAW264.7*, PEC	NF-κB translocation	TNF-α, IL-1β, IL-6, etc. CXCL10 (IP-10), CXCL11 (IP-9)	2011	[24]
Human HSP70, gp96	DC	↑HLA-DR, CD40, CD86, CD83, DC-LAMP		2001	[69]
Human & mouse, gp96 & HSP70	macs, immature DC		NO	2002	[70]
gp96	human DC	↑ MHC II,CD86	TNF-α, IL-12	2000	[71]
gp96	$CD11c^+$ cell	↑MHC II, CD80, CD86, DC migration		2000	[72]
gp96	PMN, mon		IL-8	2003	[73]
Human gp96	BMDC	NF-κB translocation, ↑CD86	IL-12	2002	[74]
Human gp96	macs		TNF-α, IL-8	2009	[75]
HSP70	Splenocytes		TNF-α,IL-1β, IL-6	2000	[76]
HSP70	BMDC		TNF-α, IL-12, IL-1β, IL-6	2000	[77]
HSP70	Tumor cells, DC	NF-κB translocation, ↑ CD80, CD86, CD40, MHC II	CXCL10	2009	[78]
Human HSP70	mon	NF-κB translocation	TNF-α,IL-1β, IL-6	2000	[79]
Human HSP70	DC		IL-12	2002	[80]
Human rHSP70	DC	↑CD40, CD86,CD83		2001	[81]
Human rHSP70	DC		IL-12p40	2003	[82]
Mtb HSP70	*THP1, KG1 cells*, DC		RANTES	2001	[83]
Mycobacteria rHSP70	Human DC	↑CD83, CCR7, CD86, CD80, HLA-DR	RANTES, IL-12, TNF-α Nitric oxide	2002	[84]
Rat HSP72	Splenocytes, macs		NO, TNF-α, IL-1β, IL-6	2003	[85]
Human Hsp70L1	DC		TNF-α, IL-12p70, IL-1β, IP-10, MIP-1α, MIP-1β, RANTES	2004	[86]
Mycobacteria/ human HSP60, HSP70	PEC		IL-12	1996	[87]

This table is adapted from Table 2 of our review of HSPs and immune responses [23]. Species is mouse unless otherwise indicated. Cell lines are italicized. Abbreviations: r, recombinant; CRT, calreticulin; mon., monocytes; PEC, peritoneal exudate cells/macrophages; macs. macrophages; DC, dendritic cell; BM, bone marrow derived; LC, Langerhaans cells; PMN, polymorphonuclear leukocytes; NO, nitric oxide.

The inflammatory responses produced by APCs treated with HSPs are expected to support development of strong CTL-mediated immunity. However, HSP interactions with other cell types may also play an important role in shaping immune outcomes. Plasmacytoid DC can also be matured by gp96, and once mature they are able to suppress HSP-stimulated monocytes [88]. Human platelets have also been reported to bind gp96, effectively sequestering this HSP from being able to stimulate DC in culture [89]. Limited reports have suggested gp96 may also directly stimulate $CD4^+$ T cells [90], due to potential expression of CD91 on these cells [91-93]. However, we have been unable to confirm CD91 expression on T cells from mice (Section 3.3.6, pg 35).

2.3 DISCOVERY OF THE HSP RECEPTOR CD91

Subsequent to the discovery of the immunogenic HSPs, it was observed that these proteins were taken up in a highly efficient and specific manner, leading to the hypothesis that a receptor must exist [38]. This section details the discovery of the HSP receptor, CD91, as well as the receptor's functions in HSP-mediated immunity.

2.3.1 Evidence for the HSP Receptor, CD91

As discussed in Section 2.1.3, simple mixtures of peptide and HSP do not stimulate protective immune responses. However, when gp96 is in complex with as little as 1-2 ng of peptide protective responses can be observed [28]. We also know HSP-mediated protection is dependent on phagocytic cells [66]. Given the rapidity and high efficiency of gp96-mediated responses, it

was proposed that professional antigen presenting cells might possess HSP-specific receptors [38]. A number of studies supported this hypothesis. Using gold labeled gp96 particles, Arnold-Schild showed in 1999 that gp96 is internalized by macrophage- and dendritic-like cell lines via clathrin coated pits [94]. Specific binding was then shown on pristane-elicited peritoneal macrophages [95], as well as non-elicited, $CD11b^+$ sorted peritoneal macrophages [96]. Additionally, fluorescent labeled gp96 binding was associated with cells expressing the individual surface markers CD11c, MHC class II, CD45, or Mac-3 from murine splenocytes, as well as human cells expressing HLA-DR, CD86, CD19 or CD14 from peripheral blood [97].

The scavenger receptor CD91 was soon identified as the major receptor for HSPs by detergent extraction of transmembrane proteins from RAW264.7 cells, a macrophage-like cell line, and isolation over a gp96 chromatographic column [98]. Specific binding of gp96 to CD91 was also observed using biochemical cross-links to transfer radioactive iodine from HSP to the receptor [98]. Blocking this receptor with anti-CD91 antibody inhibits the presentation of gp96 chaperoned peptides to antigen specific T cells, both *in vitro* (by RAW264.7 cells) and *ex vivo* (by $CD11c^+$ cells) [99]. CD91 has been confirmed as a common endocytic receptor for four of the major immunogenic HSPs (hsp70, hsp90, gp96, calreticulin) [22] and has been conserved in this capacity across species [100].

2.3.2 Alternative HSP Receptors

A number of other endocytic receptors have been implicated as receptors for immunogenic HSPs. Reports of CD91 as well as alternative uptake mechanisms are summarized in Table 2-3, adapted from our review [23]. The problems with these alternative uptake mechanisms as major mechanisms of HSP-mediated immunity have been addressed previously [101]. We do not

entirely rule out CD91-independent processes, but we and other laboratories have shown that CD91 is the primary transducer of HSP-mediated immunity.

Table 2-3. Reported cross-presenting systems for HSPs and the corresponding uptake mechanism.

Uptake Mechanism	*HSPs*	*APC*	*Year*	*Ref.*
Macropinocytosis	rHSP70 (bovine)	bovine mon.	2010	[102]
	rHSP70 (human)	*B-LCL lines L721.45, L721.174*, human mon.	2007	[103]
Receptor mediated & macropinocytosis	gp96 (porcine)	elicited PEC, *RAW 264.7, CHO, COS7, BRL*	1999	[95]
Receptor mediated, not MHC class II or DEC205	gp96	*D2SC/1, D1*, BMDC, splenic DC, macs, and B cells	2000	[97]
Receptor mediated endocytosis	rgp96	BMDC	2011	[104]
	gp96 & HSP70	*P388D1, D2SC/1*	1999	[94]
	rHSP70 (human)	*RAW264.7, RAW309Cr.1*	2008	[105]
	HSP70 (human)	human mon.	2002	[106]
	rHSP70	elicited PEC	2000	[107]
CD91	gp96	*RAW264.7*, PEC	2000	[98]
	gp96, HSP90, HSP70, CRT	BMDCs, PEC	2001	[22]
	gp96	*B-LCL*, human DC	2004	[108]
	(E.coli & Mtb) hsp70	BMDC, BM-macs	2004	[109]
CD91	gp96	*RAW264.7*, $CD11c^+$ cells	2004	[99]
	α2M	Human CD11c+lin- cells	2004	[110]
	gp96 (frog)	frog mac-like cells	2008	[100]
	rHSP70 (human)	human PBMC	2011	[111]
CD91 (not CD14 or TLR4)	rHSP70 (human), rhsp60(human)	human mon, epidermal LC	2002	[112]
CD91 (& Other)	rHSP70 (M.avium paratuberculosis)	*BoMac*, bovine DC, macs, mon	2005	[113]
CD91 (& Partial Lox-1, but not SRA)	gp96	splenic APC, $B220^+$, $CD11c^+$, $CD11b^+$, BMDC	2010	[114]
CD91 (& Partial CD36/ Scavenger Receptor)	rhsp70 (human)	Human mon, mon. derived DC	2010	[115]
Not CD91	gp96 (porcine)	elicited PEC	2002	[116]
	rgp96 (canine, NTD)	*MEF-1, PEA-13, DC2.4*	2010	[117]
Receptor mediated & macropinocytosis, Not CD91	gp96 (porcine)	elicited PEC, *RAW264.7*, BMDC	2002	[118]
Receptor dependent but not CD91 or SRA	HSP90 (human, purified), rhsp72 (hum)	*RMA-S/A*2402*, BMDC	2007	[119]
SREC-1 & not CD91	rCRT	elicited PEC, *DC2.4, MEF-1, PEA-13*	2005	[120]

Uptake Mechanism	*HSPs*	*APC*	*Year*	*Ref.*
SREC-1	gp96 (porcine) & rCRT	*CHO*, elicited PEC, BMDC	2004	[121]
Lox-1	rHSP70	human myeloid DC, mon., macs, $CD19^{+}$ cells	2002	[122]
SREC-1 & Lox-1	rHSP90 (human)	BMDC, *CHO, HeLa, RAW264.7*	2010	[123]
SRA	gp96 (porcine) & rCRT	elicited PEC, *RAW264.7, HEK*	2003	[124]
SRA (& Other)	rgp96 & rCRT	fibroblasts, BMDC, BM macs	2008	[125]
SREC-1 & SRA	rgrp170 and rhsp110	*RAW264.7, DC1.2, CHO*, BMDC	2007	[126]

Adapted from Table 1 [23]. Cell lines are italicized. Species is mouse unless otherwise indicated. Abbreviations: r, recombinant; CRT, calreticulin; NTD, N-terminal domain; mon., monocytes; PEC, peritoneal exudate cells/macrophages; macs. macrophages; DC, dendritic; BM, bone marrow derived; LC, Langerhaans cells.

2.3.3 Functions of CD91 in HSP-mediated immunity.

As described above, CD91 is required for endocytosis of the major immunogenic HSPs. Recently, our lab has shown that CD91 is also the major signaling receptor [24]. Phosphorylation of the intracellular C-terminal domain of CD91 following HSP:CD91 interaction is required for NF-κB translocation and elicitation of cytokines. With this new data, we can now place CD91 in the middle of both the innate and adaptive effects of HSPs (Figure 2-3).

Despite studies showing gp96 binding on assorted cell types, there has been no comparison of CD91 expression levels among these cells. It has also been assumed that receptor expression would directly lead to uptake of gp96 *in vivo*, however there may be other requirements that could determine specificity of uptake between cell types, such as physical access to the sites of extracellular gp96 accumulation or greater baseline levels of endocytic activity. Cellular expression of CD91 and its role in determining the cells that endocytose gp96 is explored in each of the aims in this research.

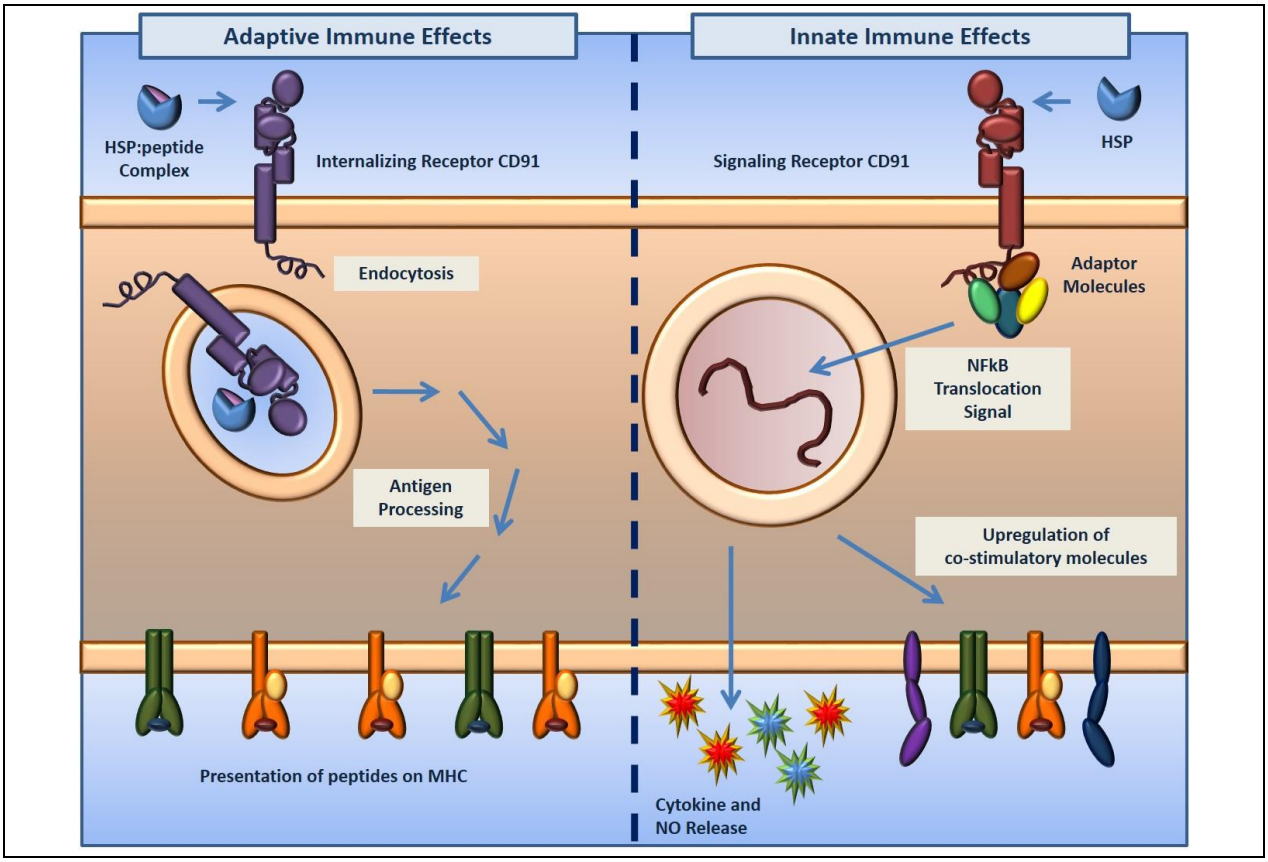

Figure 2-3. Adaptive and innate immune effects of HSP:CD91 interaction
This cartoon shows the dual nature of CD91:HSP interaction. To promote adaptive immune responses, CD91 is responsible for endocytosis of HSP:peptide complexes and delivery of these complexes to antigen processing machinery. Innate effects of CD91, dependent on signaling via tyrosine phosphorylation on the C-terminus, include activation and maturation of antigen-presenting cells, secretion of cytokines, up-regulation of co-stimulatory molecules, as well as nitric oxide production.

2.4 CLINICAL TRIALS OF HSPS

As discussed earlier, the major immunogenic HSPs have shown promising results in murine vaccination models [18]. Given these positive results, it is unsurprising that a number of groups have tested HSPs in clinical trials. One of the most popular vaccination strategies has been the use of autologous, or self-derived, HSPs. Following resection of the patient's primary tumor, HSPs are purified and then used as a therapeutic vaccine against any residual or metastatic disease. A comprehensive review of the clinical trials using autologous derived HSPs has been

published [127], and will be summarized here. Please see Table 2-4 for a complete list of autologous gp96 based clinical trials.

Positive disease outcomes from these clinical trials have been limited, potentially due to the advanced nature of most patients' disease at the time of clinical trial enrollment as well as the side-effects of standard therapy on patients' immune responses. Also, the cumulative therapeutic dose of autologous HSPs is variable from trial to trial and even within trials, as it is dependent on the amount of tumor tissue available for purification of the HSP. Furthermore, many of these

Table 2-4. Summary of clinical trials using autologous gp96

Ref.	*Year*	*Trial Phase*	*Tumor Type*	*Stage*	*# Pts*	*Vaccination Scheme*
[128]	2000	I	Varied	Late Stage	16	25ug gp96, s.c., weekly, 4x
[129]	2003	II	Colorectal carcinoma	IV	29	2.5, 25, or 100 ug gp96 i.d., weekly, 4x (1st cycle); 2.5, 25, or 100 ug gp96, i.d., biweekly, 4x (2nd cycle)
[130]	2002	II	Melanoma	IV	39	5 or 50 ug gp96, s.c. or i.d., weekly, 4x (1st cycle); 5 or 50 ug gp96, s.c. or i.d., biweekly, 4x (2nd cycle) 5 or 50 ug gp96, s.c. or i.d., monthly, 2-3x (3rd cycle)
[131]	2006	II	Melanoma	IV	38	25 ug gp96, s.c., weekly, 4x (1st cycle); 25 ug gp96, s.c., biweekly, 4x (2nd cycle) **Combined with GM-CSF and IFN-α**
[132]	2008	III	Melanoma	IV	322	25 ug, s.c., weekly, 4x (1st cycle), biweekly (2nd cycle) **Randomized to gp96 vs. Physician's Choice**
[133]	2010	I/II	Melanoma	III/IV	36	2.5, 25, or 100 ug, i.d., weekly, 4x
[134]	2003	II	NHL	Low grade	10	25 ug, weekly, 4x (1st cycle), biweekly, 4x (2nd cycle), biweekly up to 1 year (3rd cycle)
[135]	2007	II	NHL	II-IV	20	25 ug, i.d., weekly, 4x (1st cycle) 25 ug, i.d., biweekly, 4x (2nd cycle)
[136]	2007	I	Pancreatic adeno-carcinoma	I/II	10	5 ug, i.d., weekly, 4x
[137]	2008	II	RCC	II-IV	84	weekly, 4x (1st cycle) biweekly, 2x (2nd cycle) biweekly +/- IL-2, 4x (3rd cycle) Two further cycles +/- IL-2 or repeat of prior cycle
[138]	2008	III	RCC	I-IV	728	25 ug, i.d., weekly, 4x (1st cycle) 25 ug, i.d., biweekly, 4x (2nd cycle)
[139]	2012	I/II	GBM	High grade	12	25 ug, 4x, weekly or biweekly, followed by biweekly dosing

This table is adapted from Randazzo et al. Table 2 [127]. Abbreviations: Imm., immune study; QOL, quality of life; RCC, renal cell carcinoma; GBM, glioblastoma multiforme; Non-Hodgkin's Lymphoma; s.c., subcutaneous; i.d. intradermal; pts, patients; CR, complete response; SD, stable disease; DFS, disease free survival; TIL, tumor-infiltrating lymphocytes

patients are non-responders to previous therapeutic interventions, and already show compromised immune responses. Overall, the safety of gp96-based therapies has been impressive, with only mild reactions at the injection site being reported. Indeed, the worst side-effects were reported for those studies testing HSP and cytokine combination therapies, where the cytokines were the likely causative agent [131,137]. Given that not much is known about the *in vivo* processing events for HSPs following vaccination, there may be a number of targets that could be used to improve these clinical outcomes. Gaining knowledge of these targets forms the basis for this research.

3.0 AIM 1: IDENTIFICATION OF THE CELLULAR SENTINELS FOR NATIVE IMMUNOGENIC HEAT SHOCK PROTEINS *IN VIVO*

3.1 PREFACE

Data from this chapter has been published in the Journal of Immunology [140] with myself as first author. It is expanded here. Those who performed the experiments detailed in this chapter are indicated by their initials in the figure legends (Michelle Messmer: MNM; Robert Binder: RJB; Dewayne Faulkner: DF; Yu Zhou: YZ).

3.2 RATIONALE

Studies detailing the immunological effects of HSPs have used myriad APCs *in vitro*, ranging from bone marrow derived cells cultured in GMCSF with or without IL-4 [68], peritoneal exudates containing macrophages [68], B cells [141], and macrophage- and dendritic-like cell lines [142]. Expectedly, the different types of APCs produced a diversity of responses in cytokine production and cross-presentation. A compilation of APC subsets and their functional relevance to priming adaptive immunity has been reviewed elsewhere [143,144].

What then are the physiologically relevant APCs necessary for the immunological responses elicited by vaccination with HSPs? One experiment performed almost 2 decades ago

tested the requirement for APCs during HSP immunization by using the broadly acting reagent carrageenan, which inhibits the function of all phagocytic cells; T cell priming was abrogated in those studies [66]. One decade ago we showed that $CD11c^{+}$ cells from lymph nodes of gp96-immunized mice could transfer tumor immunity, but the phenotype of these cells and whether they endocytosed gp96 was not further characterized [72]. More recently, the efficiency of priming anti-tumor immune responses with a genetically engineered and secreted form of gp96 (gp96-Ig) was explored. Those studies showed that intraperitoneal vaccination with these fusion proteins caused a dramatic increase of $CD11c^{high}MHCII^{high}CD103^{+}$ cells in the peritoneum [145]. While these APCs were able to induce the expression of gut-homing receptor CCR9 in responding T cells *in vitro*, their requirement for priming *in vivo* was not tested. APC subset dynamics with regards to native, murine gp96, following deposition in the skin, as well as their expression of CD91, remains unexplored and warrants investigation.

Following introduction of extracellular gp96 via immunization in mice, gp96 was shown to preferentially localize to cells expressing CD11b and CD11c. Subsets of APCs are further characterized with respect to CD4, CD8, Gr1.1, MHC class II, F4/80, CD103 and CD207 expression. Anti-tumor immunity could be transferred to naïve mice by adoptive transfer of cells positive for gp96 acquisition. While CD91 expression is essential for gp96 uptake, location of APCs within the lymph node was another determining factor for acquiring HSP. These results are extrapolated to HSPs in the extracellular environment following active release by, or necrotic death of, aberrant cells. This study is important for development of novel HSP-based vaccines and for improvement of on-going clinical trials. Finally, these studies will shed light on the observations that HSPs are capable of priming Th1 [7,18,66,99,145], Th2 [57,146], Th17 [24] and Treg [147,148] responses under different immunization conditions.

3.3 RESULTS

3.3.1 Rapid draining of gp96 to lymph nodes

For tracking vaccine administered HSPs *in vivo*, apparently homogenous preparations of gp96 were labeled with Alexafluor 488 ($_{A488}$). We confirmed labeling by SDS-PAGE and immunoblotting (Figure 3-1A). Alexafluor 488-labeled gp96 ($gp96_{A488}$) remained functional as determined by binding to and uptake by the CD91-expressing, macrophage cell line RAW264.7. RAW264.7 cells incubated with $gp96_{A488}$ endocytosed significant protein as measured by flow cytometry (Figure 3-1B) and microscopy (Figure 3-1C). Gp96, labeled on primary amines in a similar manner, has previously been shown to retain its immunological property of priming T cell responses [96].

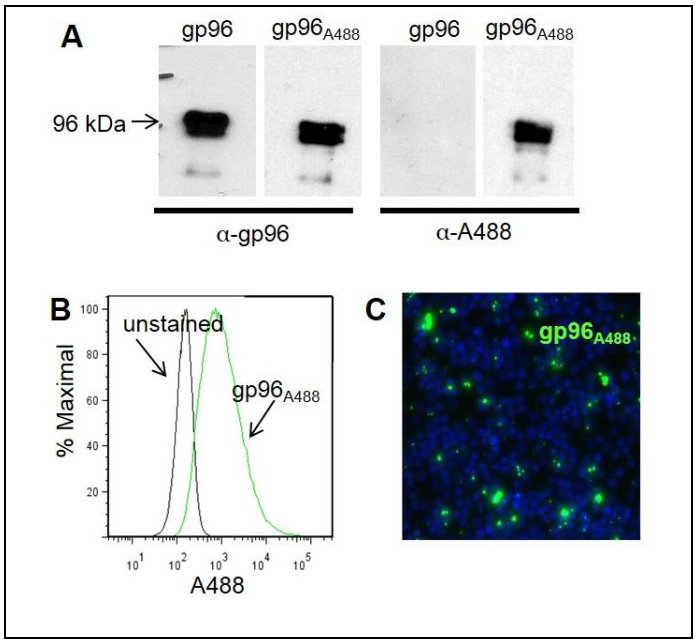

Figure 3-1. Purification and labeling of gp96 with Alexa fluor 488.
(A) gp96 was purified to homogeneity, labeled with Alexafluor 488 and analyzed by SDS-PAGE and immunoblotting. (B,C) Biological integrity of $gp96_{A488}$ was verified by testing its endocytosis by $CD91^+$ RAW264.7 cells. RAW264.7 were incubated with $gp96_{A488}$ for 30 mins and analyzed by (B) flow cytometry and (C) microscopy. Performed by MNM.

Mice were then immunized intradermally with titrated doses of $gp96_{A488}$. A dose of 1-10 μg administered via this route has routinely been used to elicit tumor-specific T cell responses [7,18,66,99,147]. Single cell suspensions of draining axillary and inguinal lymph nodes (LNs) were analyzed by flow cytometry 8 hrs post immunization (Figure 3-2A). Significant A488

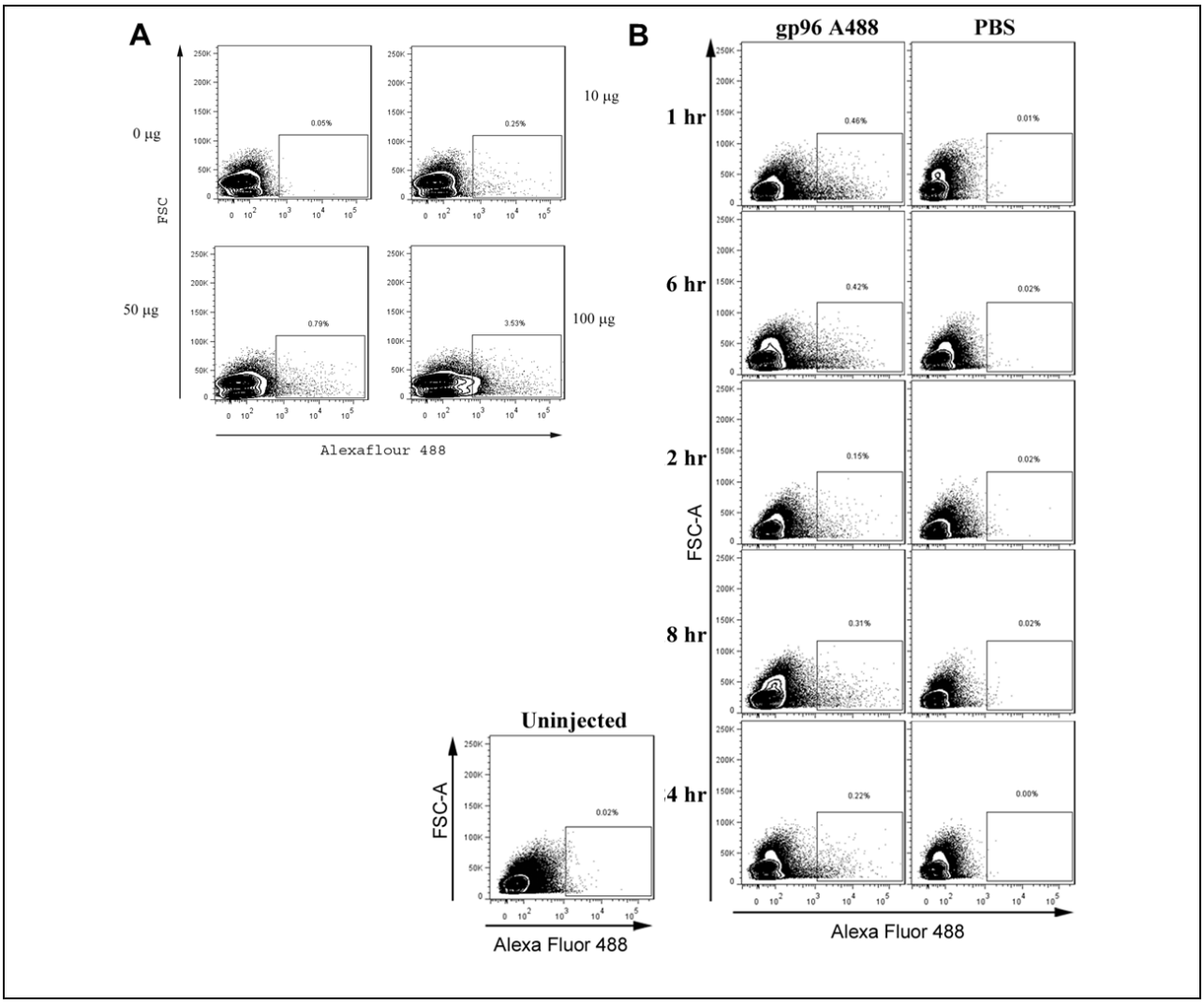

Figure 3-2. Flow dot plots show increasing A488$^+$ cells with increasing gp96$_{A488}$ dose in vivo.
(A) C57BL/6 mice were treated with titrated doses of gp96$_{A488}$ delivered via intradermal injection. Axillary/brachial and inguinal lymph nodes (LN) were harvested 8 hrs later and processed into single cell suspensions for flow cytometric analysis. Increasing doses increased the percent of cells positive for A488. Data are representative of 3 independent experiments, and were quantified in Figure 3-3A. (B) Mice were treated with 10 µg gp96$_{A488}$ and lymph nodes were harvested at the indicated times and processed into single cell suspensions for flow cytometry. Data are representative of three experiments, and were quantified in Figure 3-3B. Performed by MNM.

signal was detected in the lymph nodes at ≥10 µg dose when compared to lymph nodes from mice immunized with PBS (Figure 3-3A).

To analyze the kinetics of gp96$_{A488}$ appearance in the LNs, we immunized sets of mice with 10 µg gp96$_{A488}$ and harvested draining LN at the indicated time points (Figure 3-2B). Fluorescent gp96 was observed in the LN as early as 1 hour following immunization and peaked

at that point (Figure 3-3B). The signal gradually decreased thereafter but was still detectable 72 hrs post immunization.

Additionally, we visualized the presence of $gp96_{A488}$ within LN cells by fluorescent microscopy (Figure 3-3C). Two populations of cells differing in the amount of $gp96_{A488}$ internalized could be discerned. These results demonstrate that gp96 can be rapidly detected in the LN following intradermal immunization and suggests differential uptake by cell populations.

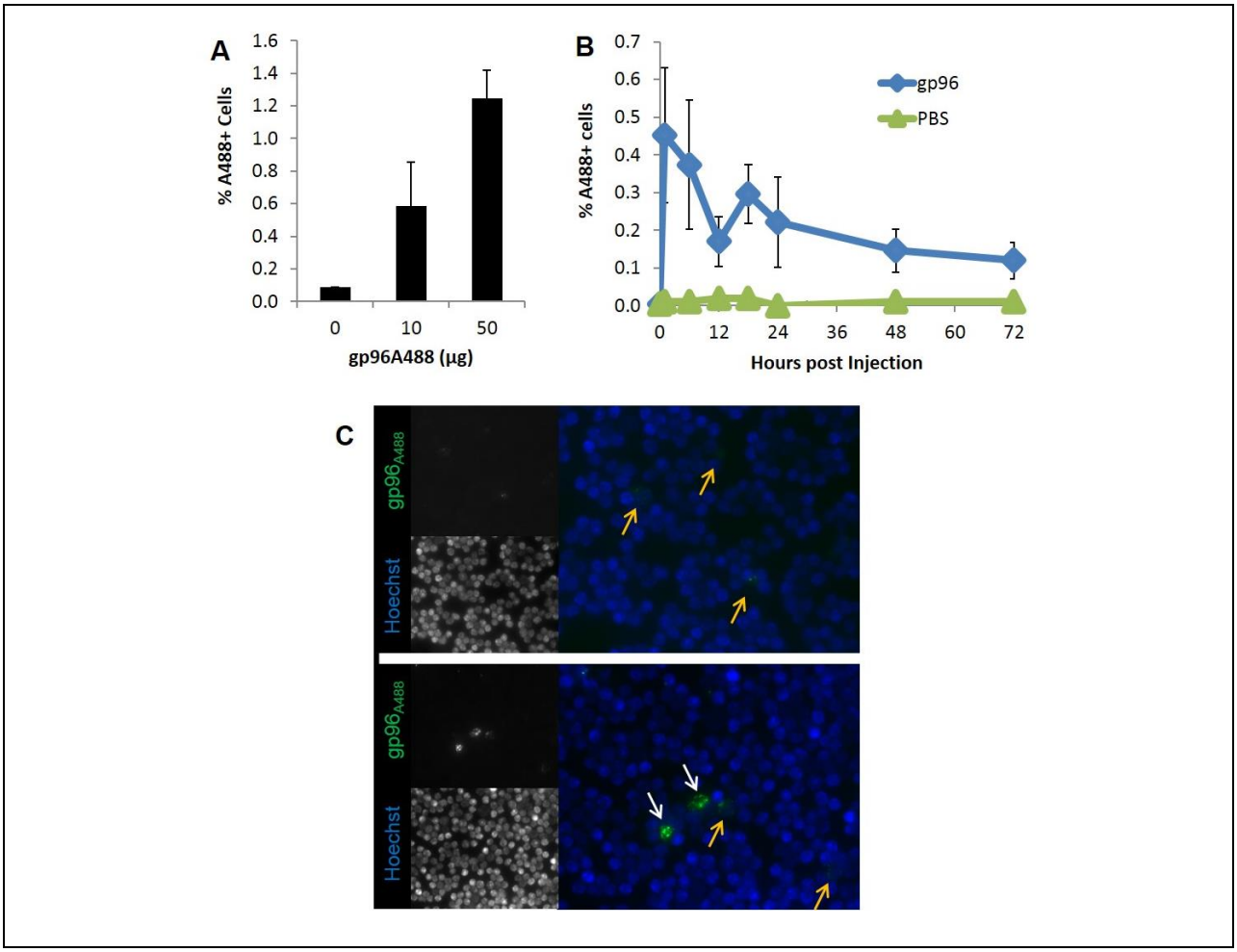

Figure 3-3. Rapid localization of gp96 in lymph nodes following intradermal immunization.
(A) C57BL/6 mice were treated with titrated doses of $gp96_{A488}$ intradermally. Draining lymph nodes were harvested 8 hours later and analyzed by flow cytometry. Results shown are averaged from 3 independent experiments, of 4-8 mice per group. (B) Lymph nodes from mice receiving 10 µg $gp96_{A488}$ were harvested at the indicated time points and analyzed as above. Data are representative of three experiments, of 5 mice per time point for gp96 group and 2 per time point for PBS. (C) Lymph nodes from mice receiving 10 µg $gp96_{A488}$ were harvested at 5 hours, disrupted into single cell suspensions and analyzed by microscopy. Nuclei were stained with Hoechst dye (blue), A488 is shown in green. Two images at 40x magnification are shown to demonstrate cells with low (yellow arrows) and high (white arrows) $gp96_{A488}$ staining. Data (A,B) are represented as mean +/- SEM. Performed by MNM.

3.3.2 Acquisition of gp96 by CD11b$^+$ and CD11c$^+$ cells

To characterize the cells responsible for the observed $gp96_{A488}$ signal in the draining LN, we adopted a flow cytometric approach including a number of surface markers for APC subsets for analysis. Our initial gating strategy was based on a review by Heath et al. showing selective characterization of the major APC subsets known at that time (Table 3-1 [143]). As our studies progressed, we added additional markers for clarification of APC types and in keeping with current publications.

Our systematic analysis of lymph nodes began with a broad screen based on the surface markers CD11c and CD11b, markers associated with professional cross-presenting APCs. The experimental gating strategy is outlined in Figure 3-4. The total LN was observed to have ~2% CD11c$^+$ cells and ~10% CD11b$^+$ cells (Figure 3-5A). These subsets can be further divided on additional functionally relevant markers including MHC class II, CD4, CD8, F4/80, Gr1.1,

Table 3-1. Major DC Subsets

DC Subtype	Surface Marker Expression						Tissue Source
	CD11c	CD8 α	CD4	CD205	CD11b	CD45RA	
CD8 DC	+	+	-	+	-	-	T-cell areas, spleen & LNs
CD4 DC	+	-	+	-	+	-	Marginal zone of spleen, move once activated
CD4-CD8- DC	+	-	-	-	+	-	Marginal zone of spleen, move once activated
Langerhans' Cell	+	-/low	-	+++	+	-	Skin
Dermal/ Interstitial DC	+	-	-	+	+/-	-	All tissues
Plasmacytoid DC	low	+/-	+/-	-	-	+	Spleen/blood/ tissues

Adapted from Heath et al. [143]

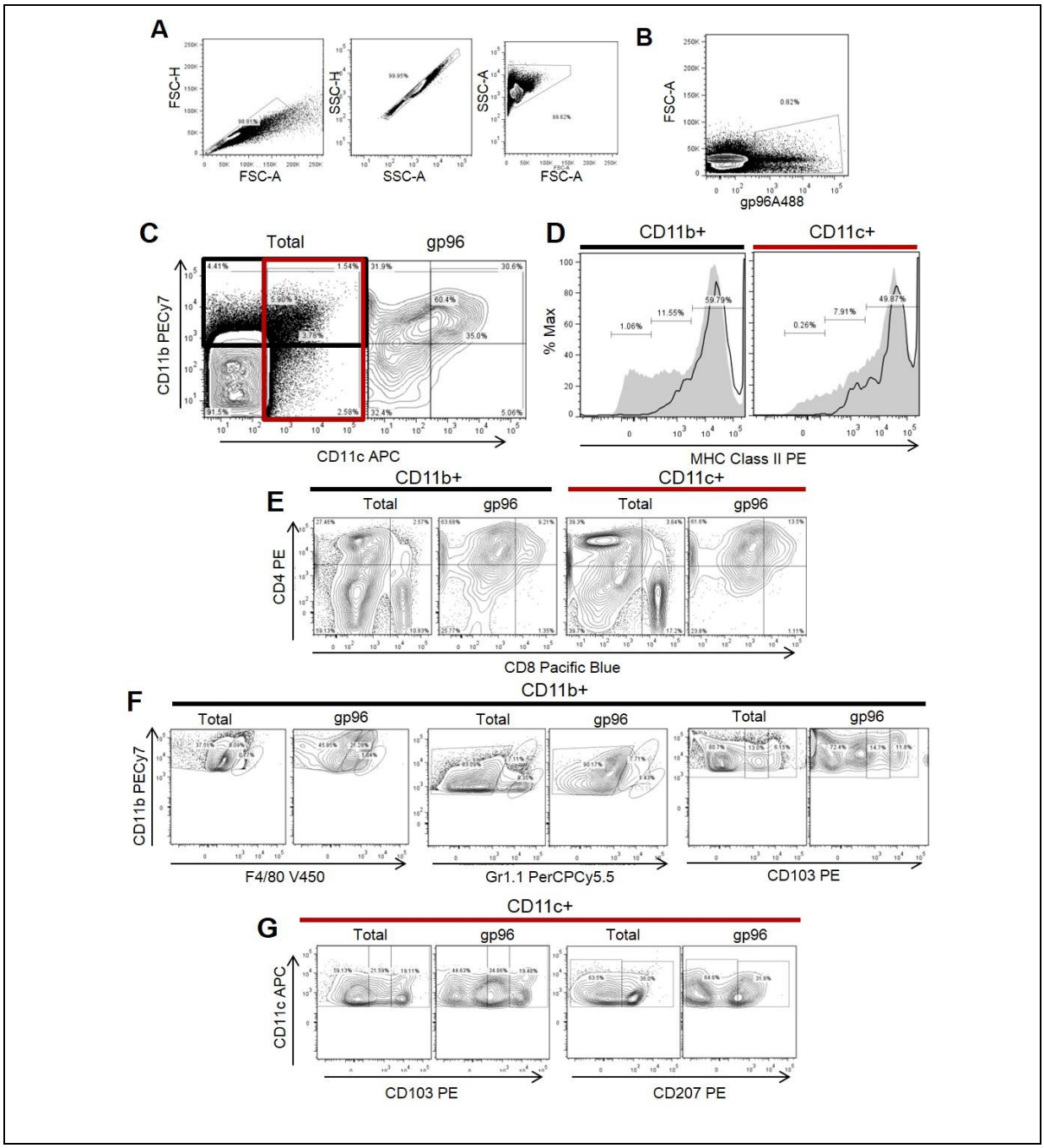

Figure 3-4. Gating strategy for phenotypic analysis of LN cells.
(A) Gating of lymph node cells based on forward scatter (FSC) and side scatter (SSC) properties to reduce doublets and cell debris, with the final FFC-A by SSC-A gate termed "Total". Total lymph node cells were analyzed directly for surface marker expression or further gated on A488$^+$ cells (B). (C) Cells were gated on CD11b (solid line) or CD11c (red line). (D) CD11b$^+$ and CD11c$^+$ cells were analyzed for their MHC class II expression (filled, grey histogram is total lymph node; open, black line histogram is gp96$_{A488}{}^+$). (E) CD11c$^+$ or CD11b$^+$ cells were analyzed for expression of CD4 and CD8. (F) Additional markers analyzed on CD11b$^+$ cells were F4/80, Gr1.1, and CD103, with 3 gates (high, med, negative) for each as shown. (G) Additional markers analyzed on CD11c$^+$ cells were CD103 and CD207. Gates for all samples were based on single color controls as well as "fluorescence minus one." Shown are representative plots from a minimum of 3 mice for each test. Frequencies were quantified and averages are shown in Figure 3-5. Performed by MNM.

CD103 and CD207 as shown in Figure 3-4D-G. By applying this analysis to draining LNs harvested from mice immunized with 10 μg $gp96_{A488}$ at 8 or 48 hours after immunization, we were able to determine the subsets of cells that contained $gp96_{A488}$ at each time point. At 8 hrs, $CD11b^+$ cells ($CD11c^{+/-}$) comprised ~70% of the $gp96_{A488}^+$ cells (Figure 3-5A). These $CD11b^+gp96^+$ cells were additionally phenotyped for CD4, CD8, Gr1.1, F4/80, and MHC class II (Figure 3-5B, Figure 3-4D-F). $CD11b^+gp96^+$ cells were primarily $CD4^+$, $CD8^-$, $Gr1.1^-$ with low or no F4/80 expression and abundant MHC class II expression (Figure 3-5B). About 30% of $gp96_{A488}^+$ cells in the LN were $CD11c^+$ ($CD11b^{+/-}$) at 8hrs (Figure 3-5A). These cells were further phenotyped for CD4, CD8, CD207, CD103, and MHC class II (Figure 3-4D,E,G). $CD11c^+gp96^+$ cells also had abundant MHC class II expression, while the expression of CD103 and CD207 was heterogeneous (Figure 3-5C). A greater percentage of the cells had no CD207 or CD103 expression. Cells that were $CD11b^-CD11c^-$, comprising the bulk (~93%) of the lymph node, accounted for the remaining 30% of $gp96_{A488}^+$ cells, potentially representing B and/or T cells (Figure 3-4C).

We next compared the overall distribution of cell types with $gp96_{A488}$ at 8 hrs with those at 48 hrs. At 8 hrs, a significantly greater percentage of $CD11b^+CD4^+$ cells acquired $gp96_{A488}$ compared to $CD11b^+CD4^-$ cells (Figure 3-5D, Figure 3-4E). $CD11c^+$ cells were a smaller fraction of $gp96^+$ cells and included both $CD8^+$ and $CD8^-$ cells, though $CD8^-$ cells were the major $CD11c^+$ fraction. (Figure 3-5D). At 48 hrs post immunization, the distribution of $gp96_{A488}$ was essentially the same (Figure 3-5D,E); $CD11b^+$ cells were still the larger percentage of $gp96_{A488}$ compared to $CD11c^+$ cells. However the percentage of $gp96_{A488}^+$ that were $CD11c^+CD8^+$ doubled

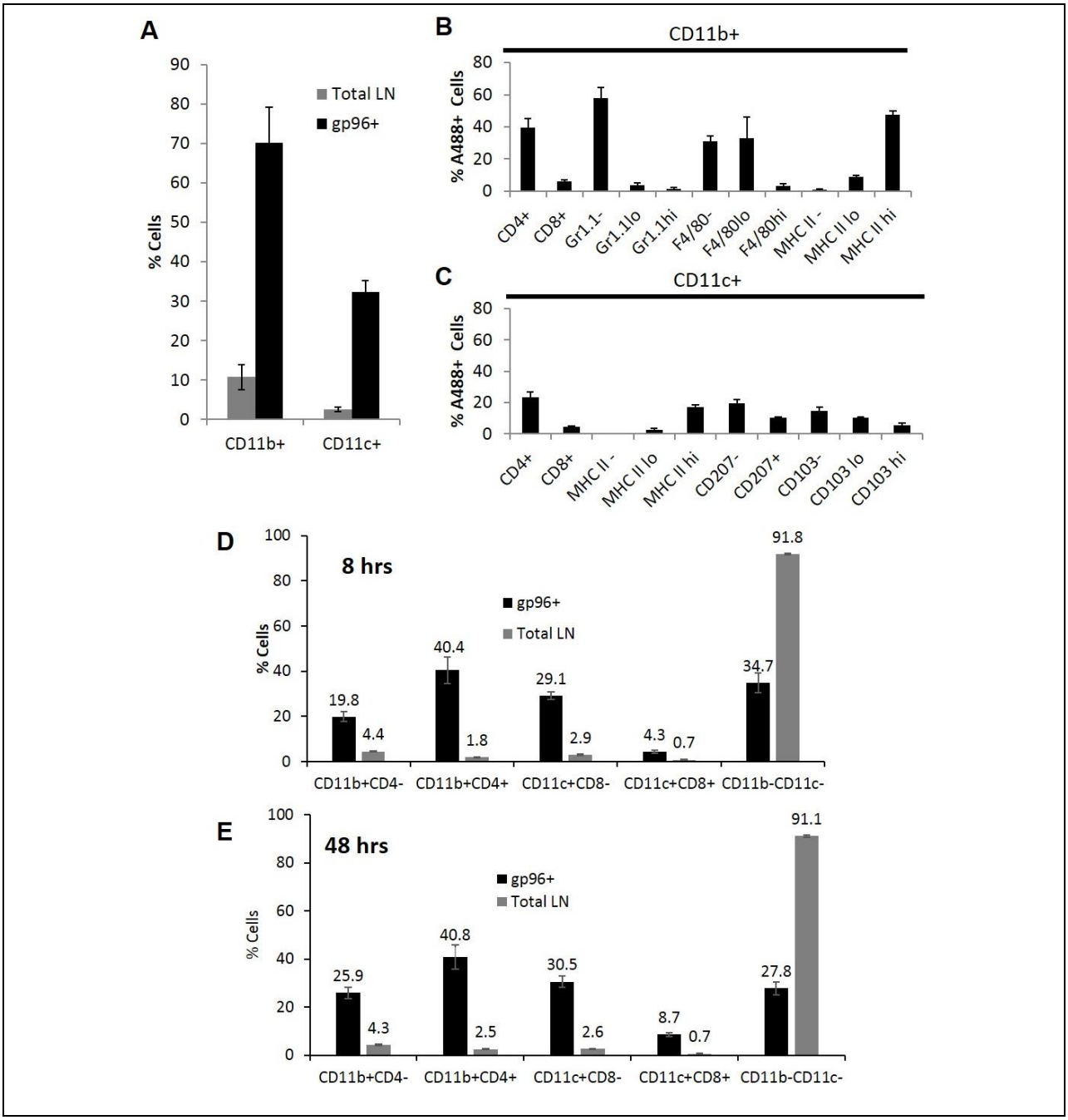

Figure 3-5. Phenotypic analysis of lymph node cells associated with gp96A488.
Lymph nodes from unimmunized or gp96 immunized mice were analyzed by multi-color flow cytometry as shown in Figure 3-4. (A) At 8 hrs post immunization with 10 μg $gp96_{A488}$, total lymph node and $gp96^{+}$ cells were phenotyped for CD11c and CD11b expression. The CD11c population was $CD11b^{+/-}$ and $CD11b^{+}$ population was $CD11c^{+/-}$. (B) $A488^{+}CD11b^{+}$ lymph node cells were additionally phenotyped for CD4, CD8, Gr1.1, F4/80 and MHC class II. (C) $A488^{+}CD11c^{+}$ lymph node cells were additionally phenotyped for CD4, CD8, CD207, CD103 and MHC class II. At 8 (D) or 48 (E) hours post immunization with 10 μg $gp96_{A488}$, lymph nodes were harvested and phenotyped for the indicated populations. The distribution of gp96 in each population is indicated as a percentage and compared to the percentage of that population in the total lymph node. Percentages are the average from 5 mice, and representative of 2 experiments. Data are represented as mean +/- SEM. Performed by MNM.

at 48 hrs compared to the 8 hr time point. These data characterize the distribution of gp96 in draining lymph nodes following immunization at early and late time points.

3.3.3 Dose dependent targeting of gp96 to LN cells

The dose of gp96 used for immunization has a profound effect on the immune response generated. At 'high' doses, 5-10 times the 'optimal' immunogenic dose determined for each route of administration, anti-tumor response is abrogated by T regulatory cell responses [147]. While the immune responses to optimal gp96 doses is peptide-dependent, the immunosuppression generated by high-dose gp96 is independent of chaperoned peptides. Additionally, high dose gp96 only suppresses concurrently developing immune responses (Figure 3-6). Indeed, high-dose gp96 vaccination suppresses any active T cell response, and has been used as therapy to reverse autoimmunity [148]

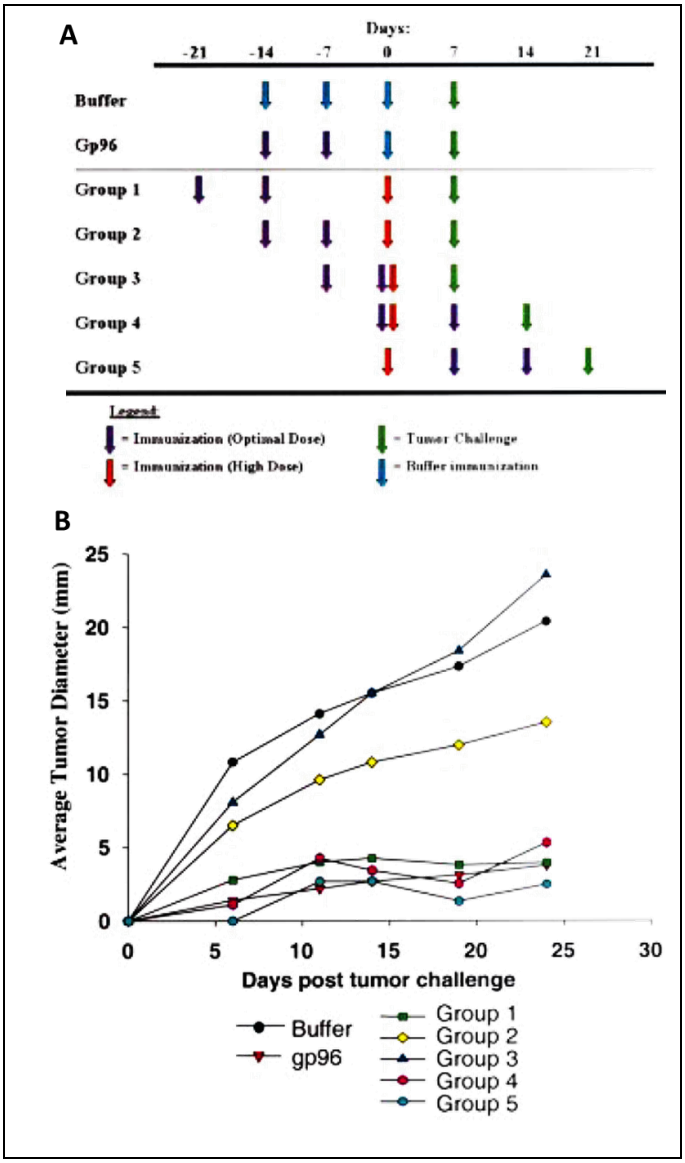

Figure 3-6. High dose gp96 suppresses developing immune responses.
After identifying an intradermal immunogenic dose (10 µg) and a tolerogenic dose (100 µg), Chandawarkar compared the timing and specificity of immunosuppression (Fig. 2 [148]). (A) Study design; animals were immunized with immunogenic dose (purple arrow) and/or a suppressive dose (red arrow) or buffer (blue arrow) at indicated time points, and challenged with 100,000 Meth A tumor cells (green arrow). (B) Tumor growth curves for each of the treatment regimens shown in A. N = 5+ mice per group.

and to prolong tissue transplant survival [149]. Abrogation of tumor immunity is transferable by $CD4^+CD25^+$ T cells [148], and the expansion of such regulatory T cells following high dose gp96 was shown to outpace CTL expansion and actively suppress effector T cells [150].

We were interested in determining whether there are changes in the subsets of LN cells targeted by high dose gp96 versus low, 'optimal' dose. At 8 hrs post intradermal injection with 100 µg ('high') or 10 µg ('low') $gp96_{A488}$, it appeared that mice given the low dose had an increase in the percentage of $CD11b^+$ cells in the lymph node compared to mice injected with 100 µg (Figure 3-7A), but this was not a statistically significant difference. Indeed, no differences were observed for $CD11c^+$ populations, nor for CD4 and CD8, despite significantly increased total cellularity in LNs from mice injected with the high dose (approximately 4 times more cells compared to dLN of mice injected with 10 µg).

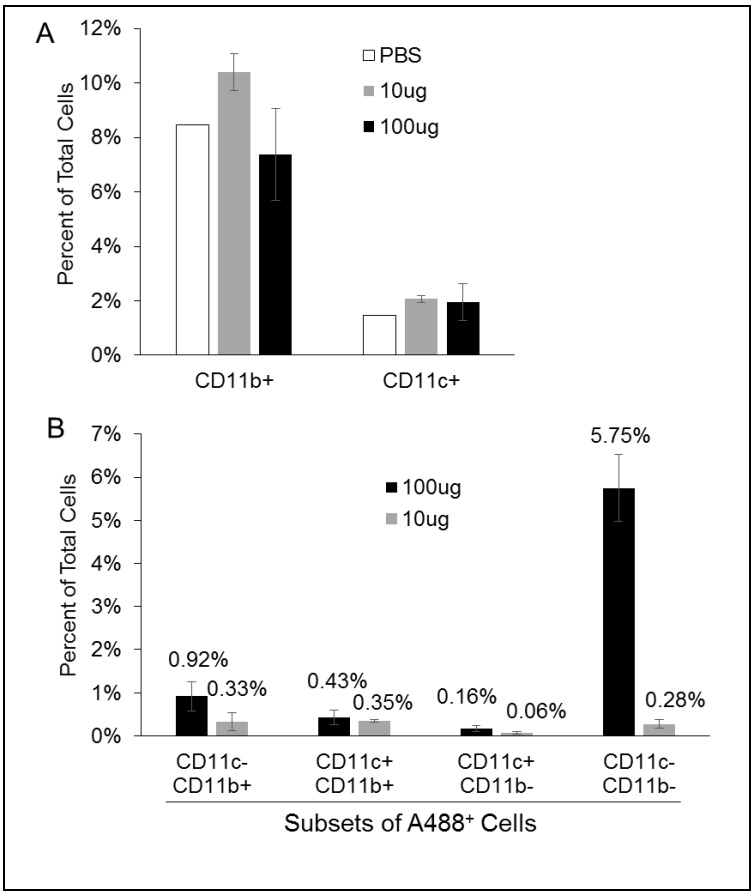

Figure 3-7. High dose of gp96 targets alternate cell subsets. C57Bl/6 mice were given intradermal injections of 10 µg gp96, 100 µg gp96 or PBS and draining LNs were harvested 8 hrs later and analyzed by flow cytometry as in Figure 3-4. (A) The number of CD11b or CD11c cells in the draining LN is expressed as a percentage of the total LN. (B) Cells were gated on A488 signal and then analyzed for CD11b and CD11c expression. Each population is shown as a percent of the total LN. N=2 mice. Performed by MNM.

We then analyzed the subsets of $A488^+$ cells as described in Figure 3-4. A dose of 100 µg $gp96_{A488}$ resulted in significantly more $A488^+$ cells in the total lymph node (~7% compared to ~1% in mice injected

with 10 µg $gp96_{A488}$). Comparing the expression of CD11b and CD11c on these cells, this increase was not evenly distributed among the subsets (Figure 3-7B). The only subset to show a significant difference between 100 µg and 10 µg $gp96_{A488}$ injected mice was $CD11c^{-}CD11b^{-}$ cells ($p = 0.01$). While APC subsets marked by expression of CD11b and/or CD11c that took up $gp96_{A488}$ only marginally increased, this $CD11c^{-}CD11b^{-}$ subset increased almost 20 times as a fraction of the total LN cells. Thus, there is a large difference in the cells that appear to take up gp96 at high doses.

3.3.4 Gp96 is localized to cells of the subcapsular region of draining LNs

We used fluorescent microscopy to visualize the location of HSPs in the draining LNs following immunization with $gp96_{A488}$. Mice were immunized with 10 µg $gp96_{A488}$ and sequential tissue sections were prepared 8 hrs post injection. As shown in Figure 3-8, $gp96_{A488}$ localizes to the subcapsular region of the LN. This region is populated primarily by $CD11b^{+}$ cells, highlighted in the region of interest (Figure 3-8B), and is distinct from T cell zones as shown by co-staining for CD8 (Figure 3-8C). Overlap of $gp96_{A488}$ signal with CD11b and/or CD11c was quantified using IMARIS software and substantiates the results obtained by flow cytometry in Figure 3-5; early after immunization (8 hrs) $gp96_{A488}$ is associated more with $CD11b^{+}$ than $CD11c^{+}$ cells (Figure 3-8D). Draining LN sections from mice immunized with $gp96_{A488}$ were stained for CD207 (Langerin) at 8 hrs (Figure 3-8E). A small fraction, of $gp96_{A488}$ co-localizes to CD207, consistent with observations in Figure 3-5C. We next examined the overlap of $gp96_{A488}$ with CD103, an integrin that identifies a subset of LN DC. We observed some co-localization of $gp96_{A488}$ with CD103 although this association was variable (Figure 3-8D,F,G). These data are consistent with the flow cytometry data in Figure 3-5.

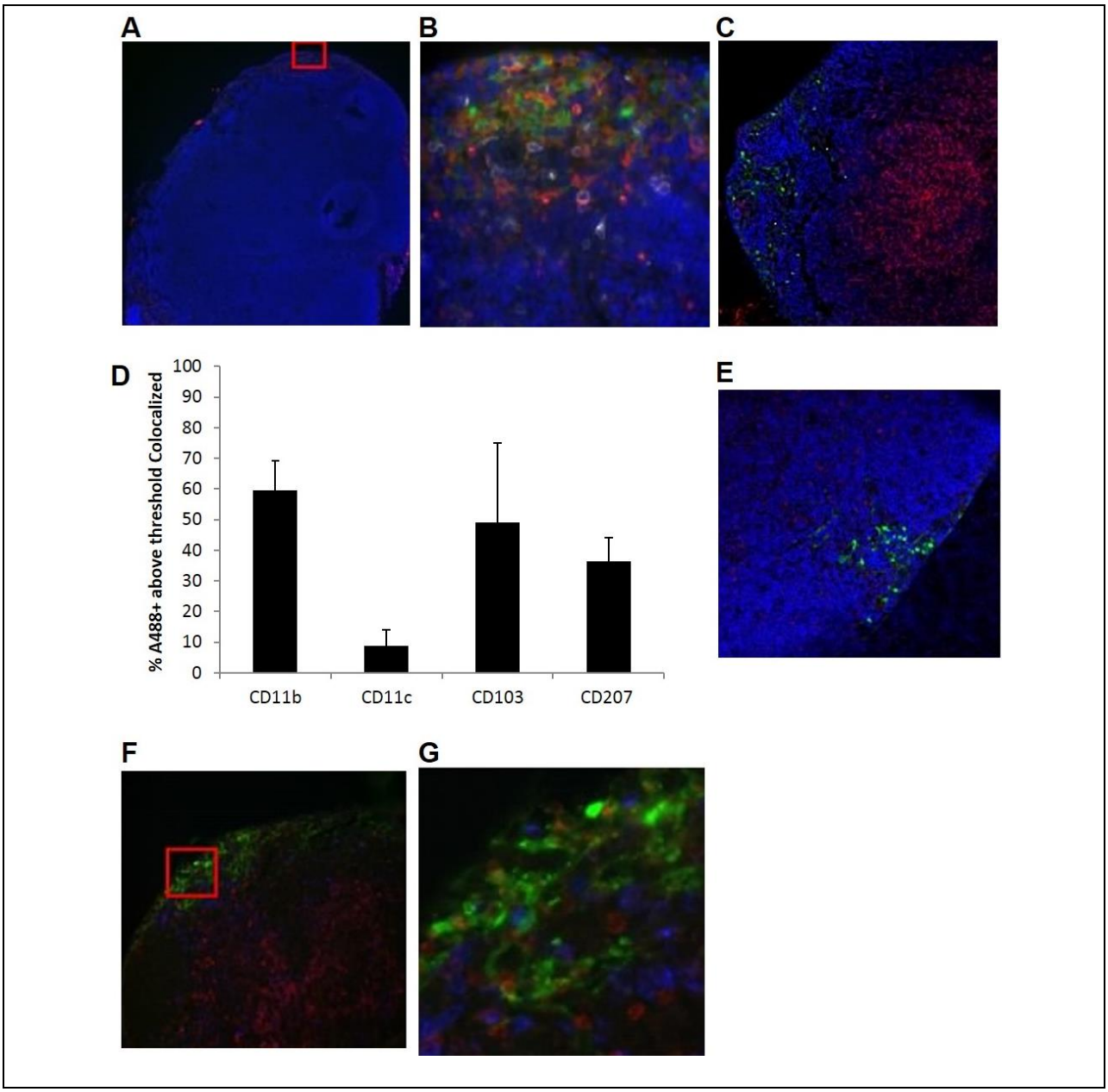

Figure 3-8. Distribution of gp96$_{A488}^{+}$ cells within the LN.
Mice were immunized with 10 µg gp96$_{A488}$ and draining LNs were harvested 8 hrs later and analyzed by fluorescent microscopy. Green indicates gp96$_{A488}$ fluorescence and blue is Hoechst nuclear staining. (A) Images captured at 10x magnification. Region of interest (ROI, red box) was selected for further analysis. (B) ROI is analyzed for CD11b (red) and CD11c (white). (C) Image at 20x magnification showing CD8 stain to reveal T cell zones. (D) Images were analyzed using IMARIS and the co-localization of each marker indicated with gp96$_{A488}$ was quantified and expressed as percent A488^{+} above threshold that co-localized. Each marker (red or white) was analyzed separately and there is potential overlap with other indicated markers. Data are the average value from 3 ROIs analyzed. Data are represented as mean +/- SEM. (E) Sections at 20x magnification were stained for CD207. Co-localization of CD207 with gp96$_{A488}$ was quantified (D). (F) Sections at 40x magnification were stained for CD103 (red). (G) ROI from (F) showing co-localization of CD103 (red) with gp96$_{A488}$ (green). Co-localization was quantified (D). Images and calculations are representative of 2 independent experiments. Performed by MNM.

3.3.5 Functional gp96^{+} APCs transfer tumor-specific immunity

As shown in previous studies conducted *in vitro*, gp96 stimulates APCs rendering them capable of providing signals for priming T cells. In addition, peptides (including tumor antigens) chaperoned by gp96 are cross-presented by the same APCs. We set up an antigenic system based on the CMS5 tumor and its immuno-dominant peptide ERK [151], to test whether the APCs that captured gp96 *in vivo* were immunogenic (Figure 3-9A). Gp96$_{A488}$ was complexed to the ERK peptide (gp96$_{A488}$-ERK) or left uncomplexed (gp96$_{A488}$). Mice were immunized with 10μg of gp96$_{A488}$-ERK, gp96$_{A488}$, ERK peptide alone or PBS. Draining LN cells were harvested from each group of mice after 6 hrs and A488^{+} cells were isolated by FACS (Figure 3-9B). A488^{+} cells from gp96$_{A488}$-ERK or from gp96$_{A488}$ group, or bulk lymph node cells from ERK peptide or PBS immunized group, were transferred to naïve BALB/c mice retro-orbitally. Recipient mice were challenged one week later with CMS5 cells and tumor growth rate was measured (Figure 3-9C).

Tumor growth was significantly retarded only in mice that received A488^{+} cells from donors immunized with gp96$_{A488}$-ERK. Tumors grew with identical kinetics in mice receiving A488^{+} cells from donors immunized with gp96$_{A488}$, or mice receiving bulk LN cells from donors immunized with ERK peptide or PBS (Figure 3-9C). We tested whether the protective effect was dependent on the cross-priming ability of donor (A488^{+} cells) or recipient APCs. Cells from donors immunized with gp96$_{A488}$-ERK or gp96$_{A488}$ were irradiated prior to adoptive transfer to recipient naïve mice as above. Recipients were then challenged with CMS5. Tumor growth rate was measured (Figure 3-9D). The protective effect of A488^{+} cells from gp96$_{A488}$-ERK immunized mice was abrogated when the cells were irradiated, as the tumors grew with identical kinetics to control treated or untreated mice. This demonstrates that the transferred (donor) APCs

were actively involved in priming anti-tumor immunity through events that may include antigen transfer, cross-presentation and migration.

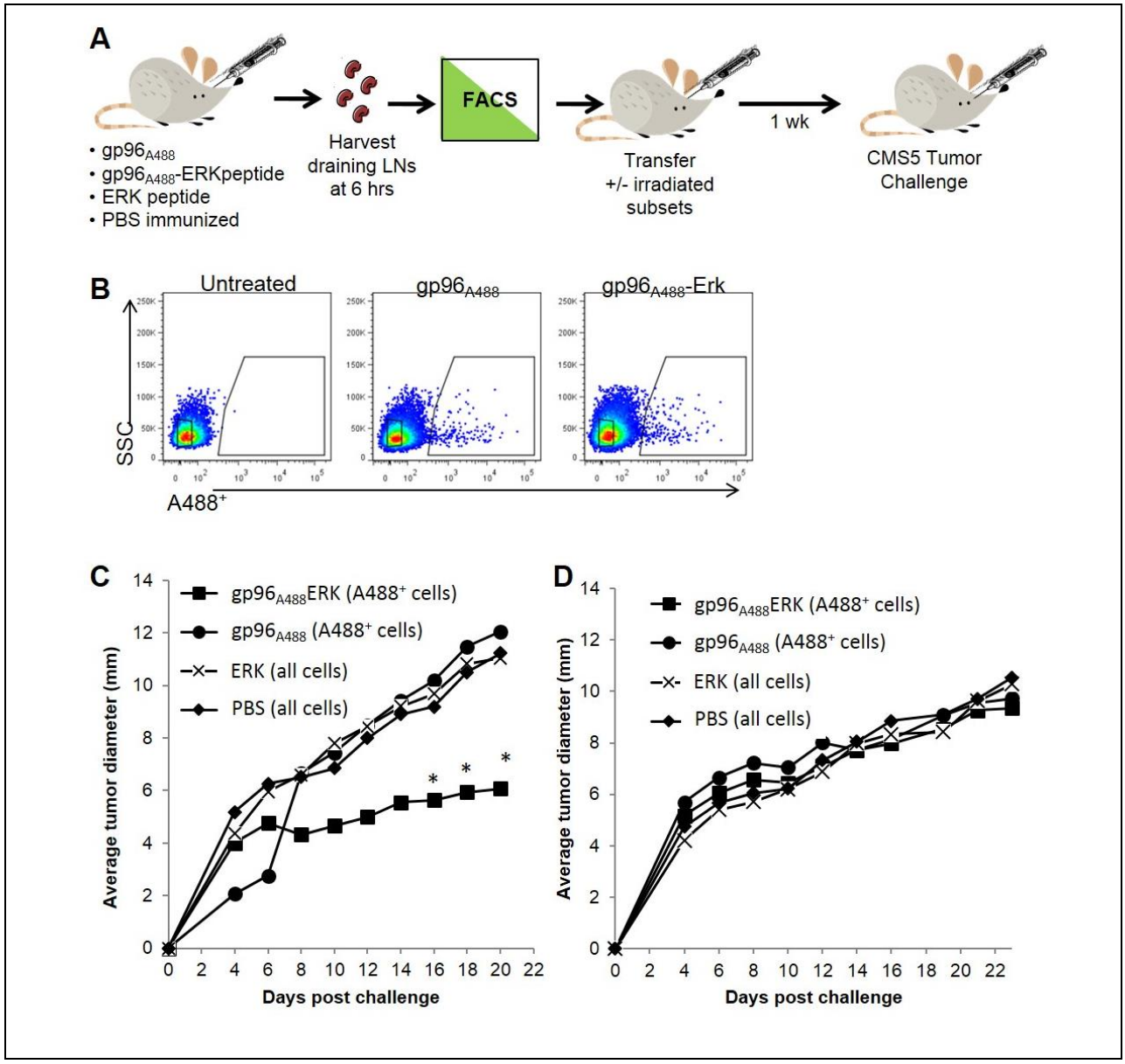

Figure 3-9. Adoptive transfer of tumor immunity by gp96$_{A488}^{+}$ lymph node cells.
(A) A schematic of adoptive transfer of tumor immunity. Groups of mice were immunized with gp96$_{A488}$-ERK or gp96$_{A488}$. Draining lymph nodes were harvested 6 hours later. Gp96$_{A488}^{+}$ cells were purified by FACS and transferred to naïve mice. Whole lymph node cells from mice immunized with ERK alone or PBS were transferred into other naïve mice. Recipient mice were challenged with CMS5 tumor 1 week later. Tumor growth was monitored. (B) Representative FACS plots showing gated cells that were transferred. (C) CMS5 growth curves in recipient mice following transfer of donor cells. Average values calculated from 2-8 recipient mice from 2 independent experiments. *$p < 0.05$, compared to gp96$_{A488}$ recipients. (D) CMS5 growth curves in recipient mice following transfer of irradiated donor cells. Average values are from 2-5 recipient mice per group. Primarily performed by MNM with help from DF (cell sorting), RJB (retro-orbital adoptive transfer), and YZ (tumor cell challenge).

3.3.6 Differential expression of CD91 in APC subsets.

We have previously shown that CD91 expression is essential for gp96 uptake. Thus we tested the relative expression of CD91 by APCs in the LN as characterized by their expression of CD11b and/or CD11c (Figure 3-10A). Cells were stained for CD91 simultaneously with CD11b and CD11c and analyzed by flow cytometry. CD91 expression was observed to vary with each population (Figure 3-10B, Figure 3-10A-C). $CD11c^{+}CD11b^{+}$ cells had the most robust CD91 expression as measured by geometric MFI followed by $CD11c^{-}CD11b^{+}$ cells. CD91 expression on $CD11c^{+}CD11b^{-}$ cells, while barely detectable, was still significant over background staining with secondary antibody alone. CD91 expression was not significantly detected on $CD11c^{-}$ $CD11b^{-}$ cells in this assay although this observation does not conflict with the possibility that a

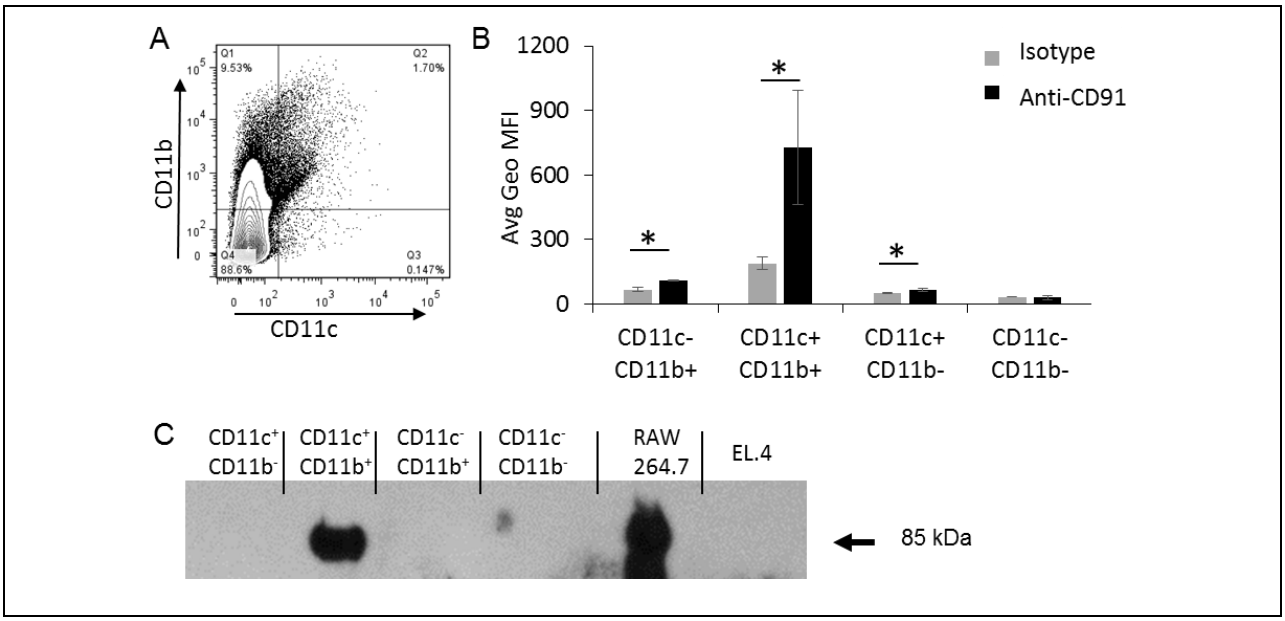

Figure 3-10. Expression of CD91 on subsets of APCs in the lymph node.
Lymph node cells were analyzed by multi-color flow cytometry for CD11b, CD11c, and CD91. (A) Cells were first gated on CD11b and CD11c subsets, and then the average geometric mean fluorescence intensity for CD91 was quantified for each population and compared to secondary alone (B). Data are averages for three mice +/- SEM, and representative of 3 experiments. (C) CD91 expression on CD11c/CD11b populations was confirmed by FACS sorting followed by SDS-PAGE and immunoblotting. CD91 β-chain (85 kDa) is identified by the arrow. Positive and negative control cell lines for CD91 were RAW264.7 and EL.4 respectively. Performed by MNM with help from DF (cells sorted for C).

minor cell type in this large and varied population does so [90,93]. The results in Figure 3-10B were confirmed by immunoblotting. FACS purified APC populations from the lymph node were lysed and analyzed by SDS-PAGE and immunoblotted for the β-chain of CD91 (85kDa). CD91 expression was easily detectable in $CD11c^{+}CD11b^{+}$ populations and more difficult to discern in $CD11c^{-}CD11b^{+}$ and $CD11c^{+}CD11b^{-}$ populations (Figure 3-10C). The macrophage cell line RAW264.7 served as a positive control and EL.4 thymoma cells as the negative control for CD91 expression.

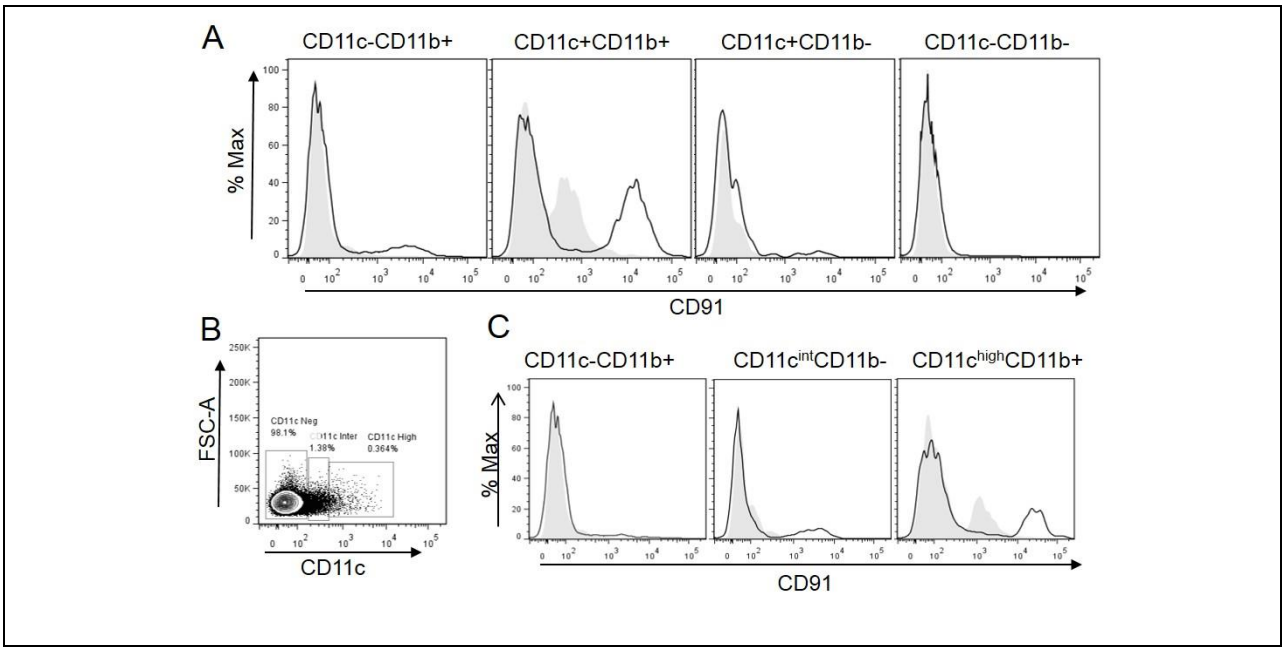

Figure 3-11. Histograms of CD91 expressing APC subsets.
Lymph node cells were analyzed by multi-color flow cytometry for CD11b, CD11c, and CD91. Cells were first gated on CD11c or CD11b expression as in Figure 5A. (A) The fluorescence intensity of CD91 (solid black line) versus secondary antibody alone (filled histogram) is shown for each gated population. Average geometric mean was quantified for each population from three mice was quantified for Figure 5B. (B) Alternative gating on CD11c high, intermediate, or negative cells followed by CD11b gating was conducted to investigate CD91 expression on migratory versus resident cells. (C) Fluorescence intensity of CD91 (solid line) versus secondary alone (filled histogram) is shown for each subset. Performed by MNM.

3.3.7 CD91 expression correlates with superior gp96 endocytic capacity

To determine the endocytic capacity of LN cells for gp96, we harvested naïve LNs, processed the cells into single cell suspensions, exposed these cells to sub-saturating levels of $gp96_{A488}$ *in*

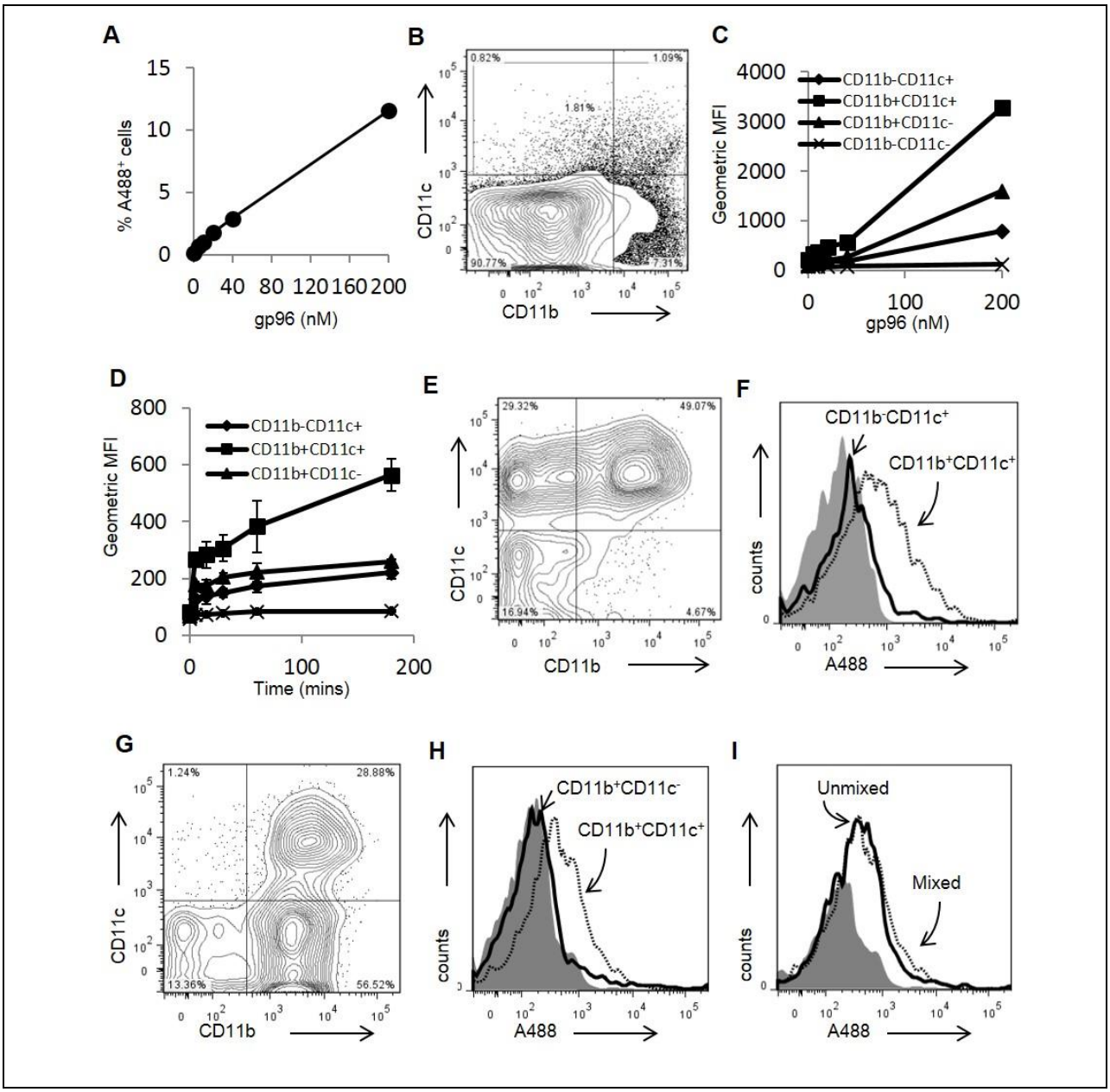

Figure 3-12. Differential capacities of APC subsets to endocytose gp96.

(A) Isolated lymph node cells were incubated with titrated doses of $gp96_{A488}$. Cells were analyzed by flow cytometry for A488 positivity and expressed as a percentage of the total population. (B) The lymph node cells were gated into populations expressing $CD11c^+$ and/or $CD11b^+$. (C) Following incubation of lymph node cells with varying doses of $gp96_{A488,}$ these populations were analyzed for endocytosis of $gp96_{A488}$. Experiments were performed in duplicates. (D) Endocytosis of $gp96_{A488}$ by the indicated populations was tested by incubating lymph node cells with 20 nM $gp96_{A488}$ for the indicated time. Experiments were performed in duplicates. (E) Competitive endocytosis was examined by mixing purified populations of $CD11b^-CD11c^+$ and $CD11b^+CD11c^+$ cells with sub-saturation amount of $gp96_{A488}$. A representative FACS plot of the cell mixture is shown. (F) An analyses of the two populations of cells from (E), for A488 positivity are presented as histograms. (G) Competitive endocytosis was examined by mixing purified populations of $CD11b^+CD11c^-$ and $CD11b^+CD11c^+$ cells in the presence of sub-saturation amount of $gp96_{A488}$ cells. A representative FACS plot of the cell mixture is shown. (H) An analysis of the two populations of cells from (G), for A488 positivity are presented as histograms. (I) The endocytosis of sub-saturating amounts of $gp96_{A488}$ by $CD11b^+CD11c^+$ cells, in the presence or absence of $CD11b^+$ cells, is shown. Data (A,C,D) are represented as mean +/- SEM. Performed by MNM with help from DF (cell sorting).

vitro and analyzed them by flow cytometry (Figure 3-12). Consistent with the data in Figure 3-3A, the percent of $gp96_{A488}^{+}$ cells was titratable with increasing amounts of $gp96_{A488}$ (Figure 3-12A). LN cells were phenotyped for CD11b and CD11c expression (Figure 3-12B). Regardless of the amount of $gp96_{A488}$ provided, $CD11b^{+}CD11c^{+}$ cells endocytosed the most $gp96_{A488}$ as measured by geometric mean fluorescence intensity (Figure 3-12C); cells expressing the highest levels of CD91 (Figure 3-11). As a population, $CD11c^{-}CD11b^{-}$ cells appeared to acquire very little $gp96_{A488}$ (Figure 3-12C), correlating with their lack of CD91 expression. In addition, incubations of cells with $gp96_{A488}$ for different lengths of time did not change the outcome; significantly more $gp96_{A488}$ was associated with $CD11c^{+}CD11b^{+}$ cells than other cells at all time points measured (Figure 3-12D).

We next investigated the efficiency of $gp96_{A488}$ uptake in competition studies by isolating each cell subset and performing the same experiment with individual or mixed combinations of cells in sub-saturating concentrations of $gp96_{A488}$. LN cells were sorted into $CD11c^{+}CD11b^{-}$ or $CD11c^{+}CD11b^{+}$ populations. These two populations were mixed in comparable numbers (Figure 3-12E) and incubated with $gp96_{A488}$. Cells were analyzed by flow cytometry for $gp96_{A488}$ incorporation (Figure 3-12F). $CD11c^{+}CD11b^{+}$ cells were observed to incorporate significantly more $gp96_{A488}$ than $CD11c^{+}CD11b^{-}$ cells. A similar experiment was performed with isolated $CD11c^{+}CD11b^{+}$ cells mixed with $CD11b^{+}CD11c^{-}$ cells (Figure 3-12G). $CD11c^{+}CD11b^{+}$ cells were again observed to incorporate significantly more $gp96_{A488}$ than $CD11b^{+}CD11c^{-}$ cells (Figure 3-12H). The acquisition of $gp96_{A488}$ by $CD11c^{+}CD11b^{+}$ cells was unaffected by the presence (mixed) or absence (unmixed) of other $CD91^{+}$ ($CD11b^{+}CD11c^{-}$) cells (Figure 3-12I). We thus conclude that $CD11c^{+}CD11b^{+}$ APCs, characterized by robust CD91 expression, appear superior at endocytosis of gp96 compared to other LN cells with lesser or no CD91 expression.

3.3.8 Loss of CD91 on CD11c$^+$ cells does not alter early gp96$^+$ subsets.

Given that CD91 is required for uptake of HSPs, we were interested in determining if CD91 loss would alter the subsets targeted by vaccination. CD11c-specific CD91 KO mice were generated as described in Materials & Methods and are further characterized in Aim 2. CD91 KO mice and Cre$^-$ littermates were given intradermal injections with 10 µg gp96$_{A488}$. Draining LN cells were then harvested 8 hrs later and analyzed by flow cytometry as previously described (Figure 3-4). A trend was observed toward an increased percent of gp96$_{A488}^+$ cells in the LN of CD91 KO mice, but this did not reach significance (Figure 3-13A). Comparing the ratios of CD11b$^+$ cells in the total LN and gp96$^+$ cells, there was no difference between CD91 KO and WT in the total LN but a trend toward a decrease in CD11b$^+$ cells for the gp96$^+$ subset of CD91 KO mice was observed (Figure 3-13B). No differences were observed for CD11c$^+$ subsets (Figure 3-13C), or for other markers tested (not shown). Thus, despite CD91 deficiency on CD11c$^+$ cells, uptake at early time points in the draining LN was unaffected.

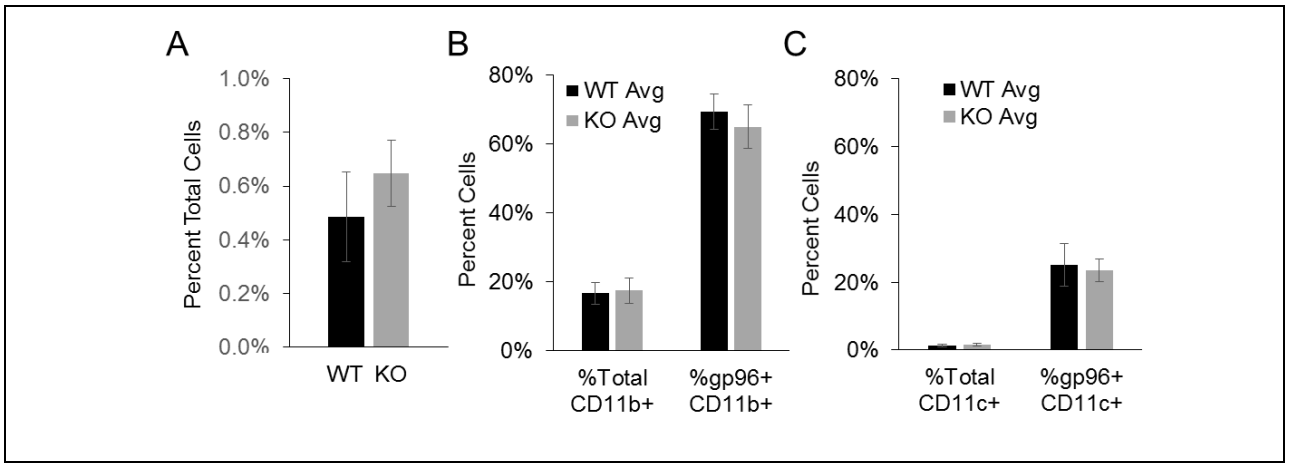

Figure 3-13. Initial uptake of gp96 in dLN is not altered in CD91 KO mice.
(A) CD91 KO mice injected with 10 µg gp96$_{A488}$ show slightly higher levels of A488$^+$ cells in dLN compared to WT mice 8 hours after i.d. injection. (B) LN cells were analyzed for CD11b expression. The percent of CD11b$^+$ cells from the total LN population vs. the gp96$^+$ population is compared for WT and KO. (C) LN cells were analyzed for CD11c expression. The percent of CD11c$^+$ cells from the total LN population vs. the gp96$^+$ population is compared for WT and KO. No significant differences were detected for any markers tested. N = 4 WT, 4 KO. One of two representative experiments shown. Performed by MNM.

3.4 DISCUSSION

We and others have routinely tested the cross-presentation of HSP-chaperoned peptides and provision of co-stimulation by APCs *in vitro* [22,24,68,96-98,100,106,109,114,152]. Recent observations that HSPs can prime diverse T cell and B cell responses [7,24,57,146-148] suggest that immune responses can be skewed by the responding APC, as shown in other settings [143]. This appears to be dependent on the sum total of co-stimulation and efficiency of peptide cross-presentation by APCs.

This chapter characterizes the APCs relevant for HSP-mediated immune responses. Cells that acquired gp96 predominantly express CD11c and/or CD11b in the LN. These populations included $CD11c^{+}CD11b^{+}$ cells which have been described as LN resident APCs [153,154]. $CD11c^{int}$ ($CD11b^{-}$) cells, compatible with migratory APCs were included in the $gp96^{+}CD11c^{+}$ population. However, other markers of migratory APCs such as CD207 and $CD103^{high}$ were a minor percentage of the total $gp96^{+}$ population suggesting migratory APCs play a small role in early gp96 trafficking. Since CD207 analysis was performed at 8 hrs post immunization our observations do not rule out a greater role for migratory cells in gp96 trafficking at later time points. Interestingly, distribution of gp96 in $CD11c^{+}$ cells changed slightly with time, increasing in $CD8^{+}$ cells at a later time point. However more gp96 appeared to associate with $CD11b^{+}$ than $CD11c^{+}$ cells at both time points.

Several mechanisms may explain this observation and are not mutually exclusive; First, $CD11b^{+}$ cells are the densest population of cells along the periphery of the LN. These would be the first cells in contact with draining protein [155] and thus, would have preferential access to gp96 regardless of their rate of incorporation. Once gp96 begins to accumulate, $CD11c^{+}$ cells migrating to the edge of the LN may gain access. Second, gp96 may be transferred between cells

through a variety of mechanisms including intercellular communication [156], CD91 dependent capture of extracellular gp96 [157], or capture of vesicle encapsulated material [158,159]. Thus $CD91^{+}CD11b^{+}$ cells may transfer endocytosed gp96 to other cell types over time. Third, macrophages are known to rapidly degrade internalized material while dendritic cells do this at a slower rate [160]. Extended times beyond 48 hrs may favor accumulation of gp96 in $CD11c^{+}$ cells. Fourth, we have not ruled out an influx of migratory cells from the periphery at later time points although changes in the total cell distribution in lymph nodes at 48 hrs were subtle. Our findings can be compared to previous studies showing an increase in $CD11c^{high}MHCII^{high}CD103^{+}$ APCs following intraperitoneal vaccination with gp96-Ig fusion protein [145]. However, since the vaccination site, draining lymph nodes, and immunizing protein (native gp96 vs gp96-Ig) are different, it was anticipated that only a partial overlap of relevant APCs subsets would be observed.

Regardless of CD11b and/or CD11c expression, the robust expression of MHC class II on cells acquiring gp96 attests to the peptide presenting ability of these cells. We have successfully transferred anti-tumor immunity between mice through the adoptive transfer of $gp96^{+}$ cells. $Gp96^{+}$ cells are predominantly CD11b and CD11c expressing cells. While there may be contaminating cells not expressing these markers in the transferred population, the low numbers of total transferred cells renders these potential contaminating cells marginal. Transferred cells elicited antigen-specific tumor immunity in recipient mice only when viable suggesting that donor cells must be cross-priming competent.

Overall, we have resisted applying the nomenclature ‘macrophage’ and ‘dendritic cell’ to our $CD11b^{+}$ and $CD11c^{+}$ populations and we compare them with caution to previously characterized APC subsets [143,144,153,154,161] for the reason that there are examples of

CD11b and CD11c expression on both macrophages and dendritic cells. Where appropriate, we have drawn parallels to previously characterized cell types using additional markers to clarify the phenotype of cells described in our study.

Both $CD11c^+$ and $CD11b^+$ cells express some level of CD91 which satisfies one requirement for interaction with, and uptake of, HSP [22]. We demonstrate that CD91 expression closely correlates with ability of APCs to endocytose gp96. $CD11c^+CD11b^+$ cells which have been characterized as LN resident APCs [153] express CD91 which is reflected in their superior ability to endocytose gp96. $CD11c^+CD11b^-$ cells, including $CD11c^{int}$ (or migratory APCs) express less CD91 and are expectedly less efficient at endocytosis of gp96 than $CD11c^+CD11b^+$ cells. These results were largely consistent both *in vivo* and *in vitro*; *in vitro*, when gp96 is abundant and access to cells is not restricted, $CD11c^+CD11b^+$ APCs appear to be superior in taking up gp96. *In vivo*, gp96 would be accessible to $CD11c^+CD11b^+$ cells following diffusion of gp96 through the lymphatics, however we have not ruled out transfer of gp96 to these cells from migratory cells. The $CD11c^-CD11b^-$ population, in our *in vitro* and low dose *in vivo* experiments, also performs as expected based on observed CD91 expression levels. However, the observation of increased uptake of gp96 by these cells *in vivo* following administration of high, immunosuppressive doses of gp96 was unexpected. We have not ruled out the potential recruitment of immature cells to the LN following high dose administration. We are also investigating changes in expression of CD91 following inflammatory stimulation that may address this difference; perhaps this subset, after prolonged exposure to high levels of gp96 experiences induced CD91 (Aim 3). Our finding that KO of CD91 on $CD11c^+$ cells had little effect on cells in the LN that take up gp96 may be due to incomplete loss of CD91 on the predominately $CD11b^+$ population, which expresses only low levels to no CD11c. Additional

factors that may contribute to the final cross-presentation of HSPs *in vivo*, such as retention of endocytosed material, remain to be examined.

The identification of physiologically relevant APCs for HSP-mediated immunity has important implications for designing vaccines to cancer and infectious disease. However, these studies also impact our understanding of effects of extracellular HSPs resulting from necrotic lysis of cells in tumor microenvironments or cell lysis associated with pathogen infection and trauma [68]. Thus release of gp96 from cells and its rapid drainage to regional LNs will serve to alert the immune system of cellular compromise. In the setting of immune surveillance, this mechanism may be responsible for the observed anti-tumor immunity associated with tumorigenesis. These studies identify a crucial step in priming HSP-associated immune responses.

4.0 AIM 2: EXAMINATION OF IMMUNE RESPONSES INDUCED BY HEAT SHOCK PROTEINS RELEASED FROM TUMOR CELLS

4.1 PREFACE

Some of the data in this chapter is part of a manuscript that has been favorably reviewed by the journal Cancer Immunology Research and is here included with permission from the primary author, Yu Zhou. I am the second author on this manuscript. Those who performed the experiments detailed in this chapter are indicated by their initials in the figure legends (Michelle Messmer: MNM; Yu Zhou: YZ; Robert Binder: RJB).

4.2 RATIONALE

Adaptive immune responses against tumors are routinely detected in tumor bearing hosts. In cancer patients and in murine experimental tumor systems, recognition of tumor by the host's immune system results in priming of concomitant immunity and immunoediting [162-164]. Conventional mechanisms of priming immune responses to pathogens do not generally apply to tumors because, wherever tested, tumors generally lack sufficient antigen as a native protein for cross-priming [165,166]. In addition, being of self-origin, tumors largely exist in a sterile environment lacking the classical pathogen-associated molecular patterns that give rise to innate

immune activation and provision of co-stimulation necessary for priming T cells. Given the ability of endogenous, purified HSPs to efficiently prime specific immune responses under conditions of limiting antigen [7,166] we tested the role of tumor-derived HSPs *in situ* and their receptor CD91 in initiation of immune responses to tumors.

We have explored the HSP-CD91 axis as a mechanism for host priming of anti-tumor immunity for two reasons; 1) antigens in the form of peptides are chaperoned by HSPs and are efficiently cross-presented by APCs [28,53,65,108,114]. The increase in efficiency of cross-presentation of HSP-chaperoned peptides versus peptides alone, is several thousand fold and is made possible through the cell surface receptor CD91 on antigen presenting cells [22,98,99,109,111,166]. 2) We have recently shown that HSPs signal through CD91 to activate APCs to provide co-stimulation through secretion of pro-inflammatory cytokines including IL-1β, TNF-α, IL-6 and increased expression of CD40, MHC class II and CD86 [24,68,84,167].

The immunological properties of HSPs make them prime candidates for the initiation of immune responses to tumors. However, HSPs are necessary for cell survival so testing their requirement for priming tumor-specific immune responses *in vivo* through simultaneous or sequential deletion is not possible. Instead, we tested their requirement by targeting and selectively blocking the HSP receptor CD91. This approach is possible because, while structurally unrelated, four of the immunogenic HSPs (gp96, hsp90, hsp70 and calreticulin) utilize the same receptor CD91 to elicit immune responses [22,24,98,99,101]. We show that, unlike wild type mice, mice lacking CD91 expression on $CD11c^+$ cells have reduced anti-tumor immune responses. These responses can also be abrogated by the receptor associated protein (RAP), an endogenous inhibitor of the HSP-CD91 pathway, which prevents exposed HSPs from binding to CD91. Expression of RAP by tumor cells reduces the localization of fluorescent

labeled gp96 in tumor-draining LNs. Our findings demonstrate that early in tumor development, the HSP-CD91 pathway is critical for establishment of anti-tumor immunity.

4.3 RESULTS

4.3.1 Characterization of APC from CD11c-specific CD91 KO mice

Conventional CD91 knock-out mice are embryonically lethal [168], thus we created mice lacking CD91 expression in $CD11c^+$ cells. To test the requirement for CD91 in gp96-mediated

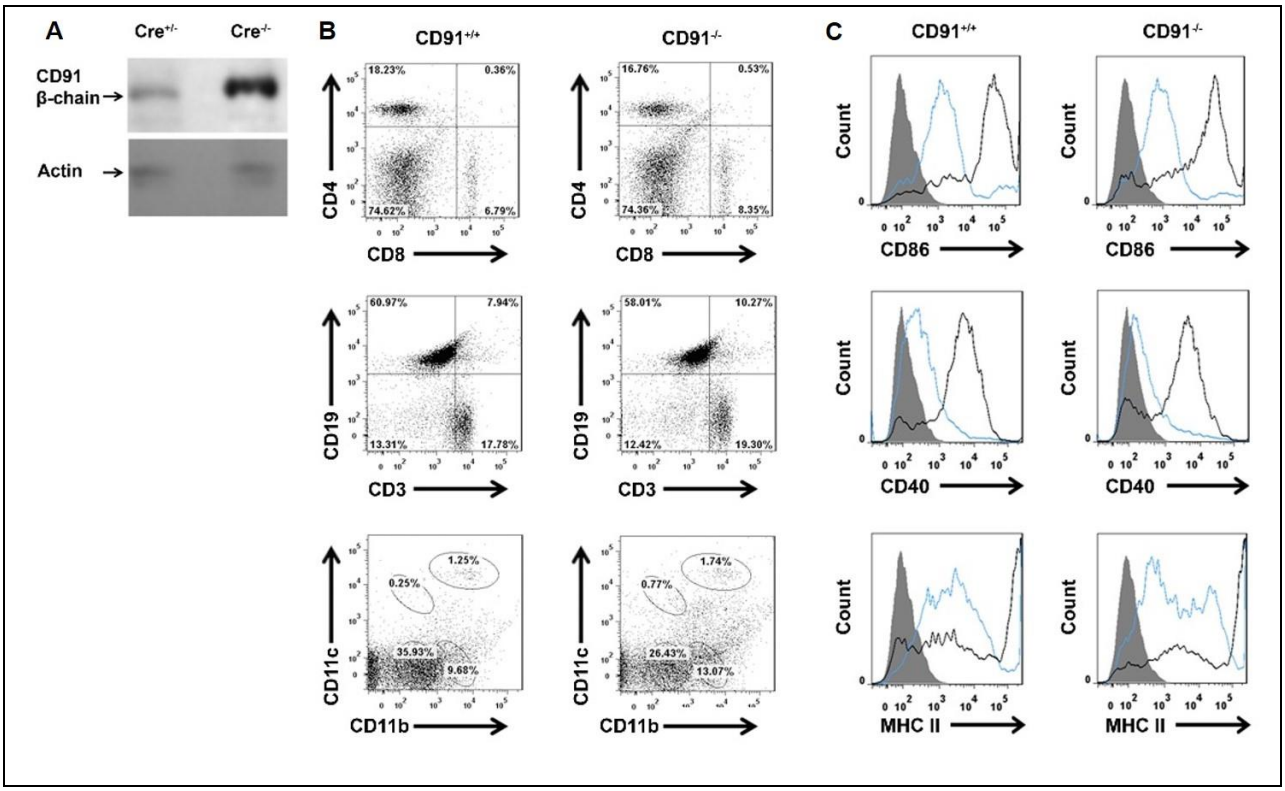

Figure 4-1. Phenotyping of CD91 KO mice.
Data from Zhou, et al. (A) Cre^+ and Cre^- BMDC purified to 96% $CD11c^+$ were analyzed by western blot for their expression of CD91. (B) Immune cell populations from Cre^+ and Cre^- lymph nodes were analyzed by flow cytometry. (C) BMDC generated from Cre^+ or Cre^- mice were stimulated with LPS for 24 hours (black line) and activation marker expression was analyzed by flow cytometry, compared to unstimulated (blue line). Performed by RJB.

anti-tumor immunity, CD11cCre mice were bred to CD91flox mice to generate mice lacking CD91 on their $CD11c^+$ cells (CD91 KO mice). For more information on the CD91 KO mice, see "Material & Methods 7.1.1 Generation of CD11c specific CD91 knockout mice," pg. 77. CD91 KO BMDCs were generated as described and purified by magnetic activated cell sorting on CD11c expression (purity = 96%). Lack of CD91 expression was confirmed by SDS-PAGE and immunoblotting for CD91 protein expression (Figure 4-1A). Analysis by flow cytometry showed CD91 KO mice had equal percentages of CD4 and CD8 T cells, B cells, macrophages and DCs compared to Cre^- littermates (Figure 4-1B). Maturation of CD91 KO BMDCs was tested by pulsing with LPS for 24 hours and measuring expression of CD86, CD40 and MHC class II by flow cytometry (Figure 4-1C). All were up-regulated in response to LPS, comparable to increases seen for Cre^- littermates. CD91 KO BMDCs were also able to respond to LPS by secreting IL-1β, however, they failed to secrete IL-1β in response to gp96 (not shown), consistent with our previous observations [24,68].

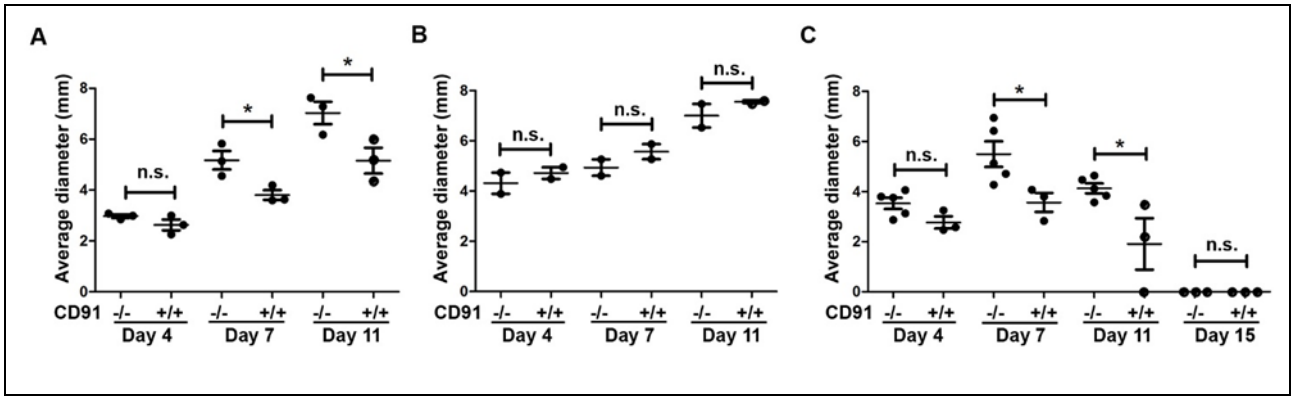

Figure 4-2. CD91 is required for priming anti-tumor immune responses.
Data from Zhou, et al. (A) CD91 KO mice or Cre- littermates were challenged intradermally with D122 tumor cells, average tumor diameter from tumor measured on two axes shown. (B) $CD8^+$ T cells were depleted from CD91 KO mice or CD91 Cre- littermates 24 hours prior to implantation of intradermal D122. CD8 depletion was continuous for >5 days. Tumor growth was monitored as in (A). (C) SVB6 tumor was implanted intradermally into CD91 KO mice or CD91 Cre- littermates. Tumor growth was monitored as in (A). n.s., not significant; * $P< 0.05$. Experiments were performed multiple times with 3-5 mice per group. Performed by YZ.

4.3.2 Loss of CD91 expression on CD11c$^+$ cells abrogates anti-tumor immunity

To test the requirement for CD91 expression on CD11c cells in initiating anti-tumor immunity, we tested tumor growth rates in the CD11c-specific CD91 KO mice. After inoculating mice with $8x10^5$ cells of the moderately immunogenic Lewis Lung Carcinoma, D122, tumor growth rate was significantly faster in CD91 KO mice versus Cre$^-$ littermate controls early after initial challenge and through day 11 (Figure 4-2A). After day 11, tumor growth rates were comparable. To determine the role of adaptive immune responses, we depleted CD8$^+$ T cells from the CD91 KO mice or Cre$^-$ littermate controls. In the absence of CD8$^+$ cells, D122 tumors grew with identical kinetics in both groups (Figure 4-2B). This tumor growth was identical to the growth observed in CD91 KO mice in Figure 4-2A. These results suggest that CD8$^+$ T cell priming was impaired in CD91 KO mice. We tested the generality of these observations by monitoring tumor growth for the highly immunogenic, regressor SV40-transformed tumor SVB6. While SVB6 grew and was rejected in both CD91 KO and Cre$^-$ littermate controls, the tumors grew significantly larger and were rejected more slowly in CD91 KO mice (Figure 4-2C).

4.3.3 Expression of gp96$_{EGFP}$ construct in tumor cells.

We have previously shown that HSPs are a necessary and sufficient source of antigen to prime CD8 T cells [166], thus we investigated the release of HSPs from growing tumors as the source of antigen for priming that is blocked by loss of CD91. To track the release of HSPs from growing tumors *in vivo*, we constructed a gp96$_{EGFP}$ fusion protein as described in Materials & Methods. This construct was transfected into the CMS5 tumor cell line and, after growth in selective media, was found to be stably expressed. A 25 mL cell pellet was collected

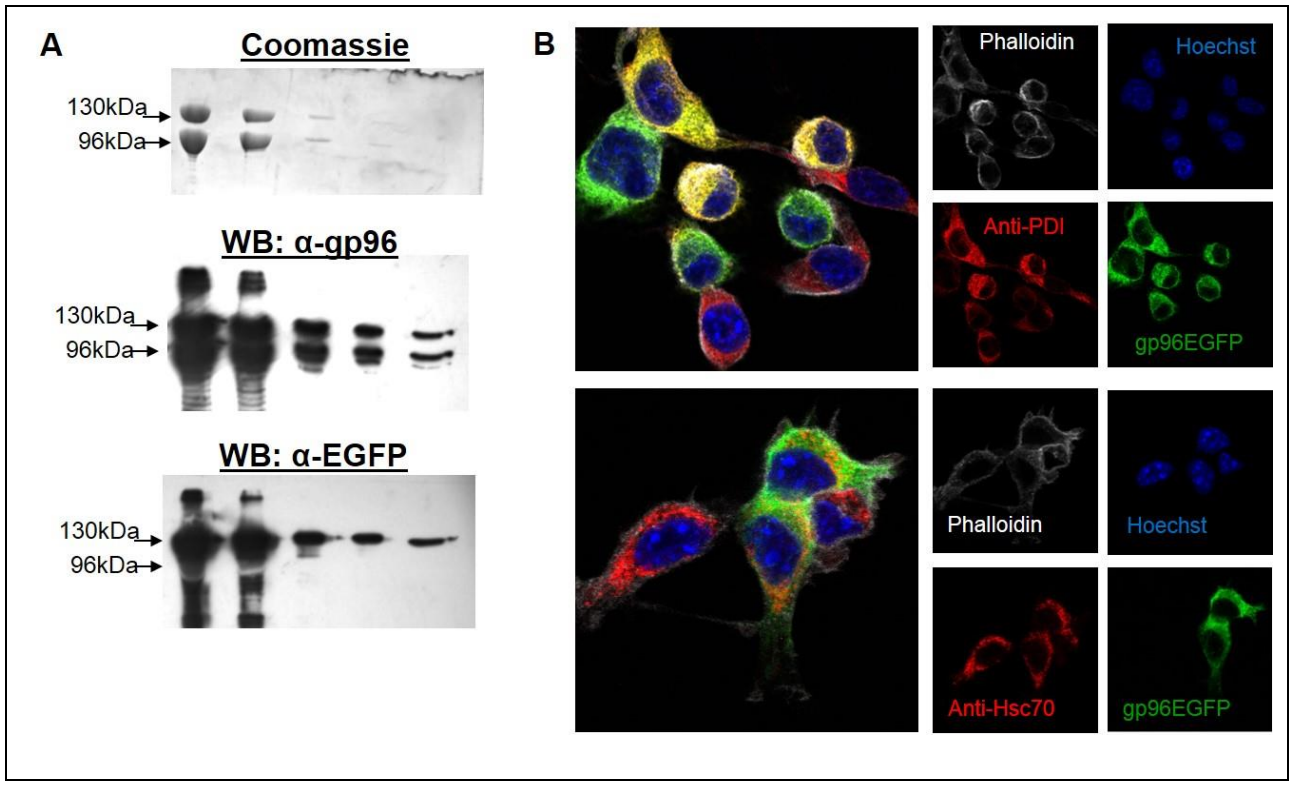

Figure 4-3. gp96$_{EGFP}$ co-purifies and co-localizes with endogenous gp96.
Gp96 was purified from frozen gp96$_{EGFP}$-expressing CMS5 tumor cell pellet after dounce homogenization. Purification was performed according to previously published methods (see Materials & Methods). (A) Individual fractions from the final chromatography separation (DEAE) were analyzed by SDS-PAGE. Equivalent protein amounts of endogenous gp96 (96 kDa) and gp96$_{EGFP}$ (130 kDa) were measured in each fraction by Coomassie staining (top) and Western blotting with anti-gp96 antibody (middle). Only one major band was observed at 130 kDa when probed with anti-EGFP antibody (bottom). (B) CMS5 cells expressing gp96$_{EGFP}$ (green) were cultured on glass coverslips and then stained with either anti-PDI antibody (top, red) or anti-Hsc70 antibody (bottom, red), as well as phalloidin (white) and Hoechst (blue). Performed by MNM.

from CMS5 gp96$_{EGFP}$ cultures and gp96 was purified as previously described [28]. SDS-PAGE and Western Blotting analysis of the final purification fractions showed that gp96$_{EGFP}$ retained the same biochemical properties as endogenous gp96 and is expressed at comparable levels (Figure 4-3A). By growing these cells on coverslips, we were able to analyze the intracellular localization of gp96$_{EGFP}$. Our construct included the ER retention sequence,

KDEL, on its C-terminus allowing for recognition by ER sorting machinery [169]. Indeed, gp96$_{EGFP}$ was found to co-localize with Protein Disulfide Isomerase (PDI), a marker for the endoplasmic reticulum, but did not co-localize with Hsc70, normally expressed in the cytosol

(Figure 4-3B). This data shows that $gp96_{EGFP}$ shares biochemical features and cellular localization with endogenous gp96.

4.3.4 CMS5 retain detectable $gp96_{EGFP}$ expression after tumor growth *in vivo*.

Expression of exogenous antigens such as EGFP may induce immune responses, increasing selective pressure on tumors *in vivo* to lose expression of this antigen. We were interested in

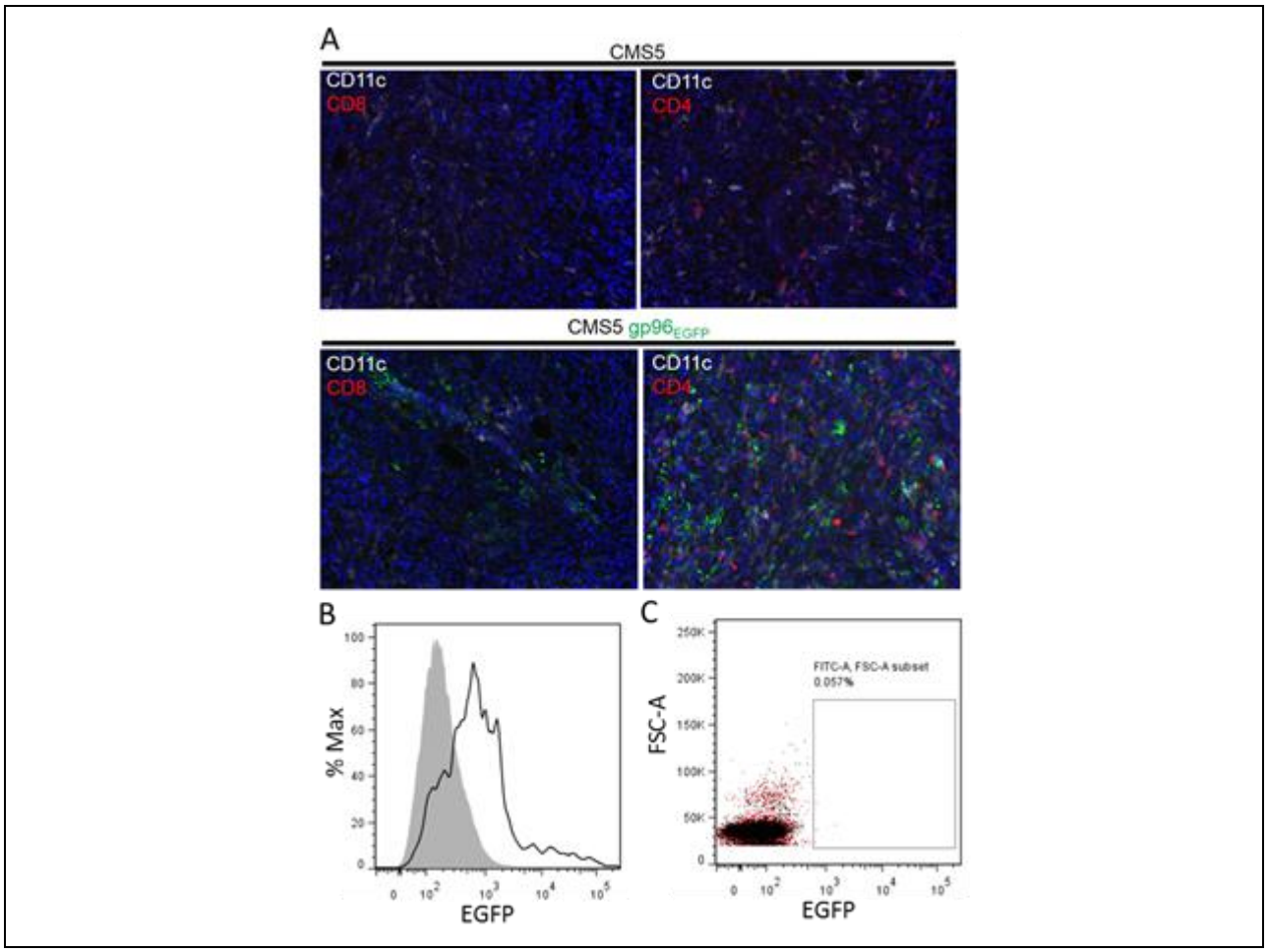

Figure 4-4. $gp96_{EGFP}$ expression by CMS5 tumors *in vivo*.
(A) Mice were intradermally challenged with $5x10^6$ wild type CMS5 cells (top) or CMS5 cells expressing $gp96_{EGFP}$ in the dorsum and followed 8 days. Tumors were harvested, sectioned in two and processed for microscopy and flow cytometry. Samples for microscopy were fixed, and prepared in sucrose as described in Methods (pg. 84). Sections were stained for CD11c (white), Hoechst (blue), and CD4 or CD8 (red). Expression of $gp96_{EGFP}$ is shown as green. (B) Tumor cells were dissociated into single cell suspensions and analyzed for EGFP by flow cytometry; untransfected CMS5 (filled histogram) vs. $gp96_{EGFP}$ CMS5 (black line). (C) Draining LN were analyzed by flow cytometry for $EGFP^+$ cells; untransfected CMS5 (red) vs. $gp96_{EGFP}$ CMS5 (black). Performed by MNM.

determining the long-term expression of $gp96_{EGFP}$ by CMS5 tumor cells *in vivo*. BALB/c mice were intradermally challenged in the dorsum with $5x10^6$ untransfected CMS5 cells or CMS5 cells expressing $gp96_{EGFP}$. At day 8, tumors and draining LNs (axillary and inguinal) were harvested and analyzed by microscopy and flow cytometry for presence of EGFP. Both untransfected CMS5 and $gp96_{EGFP}$ expressing CMS5 tumors showed infiltration by $CD4^+$ cells but lack of infiltration by $CD8^+$ cells (Figure 4-4A). A small number of $CD11c^+$ cells were also detectable in both tumors. As seen by microscopy, CMS5 retained expression of $gp96_{EGFP}$ at 8 days post implantation. This was also detectable by flow cytometry of single cell suspensions of the tumor isolates (Figure 4-4B). Comparing single cell suspensions from draining LNs from the tumor bearing mice, no difference in $gp96_{EGFP}$ was detectable 8 days post tumor implantation (Figure 4-4C). This is likely due to the number of LNs draining the dorsal region and the limited amount of protein expected to be spontaneously released.

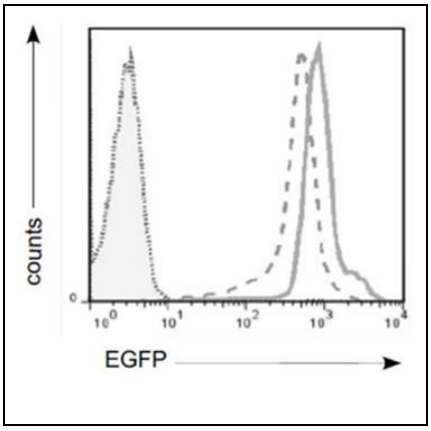

Figure 4-5. Expression of EGFP prior to tumor challenge.
Data from Zhou et al. CMS5 cells were harvested, washed in PBS, and analyzed by flow cytometry for EGFP expression prior to tumor challenge. Representative histograms for one experiment showing CMS5 $gp96_{EGFP}$ co-expressing RAP (solid line) or β-galactosidase (irrelevant protein, dashed line). Performed by YZ.

In order to reduce the number of LNs draining the tumor environment, we switched to footpad injections and harvested the popliteal LNs for analysis. We also gated on CD45 expression in the draining LN to reduce the possibility of tumor cells that may either migrate or drain to LNs after injection. Due to minor variations in auto-fluorescence observed in each mouse and in the fluorescence intensities for each $gp96_{EGFP}$ expressing cell line (Figure 4-5), the signal was normalized to these two parameters by accounting for background signal in

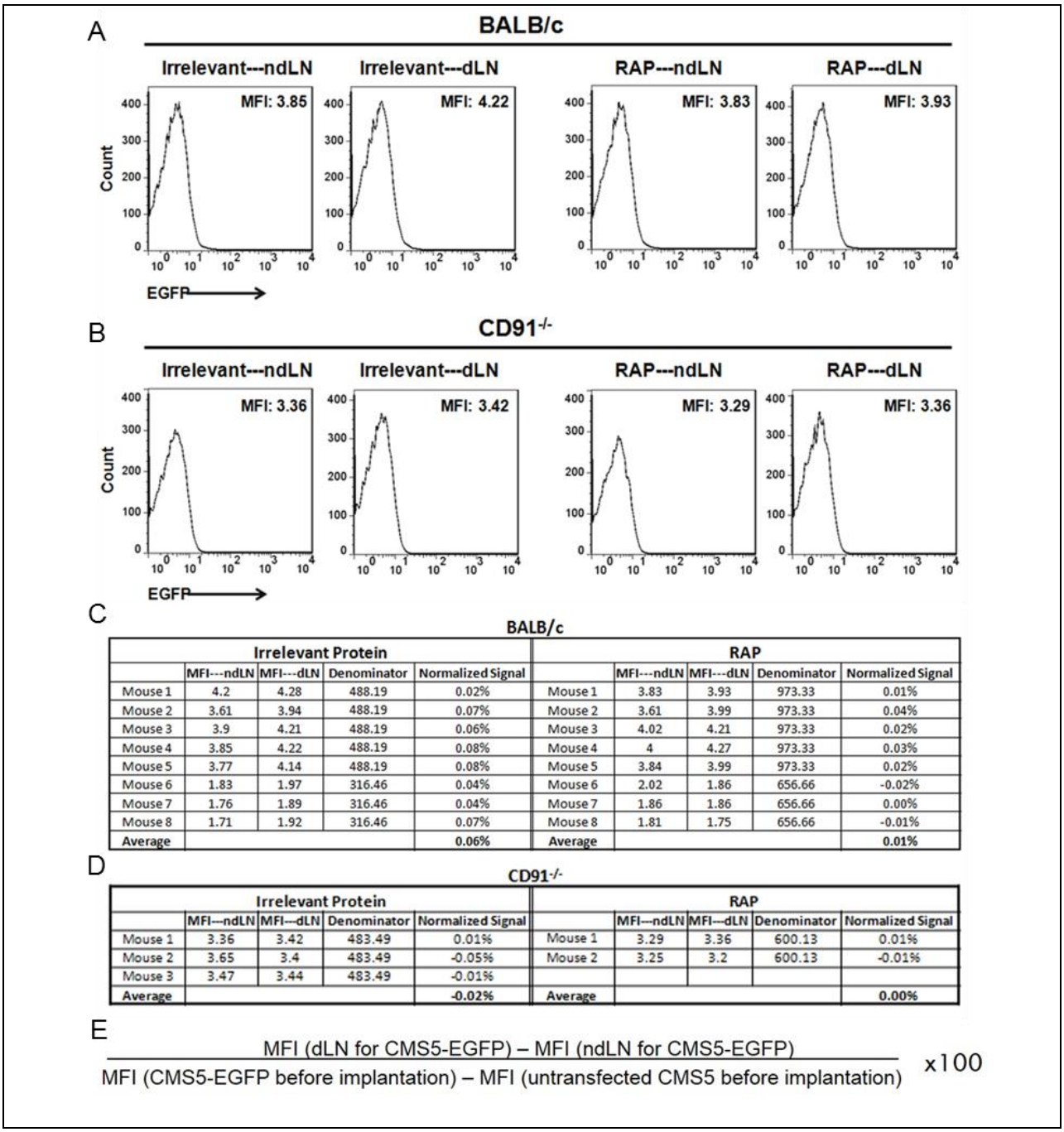

C

BALB/c

	Irrelevant Protein					RAP			
	MFI---ndLN	MFI---dLN	Denominator	Normalized Signal		MFI---ndLN	MFI---dLN	Denominator	Normalized Signal
Mouse 1	4.2	4.28	488.19	0.02%	Mouse 1	3.83	3.93	973.33	0.01%
Mouse 2	3.61	3.94	488.19	0.07%	Mouse 2	3.61	3.99	973.33	0.04%
Mouse 3	3.9	4.21	488.19	0.06%	Mouse 3	4.02	4.21	973.33	0.02%
Mouse 4	3.85	4.22	488.19	0.08%	Mouse 4	4	4.27	973.33	0.03%
Mouse 5	3.77	4.14	488.19	0.08%	Mouse 5	3.84	3.99	973.33	0.02%
Mouse 6	1.83	1.97	316.46	0.04%	Mouse 6	2.02	1.86	656.66	-0.02%
Mouse 7	1.76	1.89	316.46	0.04%	Mouse 7	1.86	1.86	656.66	0.00%
Mouse 8	1.71	1.92	316.46	0.07%	Mouse 8	1.81	1.75	656.66	-0.01%
Average				0.06%	Average				0.01%

D

CD91-/-

	Irrelevant Protein					RAP			
	MFI---ndLN	MFI---dLN	Denominator	Normalized Signal		MFI---ndLN	MFI---dLN	Denominator	Normalized Signal
Mouse 1	3.36	3.42	483.49	0.01%	Mouse 1	3.29	3.36	600.13	0.01%
Mouse 2	3.65	3.4	483.49	-0.05%	Mouse 2	3.25	3.2	600.13	-0.01%
Mouse 3	3.47	3.44	483.49	-0.01%					
Average				-0.02%	Average				0.00%

E

$$\frac{\text{MFI (dLN for CMS5-EGFP)} - \text{MFI (ndLN for CMS5-EGFP)}}{\text{MFI (CMS5-EGFP before implantation)} - \text{MFI (untransfected CMS5 before implantation)}} \times 100$$

Figure 4-6. Measurement of EGFP fluorescence intensity in draining LN.
Data from Zhou et al. CMS5 cells expressing $gp96_{EGFP}$ and either RAP or β-galactosidase as an 'irrelevant' protein were implanted into the footpad of BALB/c mice for two days before draining lymph nodes were isolated, stained for CD45, and analyzed by flow cytometry for EGFP. (A,B) Representative histograms showing the $EGFP^+CD45^+$ cells in the non-draining LN (ndLN) or draining LN (dLN) of tumor-bearing BALB/c mice (A) or CD91 KO mice (B). (C,D) MFI of all mice from one experiment are shown. (E) Formula for calculating the normalized EGFP signal taking into account autofluorescence of LN cells and the starting fluorescence of each cell line. Performed by YZ.

contralateral, non-draining popliteal lymph nodes and fluorescence of $gp96_{EGFP}$ expressing cells on the day of the experiment, respectively (Figure 4-6).

4.3.5 CD91 is required for uptake of immunogenic HSPs

To determine whether CD91 was essential for tumor-derived HSPs draining to the LN, $gp96_{EGFP}$ expressing CMS5 cells were doubly transfected with RAP, an endogenous inhibitor of CD91-HSP interaction, or control, 'irrelevant' protein β-galactosidase. BALB/c mice were challenged in the footpad and tumors were grown 2 days before harvesting draining and non-draining popliteal LNs. EGFP fluorescence was measured by flow cytometry as described (Figure 4-6). Significantly less EGFP was detected in LNs draining tumors co-expressing RAP compared to control protein ($p = 0.0002$, Figure 4-7A).

Additionally, we tested the draining of $gp96_{EGFP}$ to LNs in CD91 KO mice using the same system. CMS5 cells expressing $gp96_{EGFP}$ with or without RAP were implanted in footpads

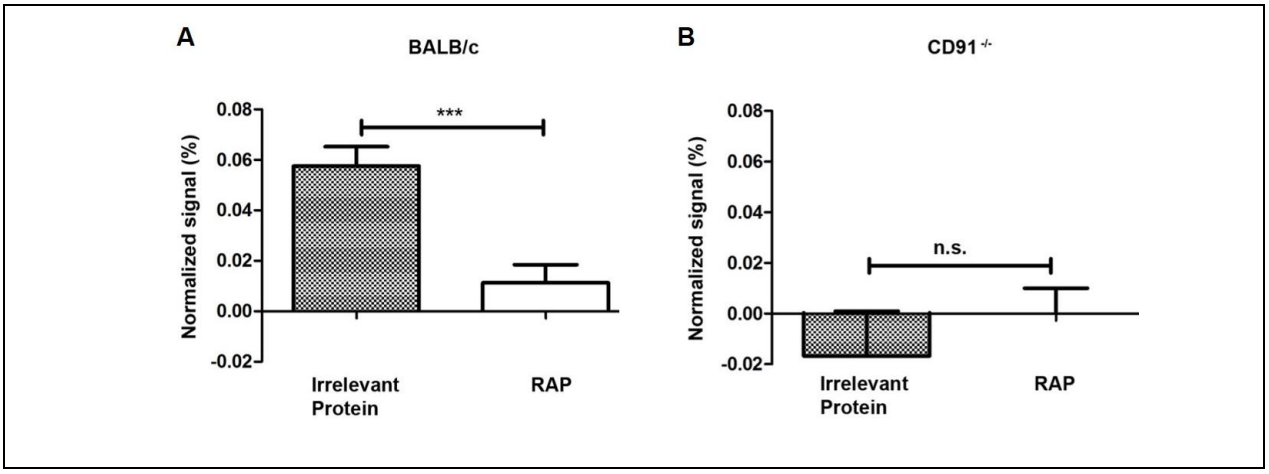

Figure 4-7. Draining of $gp96_{EGFP}$ blocked by RAP.
BALB/c mice (A) or CD91 KO mice (B) were implanted with $5x10^6$ CMS5 cells expressing $gp96_{EGFP}$ with or without RAP in the footpad. Draining and contralateral, non-draining lymph nodes were harvested two days later. LN cells were stained CD45 and analyzed by flow cytometry for EGFP. EGFP signal was normalized against starting fluorescence for each cell line and the background fluorescence of non-draining lymph nodes. ***$p < 0.001$. Experiments were performed 2 times with 8 mice per group in (A), or 3 mice per group in (B). Error bars indicated SEM. Performed by YZ.

of CD91 KO mice. Again, draining LNs were harvested after 2 days and analyzed as in Figure 4-6. We did not detect $gp96_{EGFP}$ signal in CD91 KO LNs whether or not tumors expressed RAP (Figure 4-7B). The importance of CD91 for HSP transfer and trafficking is thus highlighted in cases of deficient expression in APCs and antagonism via RAP. **HSP-mediated vaccine response is abrogated in CD11c-specific CD91 KO mice.**

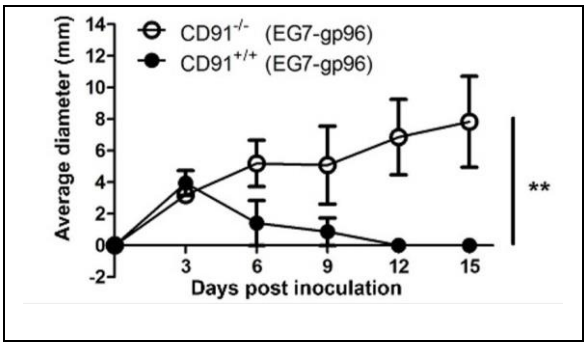

Figure 4-8. CD11cCD91 KO mice are not protected by gp96 vaccine.
$CD91^{-/-}$ or $CD91^{+/+}$ mice were immunized with 1 µg E.G7 tumor-derived gp96 twice, one week apart, followed by E.G7 tumor challenge one week later. Tumor growth was monitored. 6-10 mice per group. n.s., not significant; * P<0.05; **P<0.01. Performed by RJB.

We tested the response of CD91 KO mice to gp96 immunization in a prototypical tumor rejection assay. CD91 KO mice and littermate controls were given intradermal immunizations with 1µg gp96 purified from the OVA-expressing EL.4 thymoma, E.G7, twice, one week apart. Cre^- mice were protected from tumor challenge, while CD91 KO mice were not protected from tumor growth (Figure 4-8). Thus, CD91 KO mice appear to be incapable of priming immune responses capable of rejecting tumor cells following vaccination with extracellular HSPs.

4.4 DISCUSSION

In this chapter, we report that mice deficient in the receptor CD91 on $CD11c^+$ cells display reduced immune protection against growing tumors, dependent on $CD8^+$ T cells. In addition, mice were similarly susceptible to tumors expressing inhibitors of CD91 ligand binding. These reductions in anti-tumor immunity were due to the inability of APCs to cross-present HSP-

chaperoned antigens. To our knowledge, these findings are the first reports of a role for CD91 in antigen cross-priming *in vivo.*

When antigen is abundant, acquisition of antigens by APCs for cross-presentation and cross-priming can occur through several mechanisms as in most infectious disease settings [170]. These mechanisms are less reliant on the source of antigen or the type of APC [171]. The majority of tumor rejection antigens, however, derive from novel mutations of self-proteins which are expected to be limited in quantity at the time initial anti-tumor responses are primed [172]. As previously demonstrated for transplantable tumors, immunity to additional challenge by syngeneic tumors is established within the first week of tumor growth, when intradermal tumors are barely visible [162]. A careful quantification and titration of the amount of antigen in tumors revealed there is ~5 orders of magnitude less available for cross-presentation as required if the antigen is transferred as a whole protein [166]. Clearly, a special mechanism is necessary for efficient transfer of antigens from tumor cells to cross-presenting cells, namely receptor-targeting by chaperoning HSPs. Here we confirm that interaction of HSP-peptide complexes with CD91 provides this mechanism.

Loss of CD91 on $CD11c^+$ cells results in increased tumor burdens. However, not all immune responses were inhibited as CD91 KO mice were still capable of rejecting SVB6. At high antigenic loads, the requirement for CD91:HSP interaction may not hold (data not shown). There may also be a role for other APC that express CD91. Given the recent observation that $CD169^+$ macrophages are bonafide professional APC in the setting of apoptotic-associated antigen in LNs [159], we expect a more robust phenotype when CD91 expression is eliminated in both macrophages and dendritic cells. Studies are currently underway to create mice with loss of CD91 in both $CD11c^+$ and $CD11b^+$ cells.

It was not surprising that only low amounts of $gp96_{EGFP}$ drain to LNs of tumor bearing mice given the low rate of spontaneous cell death at only 2 days after tumor inoculation. All detectable signal was lost with co-expression of RAP or knock-out of CD91 in $CD11c^+$ cells. This decrease in EGFP signal suggests CD91 blockade inhibits transport of gp96 by a migratory subset in the tumor setting. This subset may be a minority of the cells identified in Aim 1, such as the $CD8^+$ cells observed to be increased 48 hrs after vaccination.

The effect of CD11c-specific CD91 loss on the ability to prime immune responses downstream of gp96 vaccine was striking given that no difference in the targeted subsets was observed in the draining LNs of CD91 KO mice in the vaccine setting in Aim 1 (Figure 3-13). We confirmed there is no intrinsic defect in presentation of peptides by CD91 KO mice by immunizing with OVA-8mer peptide, SIINFEKL, in Freund's adjuvant. This peptide requires no further processing for presentation; we found that CD91 KO mice and Cre^- controls generated comparable anti-SIINFEKL T cell responses (not shown). We are testing additional immunogenic models to verify there are no other disruptions in processing peptides or priming immune responses independent of the HSP:CD91 interaction.

These studies show the important role for HSP:CD91 interaction in priming anti-tumor immune responses and suggest potential mechanisms of tumor evasion by enhancing expression of CD91 inhibitors. In addition to the CD11c-specific CD91 expressing cells analyzed here, more specific cell types involved in this immunity are under current investigation.

5.0 AIM 3: ELUCIDATION OF THE PATHWAYS FOR ANTIGEN-PROCESSING FOLLOWING HSP:CD91 INTERACTION

5.1 PREFACE

Some data from this chapter has been published in the Journal of Immunology [140], and is expanded on here. Those who performed the experiments detailed in this chapter are indicated by their initials in the figure legends (Michelle Messmer: MNM; Laura Kropp: LEK; Joshua Pasmowitz: JP).

5.2 RATIONALE

Antigen processing and presentation is classically depicted as occurring along two distinct, biologically separate pathways: 1) processing of endogenous peptides by proteasome followed by transport via TAP into the ER and loading onto MHC class I complexes, or 2) processing of exogenous peptides following endocytosis and fusion of the endosome with the lysosome, acidification, and loading onto MHC class II. As we now know, exceptions to these classical processing pathways exist, exemplified by the observation of "cross presentation" of exogenous derived peptides on MHC class I molecules. The modern complexities of the MHC class I and class II processing pathways have been reviewed elsewhere [173].

We are interested in understanding the pathway taken by HSP-chaperoned peptides since, once taken into the cell, HSPs can convey their conjugated peptides to either MHC class I [99,109,166] or class II [108,174,175]. The steps between endocytosis of HSP-peptide complexes and presentation of the peptide on the cell surface are still unclear. Internalization of gp96 occurs via clathrin coated vesicles [94], dependent on interaction with CD91 [98]. After endocytosis, antigens may follow a number of different paths for presentation onto MHC class I or class II [176-181]. A number of labs have shown localization of endocytosed HSPs in early endosomal compartments that may contain MHC class I for direct loading of HSP-chaperoned peptides [88,94,118,119,182-184], however, this does not answer how even extended length peptides may be efficiently processed for presentation. Additionally, differential requirements for the proteasome and TAP have been observed [107,119], as well as localization of HSPs to other cellular compartments [88,184,185], including the cytosol [185].

The maturation state of APC can also have a major impact on the processing and presentation of antigens. When APC undergo maturation, they switch their primary directive from sampling the environment (constitutive endocytosis/phagocytosis) to professional presentation of antigens [186]. We were interested in understanding the effects of APC maturation on the expression of the HSP receptor CD91 and how this may alter the ability of APC to internalize HSPs and efficiently process and present HSP-chaperoned peptides.

We show that bone marrow-derived dendritic cells (BMDC), which share a common phenotype with the cells observed in Aim 1 as targets for gp96 *in vivo*, are capable of processing HSP-chaperoned peptides or presentation by both MHC class I and MHC class II for stimulation of two distinct restricted T cell hybridomas. We observed internalization of gp96-peptide complexes, followed by dissociation of the two molecules concurrent with gp96 crossing into the

cytosol immediately prior to peptide translocation. Finally, we found that stimulation of BMDC by LPS up-regulates expression of CD91 in a time dependent manner.

5.3 RESULTS

5.3.1 Peptides chaperoned by HSPs are cross-presented by $CD11b^+CD11c^+$ cells

Cross-presentation of HSP-chaperoned peptides after uptake by CD91 is necessary for priming effective immune responses [98,99]. To study the cross-presentation of peptides chaperoned by HSPs in detail, we adopted the use of bone marrow derived dendritic cells (BMDCs). These cells express a similar phenotype to the cells we identified as targets of gp96 following *in vivo* vaccination in Aim 1, including dual expression of CD11c and CD11b [161] as well as the HSP receptor CD91 [22]. Adopting this culture system gave us significantly more $CD11b^+CD11c^+$ cells than

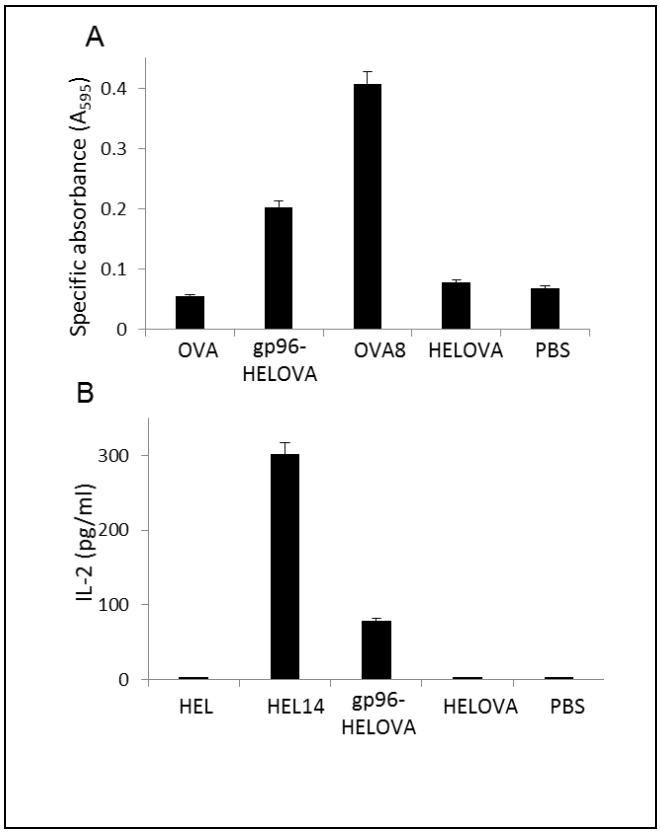

Figure 5-1. Re-presentation of gp96 chaperoned peptides by BMDC.
(A) Cross presentation of HSP-chaperoned peptides by MHC I of $CD11b^+CD11c^+$ cells was tested by incubation of cells with gp96-HELOVA. Response by B3Z was measured as specific absorbance at 595nm. Controls include cells with HELOVA alone, OVA, ova 8mer peptide and PBS. (B) Cross presentation of HSP-chaperoned peptides by MHC II of $CD11b^+CD11c^+$ cells was tested by incubation of cells with gp96-HELOVA. Response by LC21 was measured by ELISA for IL-2. Controls include incubations of cells with HELOVA alone, HEL, HEL14 mer peptide and PBS. Experiments are representative of 3 independent experiments. Error bars are standard deviation of duplicates. Performed by LEK.

could be obtained from lymph nodes and reduces concerns about different maturation/activation states at baseline.

We first confirmed that BMDCs were functionally competent in cross-presenting gp96-chaperoned peptides on either MHC class I or MHC class II molecules. Gp96 was complexed to a 22-mer peptide (HELOVA) consisting of HEL 14-mer peptide presented by H-2IA^d in tandem with the OVA8-mer peptide presented by H-2K^b, as described in detail in the Material & Methods section. BMDCs were generated from H-2^b (C57BL/6) x H-2^d (BALB/c) F1 mice and incubated in the presence of 10 μg of gp96-peptide complexes and T cell hybridomas specific for either OVA8/K^b (B3Z) or HEL14/IA^d (LC21) for 20 hrs. HELOVA peptide chaperoned by gp96 was processed into OVA and HEL epitopes which were presented by F1 BMDCs on their respective MHC molecules and subsequently detected by B3Z (Figure 5-1A) or LC21 (Figure 5-1B) respectively. As a control, HELOVA peptide alone at a concentration similar to what was introduced to the assay in a complex with gp96, was poorly cross-presented. Similarly, as we have previously shown, whole protein (OVA or HEL) was poorly cross-presented by BMDC.

Internalization of gp96 to endosomal compartments of APCs has previously been visualized [94,97], however to our knowledge no studies have shown trafficking of both HSP *and* chaperoned peptides within cells. To follow the association between HSP and peptide after endocytosis, we complexed gp96$_{A488}$ to a biotinylated 20mer peptide (b-pep20). BMDCs were incubated with 10 μg of gp96$_{A488}$-b-pep20 for the indicated times points and temperatures (Figure 5-2A-D). Cells were fixed, permeabilized and stained with streptavidin-Cy3 for detection of peptide and phalloidin for detection of actin filaments. Co-localization was quantified using IMARIS software to obtain Pearson's coefficient of co-localized volume (Figure 5-2E-G). After 5 minutes of incubation at 37°C most of the peptide localized to gp96, but by 15 minutes the two

molecules appeared dissociated (Figure 5-2A,B,E). At 15 minutes, peptide co-localized with actin suggesting translocation into the cytosol (Figure 5-2B,F). Surprisingly, gp96 was also found to co-localize with actin after only a 5 min incubation (Figure 5-2G). This suggests that, first, gp96 translocates to the cytosol independently of peptide and, second, gp96 dissociates from the peptide in the endosome prior to translocation.

BMDCs incubated with $gp96_{A488}$-b-pep20 were also stained with LAMP-1, a lysosomal marker (Figure 5-2H). Consistent with previous reports [152], gp96 did not localize with

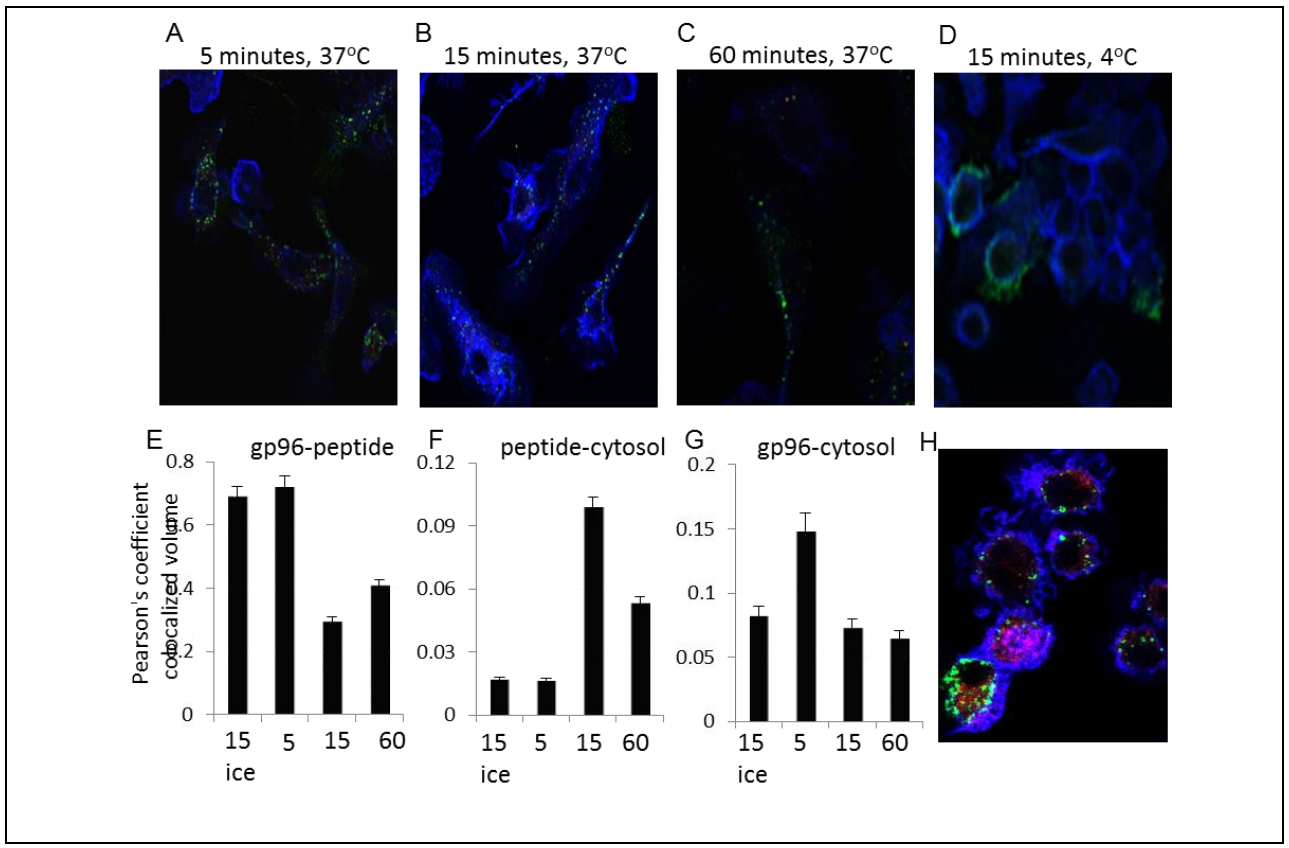

Figure 5-2. Transport of HSP-chaperoned peptides within $CD11b^+CD11c^+$ BMDCs.
(A-D) $gp96_{A488}$-b-pep20 was incubated with $CD11b^+CD11c^+$ cells on cover slips at 37°C (C-E) or 4°C (F), for the indicated time points and then stained with strepavidin-Cy3 for the peptide (red) and phalloidin (blue). $Gp96_{A488}$ appears as a green signal. (E-G) Images were analyzed using IMARIS and co-localization of $gp96_{A488}$ with peptide (E), peptide with the phalloidin (F), or gp96 with the phalloidin (G) was quantified. Experiments are representative images from numerous independent experiments. Error bars are standard deviation of multiple ROIs. Data are represented as mean +/- SEM. (H) $gp96_{A488}$ was incubated with $CD11b^+CD11c^+$ cells on cover slips for 15 mins after which cells were fixed and stained for LAMP-1 (blue) and phalloidin (red). Co-localization of $gp96_{A488}$ with LAMP-1 was quantified by IMARIS. Performed by MNM and JP.

lysosomes (Pearson's coefficient of colocalized volume =0.0065), suggesting that the rapid translocation of gp96 into the cytosol (Figure 5-2G) prevents it from being targeted to and degraded in lysosomes.

5.3.2 Activated APC up-regulate expression of CD91

We were interested in determining whether activation of BMDC alters the expression of the HSP receptor CD91, thereby altering the potential for HSP:CD91 interaction and internalization. First, we confirmed the expression of CD91 on BMDC generated from either WT (Figure 5-3A) or CD91 KO mice (Figure 5-3D). Day 7 BMDC from both mice show mixed $CD11c^+$ and $CD11c^-$ expression. WT BMDC have detectable CD91 expression on all cells, though at variable levels of intensity. As described in the Material & Methods section, CD91 KO mice are specific for CD91 depletion only on $CD11c^+$ cells. As expected, $CD11c^-$ cells from these mice retain CD91 expression (yellow arrow) while $CD11c^+$ cells were largely deficient in CD91 (white arrow). Rare $CD11c^+$ cells did show low levels of CD91 expression.

Next, we investigated the effects of LPS treatment on the expression of CD91 by these BMDC. LPS was selected for its well-studied effects on BMDC activation. After 4 hrs stimulation with LPS, both WT and CD91 KO BMDC adopted a more uniform expression pattern of CD11c by almost all cells. WT BMDC have a more dendritic appearance and show uniform expression of CD91 throughout the cell, which does not appear to co-localize to CD11c expression. CD91 KO BMDC also have a dendritic morphology and retain KO of CD91 on many of the $CD11c^+$ cells, however, with 4 hrs stimulation in LPS, a number of $CD11c^+$ cells now co-express CD91 as well. After 24 hours stimulation with LPS, WT and CD91 KO BMDC

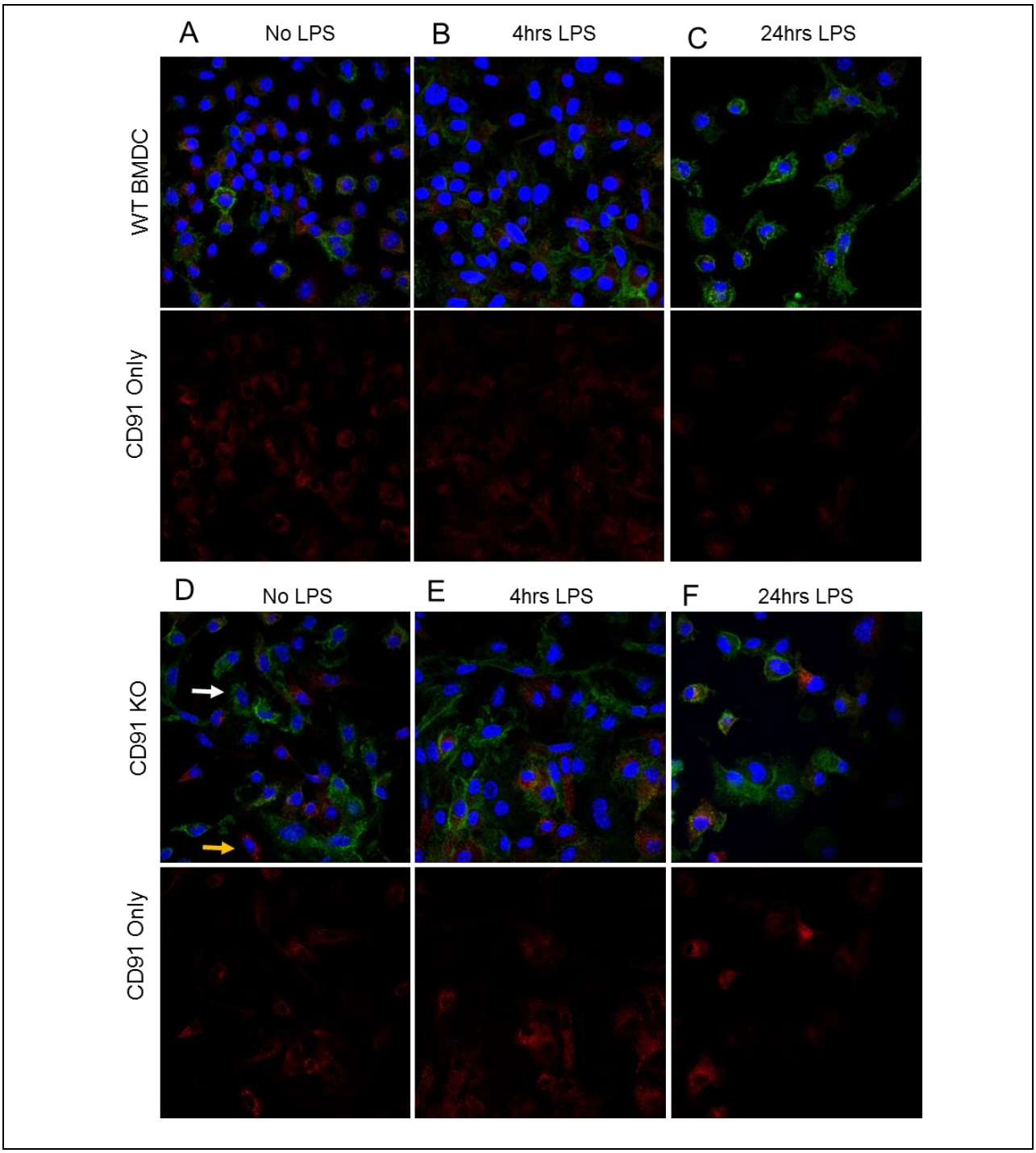

Figure 5-3. Increased expression of CD91 with LPS treatment.
BMDC were generated from Cre- littermates (A-C) or CD91 KO mice (D-F) as described in Materials & Methods. BMDC were treated with LPS on day 6 (24 hrs (C,F)) or day 7 (4 hrs (B,E)) or left untreated (0 hrs (A,D)). Cells were stained with anti-CD91 EPR3724 (red), anti-CD11c (green), and Hoechst nuclear dye (blue). Performed by MNM.

round up, adopting an appearance typically associated with migration. While WT BMDC appear to have less CD91 by microscopy, the KO BMDC have a number of CD91 bright cells.

5.4 DISCUSSION

There is a current focus on determining how material in endosomal compartments translocates to the cytosol for processing [142,185,187]. Previous studies have shown that peptides chaperoned by HSPs are processed by proteasomes and require TAP transport prior to presentation on MHC class I [22]. Following endocytosis, dissociation of peptide from gp96 occurred rapidly. This dissociation could reflect changes in pH or activity of compartment-specific enzymes [188]. Alternatively, a recently identified endosome specific 'unfolding' mechanism could cause the gp96 to relinquish the chaperoned peptide [187]. This 'unfolding' mechanism allows for stretches of polypeptides to be extruded to the cytosol. Short sequences can bypass this mechanism. Surprisingly, but consistent with this 'unfolding' mechanism, gp96 was observed to translocate to the cytosol rapidly and earlier than the peptide. This is also consistent with our observation that endocytosed gp96 is excluded from lysosomes. We expect that gp96 will be degraded in the cytosol [152]. In addition, the delay in peptide translocation to the cytosol may explain how some of these HSP-chaperoned peptides are presented by MHC class II [114]. Thus, peptide-containing vesicles may fuse with MHC class II loading compartments before peptide can be translocated to the cytosol. This concerted processing event and timed-translocation could explain how gp96-chaperoned peptides are presented on MHC class I or MHC class II by the same APC. We also observed the persistence of peptide within the cytosol of cells which could

be the result of re-association of peptide with endogenous HSPs within the APC [36,152,187,189].

Surface expression of CD91 is required for interaction with and internalization of extracellular HSPs. In our studies of BMDC, we have confirmed expression of CD91 by these cells, but have yet to clarify the localization of this receptor within cellular organelles. We are interested in determining whether CD91 localization is regulated in a similar manner to the expression of MHC class II, with maturation resulting in a redistribution from cellular stores to the cell surface [190,191]. We have also observed that expression of CD91 varies over time after maturation; this is especially clear when comparing receptor expression for the CD11c-specific CD91 KO BMDC. Given that day 6 BMDC are a relatively immature population [161], the observed co-expression of CD91 and CD11c on these cells at 4 hrs and 24 hrs may be due to novel CD11c expression on $CD11c^{-}$ precursor cells which have undergone additional differentiation with LPS stimulation [192], and may retain residual CD91 at the observed time points. Our observation that CD91 expression ultimately decreases upon LPS stimulation is supported by a number of previous reports showing down regulation of CD91 following LPS treatment [193,194], potentially mediated by increased expression of SREBP1 [195]. Interestingly, when BMDC were treated with fluorescently tagged gp96, only "immature cells" ($CD11c^{+}CD86^{neg}$) were able to bind the HSP while $CD11c^{+}CD86^{hi}$ cells showed no binding, suggesting loss of CD91 expression during normal maturation, without the need for stimulation by LPS [71]. Given that gp96 binding delivers a maturation signal through CD91 as well, we are interested in employing mutated CD91 receptors to determine if loss of this maturation signal will alter retention of gp96 and its chaperoned peptide [196]. Additional requirements for CD91 expression in the development of APCs is also under investigation.

These studies elucidate the cellular processes downstream of HSP:CD91 interaction. HSPs are ancient, stress-responsive molecules, and their ability to interact with CD91 on immune cells to generate peptide-specific immune responses is evolutionarily conserved [100]. By understanding the mechanism of HSP-chaperoned antigen presentation we gain insight into the evolutionary development of these complicated pathways.

6.0 SUMMARY & FUTURE DIRECTIONS

Heat shock proteins may be found in the extracellular environment due to membrane damage, active secretion, or by administration of HSPs as a vaccine. These HSPs are capable of generating highly efficient and specific immune responses via their interaction with the receptor CD91. The characterization of the cellular players and processes involved in generating these responses is important to understanding retention of this responsive pathway throughout evolution as well as highlighting potential means of altering immune responses via use of HSPs in various disease settings.

All of these studies rely on our ability to detect gp96 using a fluorescent molecule, either Alexa Fluor 488 for our exogenous gp96 administration or EGFP for our studies of endogenous gp96 release. While these markers are a powerful tool, they have some drawbacks. Namely, the accuracy of tracking of these proteins is dependent on the specificity of the label, limit of non-specific targeting due to label-protein interactions, and the stability of the tag. These issues will be discussed in the following paragraphs.

A488 labels free primary amines, such that any contaminating proteins in our gp96 preps may also be labeled. Thus, we may mistake off-target labeled protein binding for gp96 binding. However, as shown previously [65], and as demonstrated by Coomassie staining and immuno-blotting of our purified proteins (Figure 3-1A), our gp96 preparations are highly purified. Contaminants are unlikely to account for the majority of the signal observed. Ideally, co-staining

with an anti-gp96 antibody might clarify that the major subsets observed are specifically binding gp96 rather than a non-specific contaminant. This approach, however, is complicated by the high expression of endogenous gp96 by most cells, which would produce a high level of background staining. Genetic labeling of gp96 with EGFP reduces the question of specificity since our construct only allows EGFP expression at the C-terminus of gp96 and is unlikely to have EGFP cleaved from the fusion protein and still remain fluorescent. Purified $gp96_{EGFP}$ could be used to validate the cellular subsets identified with A488 conjugated protein. Alternatively, uptake of $gp96_{A488}$ could be competitively inhibited with unlabeled gp96 to show specificity, especially in our *ex vivo* experiments.

Another major concern associated with tracking labeled proteins is altered protein-protein interactions due to addition of the tag. Steric inhibition of normal protein interactions due to bulky tags can disrupt ligand receptor binding. The molecular weight of the Alexa fluor 488 carboxylic acid, tetrafluorophenyl ester used to label gp96 is ~885 Da, equivalent to approximately eight amino acids. Multiple A488 molecules label each molecule of gp96, and are expected to be distributed along the gp96 structure. As mentioned in Aim 1, previously published reports using gp96 similarly labeled with FITC (molecular weight of 389 Da) showed no disruption in the ability of gp96 to bind its receptor and deliver peptide for cross-presentation [96]. Thus, labeling with A488 would not be expected to block receptor binding, and our data shows that peptides associated with $gp96_{A488}$ are delivered for cross-presentation. Comparatively, EGFP is ~32.7 kDa, or 37 times larger than A488. Although EGFP is significantly larger, it is distant from the N-terminus of gp96. The N-terminus has been shown to be sufficient for binding peptides and interacting with CD91 [45]. Thus, any steric effects on receptor binding from this bulky C-terminal tag are also expected to be limited. Studies of the

ability of this fusion protein to chaperone peptides for cross-presentation are warranted to confirm that the gp96 folding and function are not compromised *in vivo*.

Some labeling dyes non-specifically interact with substrates other than the protein to which they are conjugated. Chemically, A488 carries a negative charge and is hydrophilic, limiting the amount it non-specifically interacts with other substrates [197]. Receptors for the molecules A488 or EGFP may exist; to confirm the targeted cells are not a by-product of receptor interaction with the labels rather than gp96, unconjugated A488 as a control vaccine and control tumors expressing KDEL tagged EGFP could be used.

Detection of gp96 is also dependent on the stability of the fluorescent molecules. Unlike earlier dyes, A488 is highly photostable and pH insensitive over the range of 4-10 [198]. However, the natural amino acids Trp, Tyr, His, and Met are capable of quenching this molecule [199]. This quenching is due to photo-induced electron transfer, such that if the labeled gp96 is in a compartment containing high concentrations of these amino acids or is closely associated with proteins containing these amino acids at the time of analysis, the signal may be below the limit of detection. EGFP, a relatively complex protein tag, is highly dependent on its structural stability for fluorescence. Assays for the stability of this protein showed that it is relatively stable following treatment with the protein denaturant guanidinium chloride, in elevated temperatures, as well as exposure to various detergents and proteases [200,201]. The half-life of EGFP in mammalian cells is ~26 hrs, but this can be modulated by fusion with other proteins' proteolytic groups [202]. Studies into the stability of the $gp96_{EGFP}$ fusion protein's half-life in the extracellular environment are warranted to determine the length of time $gp96_{EGFP}$ may be detectable after release from tumor cells. Both the A488 and EGFP fluorescence spectra overlap with the fluorescence spectra of many endogenous molecules, raising the limits of detection.

Alternative fluorescent proteins based on the structure of EGFP have been developed with enhanced stability and fluorescence in the red spectrum to avoid issues with high background.

Questions on our ability to detect this protein become extremely important when looking at the internalization of gp96 and its subsequent processing. As we and others have shown, internalized gp96 fails to localize to lysosomal compartments. The dyes used in this study are relatively insensitive to this pH change, allowing us to be confident in this observation. However, it is unclear if A488 tagged gp96 would lose its fluorescence immediately upon gp96 degradation or if we may continue to visualize gp96 peptide fragments after the protein may be cleaved. Thus, we need to confirm our observation of gp96 transport into the cytosol using additional methods. Potentially, we may be able to co-stain for gp96 with a fluorescent antibody and look for overlap. Alternately, we could conduct a pulse-chase experiment and isolate the various cellular compartments for analysis by Western blot to confirm if the A488 labeled bands continue to correspond to full length gp96 or to degradation bands with increasing time within the various compartments.

It is important to remember when elucidating these pathways that the various cell subsets may also utilize alternate antigen processing routes [160,203,204], and this can also depend on the maturation status of the APC. The processing pathways for the HSPs should be examined for a number of cell types, and compared between immature or matured populations.

Assuming that $gp96_{A488}$ behaves as normally purified autologous gpp96 vaccines, Aim 1 demonstrates that upon vaccination with gp96, this protein is predominately endocytosed by CD91 expressing $CD11c^{+}CD11b^{+}CD4^{+}$ cells in the subcapsular region of the LNs. These cells rapidly and preferentially take up protein both *in vivo* and *in vitro*. Given that these cells would contain the bulk of antigen for presentation, this suggests that they must play a major role in

defining immune responses to gp96. However, since our experiments with the adoptive transfer of immunogenic cells relied on bulk $A488^+$ cells rather than subdividing based on APC phenotype, an absolute requirement for this subset in gp96-mediated immune responses has not been established. Unexpectedly, there were no alterations in $gp96_{A488}{}^+$ subsets observed in CD91 KO mice. This may be due to the relatively low expression of CD11c on the $CD11b^+$ subset, such that selective deletion of CD91 only on $CD11c^+$ cells may have been incomplete for this subset. We would expect to see a greater effect on gp96 endocytosis in a dual CD11b/CD11c specific CD91 KO, as proposed in the discussion in Aim 2. However, the population identified is naturally highly endocytic and a CD91-independent A488 labeled protein, mouse serum albumin, showed no difference in cellular targets (data not shown). Thus, there may be features of these cells that lead them to uptake HSPs even when CD91 is lacking, such as increased rates of phagocytosis, pinocytosis, etc. Interestingly, in Aim 2 we show generally that immune responses to tumor, and specifically to gp96 vaccine, have a strong dependence on the expression of CD91 on CD11c expressing cells. Though we have already confirmed that these CD91 KO mice are capable of presenting a peptide for priming T cell responses independent of processing, we have not confirmed that these cells are capable of processing antigen following uptake that is not dependent on the receptor CD91.

It is important to clarify that the endocytosis of gp96 may not be the critical feature of gp96-mediated immunity disrupted in our CD11c-specific CD91 KO mice. Deficiency in gp96 signaling through CD91 on $CD11c^+$ cells may reduce effective priming. As we have shown that interaction of gp96 with CD91 elicits a variety of cytokines, it may be that this cell-specific deletion abrogates a critical cytokine response from the $CD11c^+$ cells. We may also have reduced the ability of these cells to mature in response to gp96 signaling. Although we do not show that

these cells are the major targets for endocytosis of gp96, they may receive antigen from $gp96^{+}$ cells via antigen transfer but still be dependent on an extracellular maturation signal. Indeed, we observed that transfer of $gp96_{ErkA488}^{-}$ subsets from $gp96_{ERK}$ complex treated mice were also capable of inducing protection against CMS5 tumor, with growth curves comparable to those observed for the $_{gp96ErkA488}^{+}$ group shown in Aim 1 Figure 3-9, pg 34. It is not clear if these cells received antigen from one of the $gp96^{+}$ subsets, or if they may more rapidly process internalized antigen, degrading the fluorescent signal.

We are currently investigating mice deficient in defined APC subsets, such as the Batf3 KO mice that have lost $CD8\alpha^{+}$ and $CD103^{+}$ DCs [205], for their ability to respond to HSP-based vaccines. Although our uptake data did not implicate the $CD8\alpha^{+}$ or $CD103^{+}$ subsets as major cellular populations that take up gp96, their role in cross presenting antigens in other systems has been well established [205-207]. It may be that only a very small number of these cells are indeed responsible for generating the observed immune responses. Our studies focused on the cells that quantitatively took up the majority of gp96 but did not fully assess the qualitative outcome of gp96 endocytosis, namely the processing of gp96-chaperoned peptide for presentation. Thus, we cannot rule out that deficiency in Batf3 may also abrogate gp96-mediated immune responses.

APC in the homeostatic LN are considered to be in an immature state [208]. Since our data on CD91 expression shown in Aim 1 was derived from naïve animals, it will be important to clarify if there are any changes in CD91 expression in the LNs of vaccinated mice. CD91 may increase in expression after APC stimulation, or matured APC may recruit additional CD91 expressing cells. The nature of the maturation stimulus may also differentially impact CD91

expression [196]. The effects of this regulation on antigen processing and presentation deserve more investigation.

The role of dose on immune responses to gp96 is an especially intriguing feature of these studies as we have observed differential effects in cell subsets targeted *in vivo* versus *in vitro*. The immunogenic dose of gp96 *in vivo* clearly preferentially targets cells with an APC phenotype (expressing CD11b or CD11c), and our *ex vivo* data on LN subsets confirmed these cells are the preferred endocytic cells as well. Surprisingly, increasing the dose of gp96 *in vivo* targeted an entirely different population that were negative for CD11c and CD11b, despite these cells showing no endocytic capacity *ex vivo*. The nature of the gp96 responsive $CD11b^{-}CD11c^{-}$ cells *in vivo* has yet to be clarified; this population in the high dose vaccinated LN may represent a newly recruited or expanded population not present in the isolated naïve LNs. This would explain the discrepancy in endocytic capacity, however this must also be an extremely rapid recruitment, as these differences were observed very early, just 8 hrs, after vaccination. An alternative explanation could be that the LN structure may allow transfer of high dose gp96 to the $CD11b^{-}CD11c^{-}$ via a mechanism that may be disrupted *ex vivo*, such as close cell to cell contact. Further surface marker characterization on the $CD11b^{-}CD11c^{-}$ population should be conducted to identify this population and the potential mechanism behind this observed discrepancy.

Our tumor model expressing fluorescent gp96 is an excellent tool for studying the complicated immunological processes at play in the tumor microenvironment. The role for heat shock proteins in tumor cells is controversial; while HSPs are capable of stimulating immune responses, patients whose tumors over-express HSPs often have a worse prognosis. There are multiple cell types present in the tumor microenvironment that may express CD91 and respond

to HSPs, including tumor associated macrophages, plasmacytoid dendritic cells, and myeloid derived suppressor cells. These cells may be recruited and activated by the HSPs released in the growing tumor environment and respond by suppressing anti-tumor effector cells, contributing to increased disease burden. Studies of $gp96_{EGFP}$ expressing tumor cells co-cultured with these cell types may shed light on the mechanistic pathways for immune suppression by HSP release. Also, as discussed earlier, the expression of CD91 by T cell populations remains controversial; while we have been unable to confirm CD91 on murine T cells, we have not ruled out a potential direct effect of HSPs on stimulating T regulatory cells. Additionally, as we have already shown [24], cytokines downstream of HSP signaling on APCs, when combined with the appropriate tumor microenvironment, can alter the phenotype of responding effector cells. Thus, we are very interested in following up on the cytokine production in and around cells expressing or endocytosing $gp96_{EGFP}$ in the tumor.

As introduced, HSPs have already been tested in clinical trials as cancer therapeutics. Despite promising results in murine studies, only a small number of patients showed partial or complete responses to autologous gp96 therapy. This may be due to immunosuppressive effects of the tumor microenvironment, or it may be due to differences in immune cell targeting of the gp96 vaccine. As shown in mice, dosing can play a major role in determining the outcome of the immune responses generated by HSPs. The optimal dose for humans has yet to be determined. Trials to date have used 20-50 ug of protein per dose, which is similar to the amounts of protein used to vaccinate mice. This dose was calculated based on the amount of antigen theorized as necessary to generate immune responses and with a concern to avoid giving a “high,” immunosuppressive dose. Other than clinical response, the effectiveness of the vaccine has been difficult to monitor. The studies on the effects of dose on the targeted cell populations in the

lymph node in Aim 1 suggest an approach for tracking autologous vaccine within a patient using draining lymph node biopsies. The ability to confirm appropriate dosing by analyzing the cellular subsets that have taken up the protein could assist in tailoring vaccine dose to enhance effectiveness.

All of these studies were performed with a prototypic HSP, gp96. However, as our lab has already shown, other HSPs give rise to different immune outcomes following CD91 engagement. It will be important to clarify if the findings discussed here are universally applicable or if other HSPs target different cell populations or differentially regulate CD91 expression. Given the distinctive patterns of CD91 phosphorylation after treatment with the different HSPs [24], we would predict altered cytokine responses as well as altered rates of endocytosis and the downstream signaling that results in maturation.

Overall, HSPs are clearly capable of inducing immune responses through their interactions with the receptor, CD91. Aim 1 demonstrated the major cells targeted by HSP vaccine express CD11b and high levels of CD91. Aim 2 demonstrated the dependence on HSPs and CD91 for generation of anti-tumor immune responses. Aim 3 showed the intracellular pathways critical to processing HSP and peptide for efficient presentation. These three aims lay the foundation for continuing research on the basic mechanisms of HSP-mediated immune responses that will clarify the early stages of immune system development. The pathways our immune cells developed in order to respond to stressful or dangerous conditions are clearly rooted in their ability to detect HSPs. A better understanding of these mechanisms will guide us toward the situations in which utilizing HSPs may provide the greatest benefits.

7.0 MATERIALS & METHODS

Those who performed the experiments or generating novel methods in this chapter are indicated by their initials in the figure legends (Michelle Messmer: MNM; Sudesh Pawaria: SP; Laura Kropp: LEK; Joshua Pasmowitz: JP).

7.1 MICE

Female C57BL/6, BALB/c, C57BL/6 x BALB/c "F1 mice," C.129S7(B6)-Rag1tm1Mom/J (*rag1*$^{-/-}$ BALB/c), and B6(Cg)-Rag2tm1.1Cgn/J (*rag2*$^{-/-}$ C57BL/6), C57BL/6-Tg(TcraTcrb)1100Mjb/J (OT-1), B6.SJL-Ptprc^{a}Pep^{b}/BoyJ (CD45.1) were purchased from The Jackson Laboratory (Bar Harbor, ME) and housed in the animal facility at the University of Pittsburgh. Experimental mice were used between the ages of six to eight weeks. All mice were used according

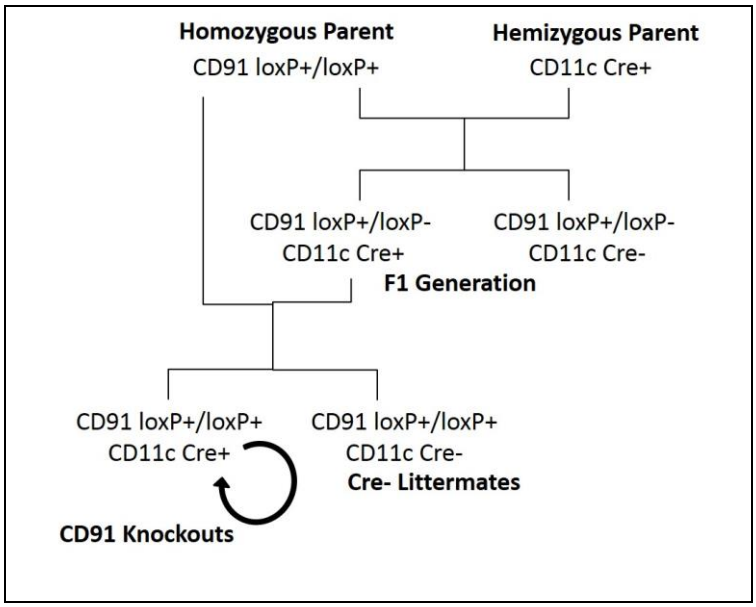

Figure 7-1. Mating scheme for CD11c specific CD91 KO mice. Development of this breeding scheme by SP.

to IACUC protocols approved by the University of Pittsburgh and in accordance with the National Institutes of Health (Bethesda, MD) guidelines.

7.1.1 Generation of CD11c specific CD91 knockout mice

B6;129S7-*Lrp1*^{tm2Her}/J (CD91$^{flox/+}$) mice originally generated by [209] were purchased from Jackson Laboratory (Bar Harbor, ME) and mated to homozygosity (CD91$^{flox/flox}$). CD11c specific CD91 knockout mice were generated by crossing B6.Cg-Tg(Itgax-cre)1-1Reiz/J (CD11c-Cre) mice with CD91$^{flox/flox}$ mice. Members of the F1 generation were then backcrossed with the homozygous CD91$^{flox/flox}$ parent and confirmed CD91$^{flox/flox}$ CD11c^{Cre+} offspring were mated for all subsequent generations (Figure 7-1).

7.2 CELLS AND REAGENTS

7.2.1 Cell lines

Lung carcinoma D122, methylcholanthrene-induced fibrosarcoma CMS5, Simian Virus 40 (SV40)-induced SVB6, and macrophage-like RAW264.7 were obtained from American Type Culture Collection (ATCC, Manassas, VA) and cultured as recommended in Dulbecco's modified Eagle's medium supplemented with 1% sodium pyruvate, 1% L-glutamine, 1% non-essential amino acids, 1% penicillin and streptomycin, 0.1% 2-mercaptoethanol and 10% fetal bovine serum (FBS) (complete DMEM, GIBCO). RAW264.7 cells previously transfected using a K^b plasmid (RAW264.7 K^b) as described [210] were also maintained in complete DMEM.

RAP or control vector-transfected CMS5 tumor cells were cultured in complete DMEM media plus blasticidin (3μg/mL, Invitrogen). Double transfected tumor cells ($gp96_{EGFP}$+RAP, or $gp96_{EGFP}$+control vector) were cultured in complete DMEM media plus blasticidin (3μg/mL, Invitrogen) and geneticin (0.7g/L, GIBCO).

Retroviral immortalized DC line D2SC/1 (a generous gift from Dr. P. Ricciardi-Castagnoli, Cellular and Molecular Pharmacology Center, Milan, Italy, [211]) were maintained in complete DMEM with heat inactivated FBS. Prior to experiments, D2SC/1 cells were treated with 12 ng/ml of recombinant INFγ (invitrogen, Carlsbad, CA) for 48 hours to increase expression of surface MHC.

T cell hybridomas, B3Z (provided by Dr. Nilabh Shastri, UC Berkeley) and LC21 (provided by Dr. Jean-Charles Guery at the Institut National de la Sante et de la Recherche Medicale, France) as well as the T cell lymphoma EL4 (ATCC) were grown in RPMI Medium 1640 supplemented with 5% FBS, 1% nonessential amino acids, 1% penicillin and streptomycin, 1% pyruvate, 1% glutamine, 1ml/L of β-mercaptoethanol.

All cell cultures were stored in a liquid nitrogen cell bank at the University of Pittsburgh in 20% DMSO/80% FBS freezing media until thawing for culture at 37˚C in a humidified atmosphere containing 5% CO_2.

7.2.2 Generation of bone-marrow-derived dendritic cells

Bone marrow derived dendritic cells were obtained by culturing bone marrow cells from F1 mice, CD91 KO mice, or Cre^- controls for 6 days in DMEM containing 10% heat-inactivated fetal calf serum (50°C for 30 minutes) and supplemented with GM-CSF on days 0 and 3 as previously described [161].

7.2.3 Purification of gp96 and labeling with Alexafluor 488

For all experiments, gp96 was purified as previously described [212]. In detail, batches of 30-50 livers from C57Bl/6 or BALB/c mice, either freshly harvested or previously frozen at -20°C, were blended into 30 mL phosphate buffered saline supplemented with additional 1.75g NaCl per liter, 300 µL Halt Protease Inhibitor Cocktail, EDTA-free (Thermo Scientific, Rockford, IL), one tablet cOmplete protease inhibitor, EDTA-free (Roche Diagnostics, Indianopolis, IN), and 30 µL 0.2M Phenylmethylsulfonyl fluoride (PMSF). Blended livers were pooled and the volume of PBS was increased to ~3 mL per liver before samples were centrifuged at 5,700 x G for 10 min. Supernatant was then subjected to ultra-centrifugation at 100,000 x G for 90 min. Supernatants were then brought to 50% Ammonium Sulfate by slow addition of the salt while stirring in an ice bath. This solution was then centrifuged at 14,000 x G for 30 min. Supernatants were then brought from 50% to 80% Ammonium Sulfate as before, followed by an additional 14,000 x G centrifugation for 30 min. The 80% salt pellet is resuspended in 10 mL per liver of 'Con A PBS' (prepared with 2L distilled H_2O, 1 packet PBS powder (Sigma Aldrich, St. Louis, MO), 12.26 g NaCl, 4 mL 1M CaCl, 4 mL 1M $MgCl_2$, and 10 mL 0.2 M PMSF) prior to application to Concanavalin A-agarose column (GE Healthcare, Chalfont St. Giles, United Kingdom). Glycoproteins were eluted by 10% methyl-α-D-mannose pyranoside Con A PBS. Eluate was then applied to sepharose gel columns (also purchased from GE Healthcare) to exchange into DEAE buffer (prepared by combining 2L 0.005M monobasic sodium phosphate solution with 2L 0.005M dibasic sodium phosphate solution to a pH of 7.2, followed by addition of NaCl to 0.3 M). Protein was then loaded onto equilibrated DEAE Sephacel columns (GE Healthcare) and eluted with 0.7 M NaCl DEAE buffer. Fractions were concentrated using a 10,000 MWCO spin column (Ultracel 10K, Amicon Ultra, Millipore, Billerica, MA). Protein

concentration was determined by Bradford analysis (Bradford reagent purchased from Biorad, Hercules, CA). Absorbance at 595 nm was measured using a Biorad Model 680 microplate reader. Protein purity was analyzed by SDS-PAGE using a 10% Bis-acrylamide gel (Biorad).

Apparently homogenous preparations of gp96 were labeled with Alexafluor A488 (Molecular Probes, Invitrogen, Grand Island, NY) using a labeling kit optimized for labeling of immunoglobulin molecules according to the manufacturers recommendation. In detail, 1M bicarbonate buffer was added to approximately 2 mg/mL purified gp96 to a final concentration of 0.1M bicarbonate before transferring the protein to a vial of the reactive Alexa Fluor 488 dye and mixing for 1 hour at room temperature. Free dye was removed by size exclusion chromatography using the provided column components. Protein concentration was measured by Bradford analysis. Labeled gp96 is referred to as $gp96_{A488}$. Protein was analyzed by SDS-PAGE and immunoblotting with anti-gp96 (Enzo Life Sciences, Inc. Farmingdale, NY) and anti-A488 (Invitrogen, Grand Island, NY) antibodies.

7.2.4 HSP:Peptide Complexes

To generate specific anti-CMS5 responses, the H-$2K^d$ restricted immunodominant epitope from ERK2 ($ERK2_{136\text{-}144,}$ QYIHSANVL)[151] was conjugated in a 100:1 peptide to $gp96_{A488}$ molar ratio as previously described [28], termed $gp96_{A488}$-ERK. To measure cross-presentation of a dual epitope peptide, HELOVA was constructed of the HEL I-A^d restricted immunodominant epitope ($HEL_{12\text{-}25,}$ MKRHGLDNYRGYSL) in tandem with the OVA H-$2K^b$ restricted immunodominant epitope ($OVA_{257\text{-}264}$, SIINFEKL). Gp96 was complexed to HELOVA as described above to obtain $gp96_{HELOVA}$. To track processing of peptides within BMDCs, an extended 20 amino acid OVA peptide containing the above epitope was biotinylated before

conjugating with $gp96_{A488}$ to obtain $gp96_{A488}$-b-pep20. All peptides were synthesized at Genemed Synthesis, Inc. (San Antonio, TX). Free peptide was removed from all conjugation reactions by size exclusion membranes.

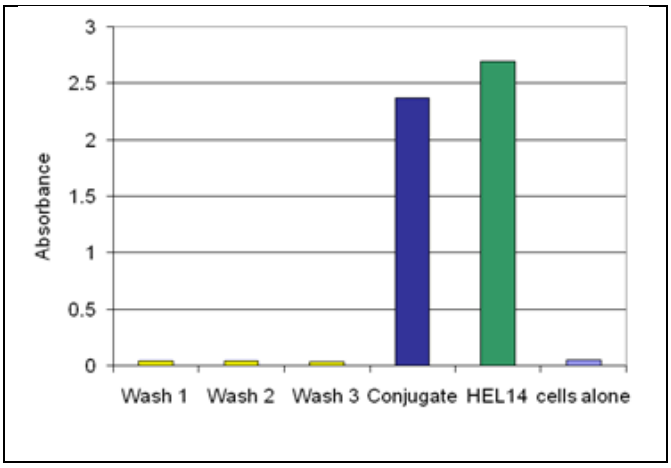

Figure 7-2. Free HELOVA peptide does not stimulate LC21.
100 µL flowthrough from preparing HSP:peptide complexes, 1 µL Hel14, or 10 µg $gp96_{HELOVA}$ complex was pulsed onto D2SC/1 cells in co-culture with LC21 for 24 hrs. Production of IL-2 was measured by ELISA. Performed by MNM.

We confirmed that immune responses to HSP:peptide complexes are due to peptides bound by HSPs and not free peptide by washing prepared HSP conjugates three times in 4mls PBS on a 10,000 MW cut off centricon. Flowthrough was saved, condensed by air drying, pulsed onto D2SC/1 cells which were cultured overnight with LC21 cells. Activation of LC21 was measured by ELISA for IL-2. As shown in Figure 7-2, even the flowthrough from wash 1 did not elicit a measurable response, while 10µg/ml of $gp96_{HELOVA}$ conjugate was able to elicit a response comparable to direct addition of 1uM of the specific MHC class II epitope, HEL14.

7.2.5 Antibodies

Dilutions and specific use for the antibodies below are included in the Experimental Methods section. Anti-CD8 depleting antibody was purified from culture supernatant of TIB210 hybridoma (ATCC).

Table 7-1. Antibodies for Flow Cytometry

Name	Clone	Isotype	Manufacturer	Conjugate
Anti-CD91	11H4	Mouse IgG1	Hybridoma from ATCC,	Unconjugated

			purified by Sudesh Pawaria	
Anti-CD91	5A6	Mouse IgG2b	abcam	Unconjugated
Anti-CD8a	53-6.7	Rat IgG2a	BD Pharmingen	Pacific Blue, APC
Anti-CD4	RM4-5	Rat IgG2a	BD Pharmingen	PerCP-Cy5.5
Anti-CD11c	HL3	Arm. Hamster IgG1	BD Pharmingen	PE, APC
Anti-CD103	M290	Rat IgG2a	BD Pharmingen	FITC, PE, BV421
Anti-CD205	205yekta	Rat IgG2a	eBioscience	APC
Anti-CD207	eBioL31	Rat IgG2a	eBioscience	PE
Anti-CD11b	M1/70	Rat IgG2b	BD Pharmingen	PE-Cy7
Anti-F4/80	BM8	Rat IgG2a	eBioscience	eFluor 450
Anti-CD45	30-F11	Rat IgG2b	Invitrogen	APC
Anti-Gr1.1	RB6-8C5	Rat IgG2b	BD Pharmingen	PerCP-Cy5.5, Alexa Fluor 700
Anti-I-A/I-E	M5/114.15.2	Rat IgG2b	BD Pharmingen	PE
Anti-CD107a	1D4B	Rat IgG2a	eBioscience	Unconjugated
Anti-CD3 Complex	17A2	Rat IgG2b	BD Pharmingen	PE-Cy5
Anti-CD3e	145-2C11	Arm. Hamster IgG1	BD Pharmingen	APC
Anti-CD19	1D3	Rat IgG2a	BD Pharmingen	APC
Anti-NK1.1	PK136	Mouse IgG2a	BD Pharmingen	PE-Cy7

Table 7-2. Antibodies for Microscopy

Name	**Clone**	**Isotype**	**Manufacturer**	**Conjugate**
Anti-CD8	53-6.7	Rat IgG2a	BD Pharmingen	Biotin
Anti-CD4	RM4-5	Rat IgG2a	BD Pharmingen	Biotin
Anti-CD11c	HL3	Arm. Hamster IgG1	BD Pharmingen	Unconjugated
Anti-CD103	M290	Rat IgG2a	BD Pharmingen	Biotin
Anti-CD207	eBioL31	Rat IgG2a	eBioscience	Biotin
Anti-CD11b	M1/70	Rat IgG2b	BD Pharmingen	Unconjugated
Anti-CD19	1D3	Rat IgG2a	BD Pharmingen	Biotin
Anti-I-A[b]	AF6-120.1	Mouse (BALB/c) IgG2a	BD Pharmingen	Unconjugated
Anti-PDI	34/PDI	Mouse IgG1	BD Transduction Laboratories	Unconjugated
Anti-CD91	EPR3724	Rabbit IgG	abcam	Unconjugated

Table 7-3. Antibodies for Western Blot

Name	**Clone**	**Isotype**	**Manufacturer**	**Conjugate**
Anti-CD91	11H4	Mouse IgG1	Hybridoma from ATCC, purified by Sudesh Pawaria	Unconjugated
Anti-CD91	EPR3724	Rabbit IgG	abcam	Unconjugated
Anti-grp94	Polyclonal	Rabbit IgG	Enzo	Unconjugated
Anti-Alexa Fluor 488	Polyclonal	Rabbit IgG	Molecular Probes	Unconjugated

7.2.6 Additional reagents

Ovalbumin, hen egg lysosome, complete Freund's adjuvant, incomplete Freund's adjuvant, and mitomycin-C were purchased from Sigma (St. Louis, MO). Ovalbumin was rendered free of endotoxin by detoxi-Gel columns (Thermo Scientific).

7.3 EXPERIMENTAL METHODS

7.3.1 Tracking vaccine gp96 *in vivo*

Mice received ventral intradermal immunizations with $gp96_{A488}$ in 100 µl saline. Doses of $gp96_{A488}$ are indicated in each experiment. In some experiments, lymph nodes were isolated after indicated incubation periods, mechanically disrupted and passed through a 20µm strainer.

7.3.2 Flow cytometry

Cells were blocked with anti-CD16/CD32 antibody (BD Pharmingen, San Diego, CA) for 10 minutes before addition of fluorescent-tagged surface antibodies for 20 minutes. Where indicated, cells were fixed in 4% paraformaldehyde and stained with anti-CD91 extracellular β-chain clone 5A6 (abcam) followed by allophycocyanin or FITC conjugated rat anti-mouse IgG2b (BD Pharmingen) according to the recommended protocol. Major subtyping was performed using the following panel of antibodies: CD11c allophycocyanin, CD11b PECy7, CD8 Pacific Blue, and CD4 PerCPCy5.5 (BD Pharmingen). Additional markers were included as indicated

(Figure 3-4). Data was collected on a Becton Dickinson LSR2 (Franklin Lakes,NJ) using Cellquest software and analyzed using FlowJo version 7 (Treestar, Inc., Ashland, OR).

7.3.3 Microscopy

Lymph node and tumor tissues were fixed in 2% paraformaldehyde and then stored in 30% sucrose solution at 4°C overnight. Tissues were frozen by submersion in 2-methyl-butane cooled by liquid nitrogen and stored long term at -80°C. Sections (8-10 μm) were prepared in Neg50 freezing media on a HM505 Microm Cyrostat, and adhered to Fisherbrand Superfrost Plus Precleaned Microscope Slides (Fisher Scientific). Slides were stored at -20°C until staining using a protocol developed by the Center for Biologic Imaging (CBI, University of Pittsburgh). Primary antibodies included biotin conjugated CD11b, CD4, CD8, CD207, CD103 and purified Armenian Hamster anti-CD11c (BD Pharmingen & eBioscience, San Diego, CA). Secondary antibodies were Cy5 conjugated goat-anti-Hamster IgG and DyLight 549 conjugated Streptavidin (Jackson ImmunoResearch, West Grove, PA).

To visualize intracellular trafficking of gp96-peptide complexes, day 6 BMDCs were grown overnight on coverslips. $Gp96_{A488}$-b-pep20 was pulsed onto BMDCs for indicated times at 37ºC or 4ºC. Cells were washed, fixed in paraformaldehyde, permeabilized and stained using a protocol developed by the Center for Biologic Imaging (CBI, University of Pittsburgh). Cells were stained with Cy3 conjugated strepavidin (Jackson ImmunoResearch), phalloidin and/or LAMP-1 specific antibody (Invitrogen).

Imaging of CD91 on BMDC was accomplished by growing $3x10^5$ day 6 WT or CD91 KO BMDC on coverslips overnight, with or without LPS. Cells were again processed using the protocol from CBI and stained with anti-CD91 β-chain clone EPR3724 and anti-CD11c followed

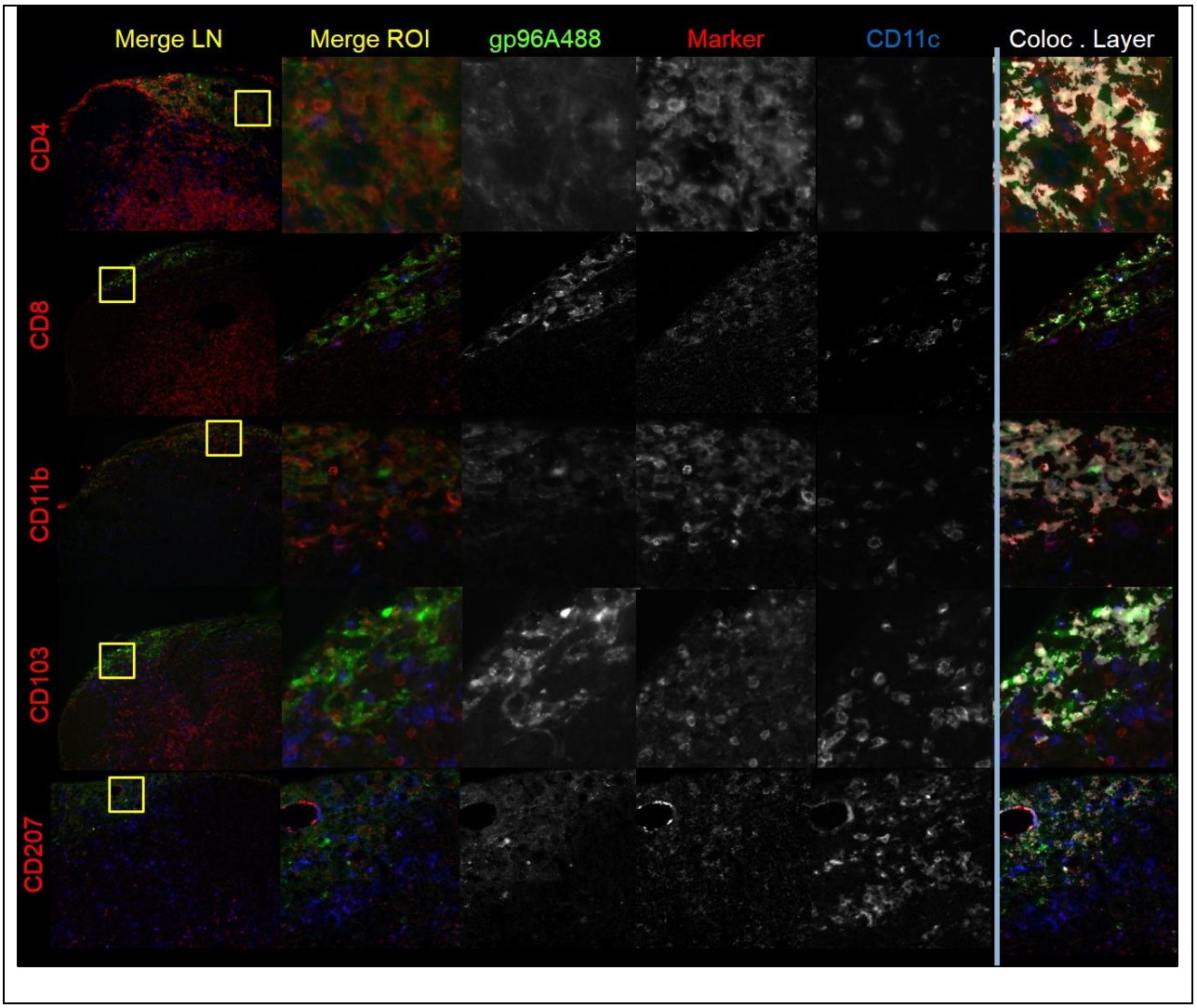

Figure 7-3. Microscopic analysis of gp96$_{A488}$ in draining LN.
LNs were harvested 8 hr post 10ug gp96A488 injection and fixed in PFA, incubated in sucrose, frozen, and serially sectioned. Sections were then stained with Cy5 (CD11c; blue) and Cy3 (separately, either CD4, CD8, CD11b, CD103 or CD207; red). Images were taken at 20x magnification by confocal microscopy (column 1). Regions of interest were selected for colocalization analysis (yellow boxes, column 1; expanded in column 2). Individual fluorescence channels are shown in Columns 3-5. Column 6 shows a colocalization channel generated using Imaris software (white; indicates regions of red and green overlap). This colocalization is quantified in Figure 3. Performed by MNM.

by Cy3 conjugated anti-rabbit and Cy5 conjugated anti-Armenian hamster secondary antibodies (Jackson ImmunoResearch).

All images were captured using an Olympus 1000 inverted confocal microscope with 60x objective and Fluoview v. 2.1 acquisition software (Melville, NY). Imaris v. 7.2.1 (Bitplane, Zürich, Switzerland) and Photoshop v. 7.0 (Adobe, San Jose, CA) were used for analysis and to

prepare the images for publication. Examples of images processed for co-localization are shown in Figure 7-3.

7.3.4 Adoptive transfer of gp96$_{A488}^{+}$ cells

Lymph node cells were harvested from BALB/c mice 6 hours after vaccination with gp96$_{A488}$ or gp96$_{A488}$-ERK and sorted by FACSAria (BD Bioscience, San Jose CA) based on A488 positivity. Sorted cells were washed in saline, and suspended at a concentration of 1x10^5 per 100 µL for transfer to naïve BALB/c mice via intravenous, retro-orbital injection. Mice were rested for one week and then challenged with 1x10^6 CMS5 cells. Tumor growth was monitored starting at day 4 and 2-3 days thereafter. For some experiments, cells were gamma irradiated with 7,000 rad prior to adoptive transfer.

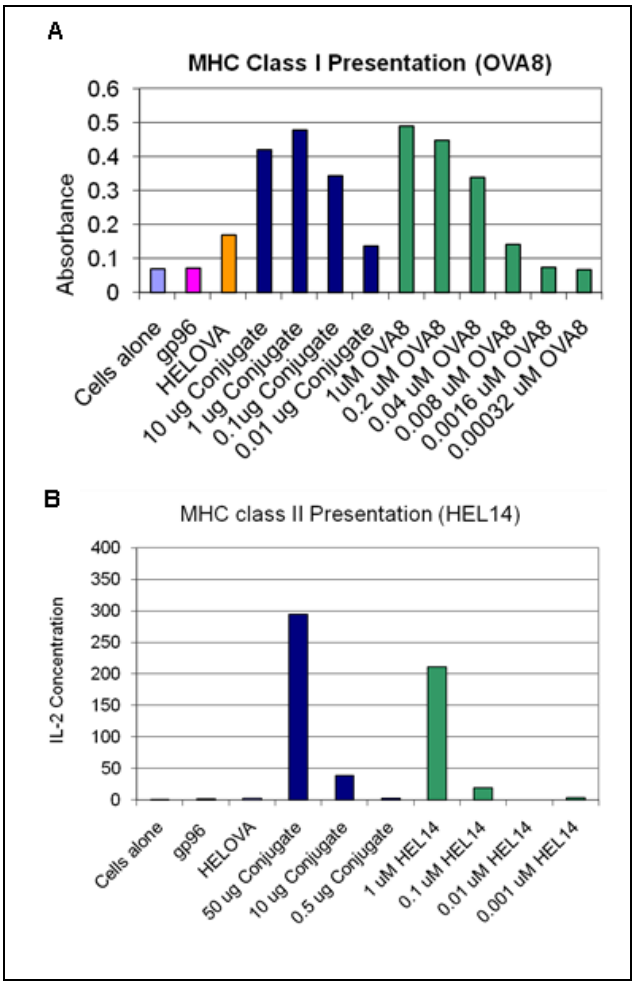

Figure 7-4. Titration of HSP:peptide complexes in the representation assay.
(A) Representation assay for MHC class I presentation of OVA. APCs used were RAW264.7 K^b, with B3Z T-cells. Activation was measured by absorption at 595 nm following cleavage of the CPRG substrate by βgalactosidase generated under the IL-2 promoter.To the right of the graph is a standard curve generated using the change in absorption in response to increasing amounts of OVA8 peptide. (B) Representation assay for MHC class II presentation of HEL. APCs used were D2SC1, with LC21 T-cells. Activation was measured by ELISA for IL-2. To the right of the graph is a standard curve generated using the change in IL-2 concentration in response to increasing amounts of HEL14 peptide. Performed by MNM.

7.3.5 Cross-presentation assay

In separate duplicate wells, BMDCs were cultured in 200 µl of complete media containing 20 µg of gp96-HELOVA, HEL or OVA, or 0.05 µg HELOVA, 0.03 µg HEL14 or 0.17 µg OVA8. T cell hybridomas B3Z specific for OVA8/K^b [213] or LC21 specific for HEL14/IA^d [214] were added at BMDC to T cell hybridoma ratio of 1:1 with $1x10^5$ cells of each. B3Z has been transfected with a gene for β-galactosidase under the IL-2 promoter, allowing for determination of activation by addition of substrate chlorophenolred-ß-D-galactopyranoside (CPRG) that produces a color change upon cleavage by β-galactosidase with absorbance measurable at 595

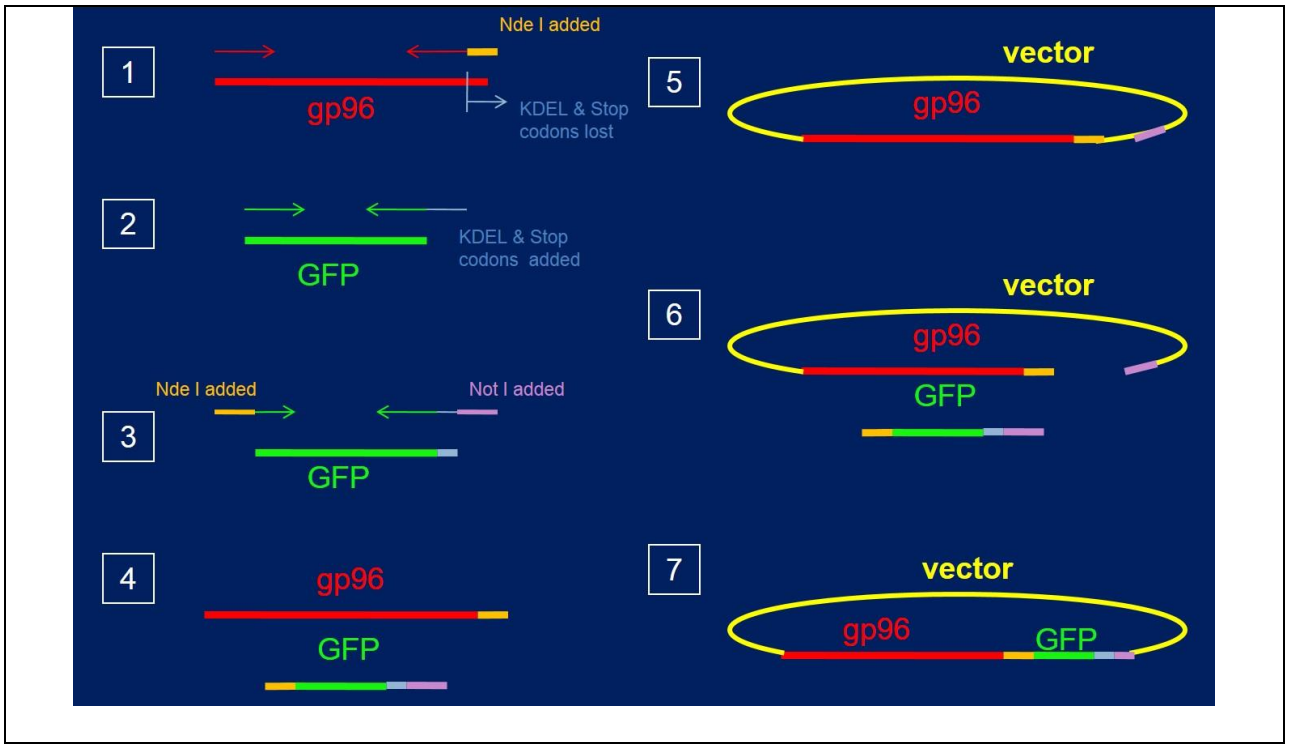

Figure 7-5. $gp96_{EGFP}$ construct schematic.
Schema for $gp96_{EGFP}$ (C-terminal fusion protein) construction by sequential PCR and subcloning. Gp96 cDNA was amplified from murine RNA using N-terminal primer, gp96NT2, and C-terminal primer, gp96CTNde1. The codons for ER retention sequence, KDEL, and the stop codon were replaced with an NdeI restriction cut site [1]. EGFP was prepared via 2-step PCR. First, EGFP cDNA was amplified from a commercial vector (Invitrogen) using complementary commercial N-terminal primer and C-terminal primer, GFPCTKDEL, with an overhang including KDEL and a stop codon [2]. EGFP was then reamplified using N-terminal primer, GFPNTNde1, with an NdeI restriction site overhang and C-terminal primer, GFPCTNot1, complementary to the previous primer's extansion, and including a NotI restriction site overhang [3]. Final products of the PCR reactions are shown at [4]. The gp96 PCR product was inserted into the pEF6/V5-His-TOPO vector and orientation was confirmed by restriction enzyme digestion and sequencing analysis [5] (Figure 7-6). The final EGFP construct was ligated into the gp96 containing vector [6] and the final product [7] was fully sequenced to confirm the sequences were in frame and that no mutations occurred during the construct assembly process. Scheme generated by MNM, with suggestions by SP.

nm [213]. LC21 activation is measured directly by the amount of IL-2 production as determined by ELISA.

7.3.6 Plasmid gp96$_{EGFP}$ construction and transfection

The gp96$_{EGFP}$ (C-terminal fusion protein) was generated by sequential PCR and subcloning. Schema for this experimental design is shown in Figure 7-5. The gp96 cDNA was amplified from murine RNA using an N-terminal primer upstream of the gp96 start codon (gp96NT2) and a C-terminal primer with complementarity starting at nucleotide 2483 (gp96CTNde1). The codons for KDEL, an ER retention signal sequence, and the stop codon were replaced with an NdeI restriction cut site. EGFP was prepared via 2-step PCR due to biochemical/physical

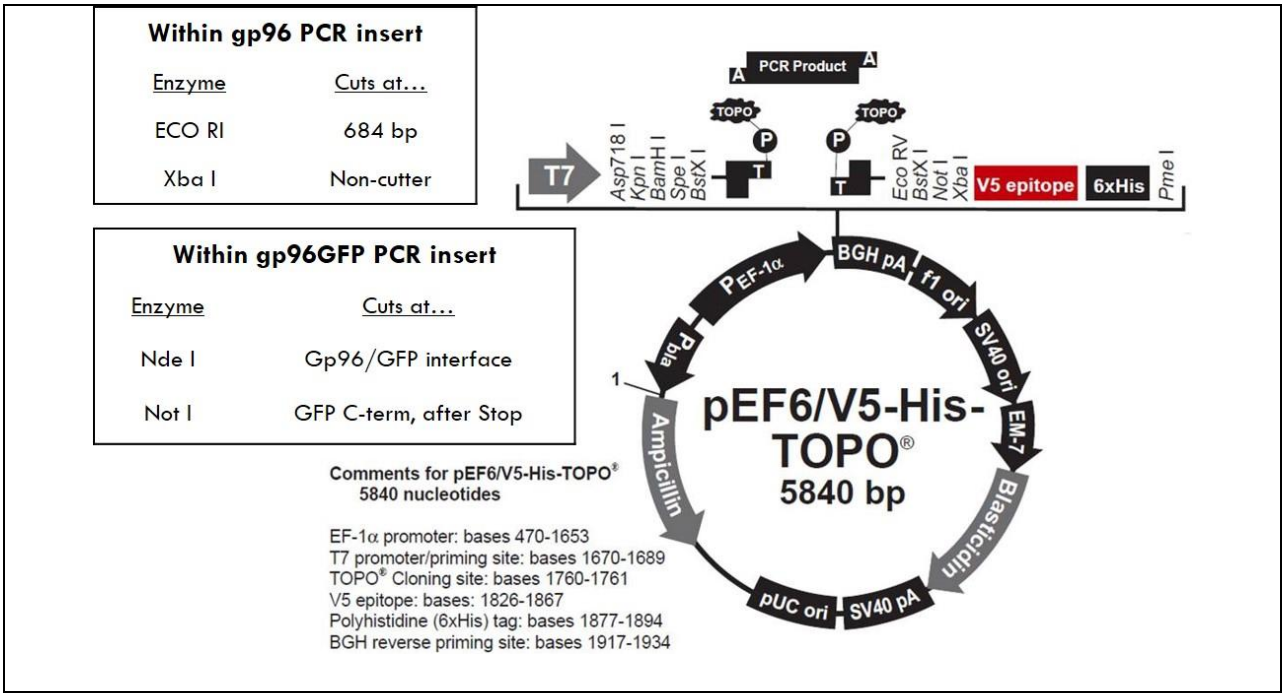

Figure 7-6. Vector map and restriction cut sites.
The gp96 PCR product was subcloned into the pEF6/V5-His-TOPO vector. Vectors containing the gp96 PCR insert were then analyzed for correct orientation by digestion with ECO RI and XbaI (Figure 7-7C). EGFP was then inserted into the vector-gp96 construct by digestion with NdeI and NotI followed by ligation, with only a single orientation possible for successful EGFP insertion (Figure 7-7D,E). Sequencing was used to confirm the final gp96EGFP containing vector was free of point mutations and in the predicted orientation. Vector map from Invitrogen.

restrictions on the number of bases that can be added by a single primer. First, EGFP cDNA was amplified from a commercial vector (Invitrogen) using a complementary, commercial N-terminal primer and a complementary C-terminal primer with an overhang for the KDEL and stop codons (GFPCTKDEL). EGFP was then reamplified using an N-terminal primer with an NdeI restriction site overhang (GFPNTNde1) and a C-terminal primer complementary to the C-terminus with KDEL and stop codons and with a NotI restriction site overhang (GFPCTNot1). Final PCR products for gp96 and EGFP are in Figure 7-7A. The PCR construct

Table 7-4. Primers for gp96$_{EGFP}$ construct.

1.	gp96NT2: 30 bases + **3 bps** for Kozak sequence
	5' **GGG** ATG AGG GTC CTG TGG GTG TTG GGC CTC TGC 3'
2.	gp96CTNde1: 20 bases not including stop codon +**NdeI site** + **3 bps**
	5' **CCC CAT ATG** CTC TGT AGA TTC CTT TTC TGT TTC CTC 3'
3.	GFPNTNde1: 20 bases + **NdeI site** + **3 bps**
	5' **GGG CAT ATG** ATG GTG AGC AAG GGC GAG GA 3'
4.	GFPCTKDEL: (1st PCR)19 bases + **KDEL** + **Stop**
	5' **TTA CAA TTC ATC CTT** TCT AGA TCC GGT GGA TCC C 3'
5.	GFPCTNot1- (2nd PCR) (GFP+**KDEL**+Stop) + **Not I site** + **3 bps**
	5' **GGG GCG GCC GCT TAC AAT TCA TCC TT**T CTA GAT CCG 3'

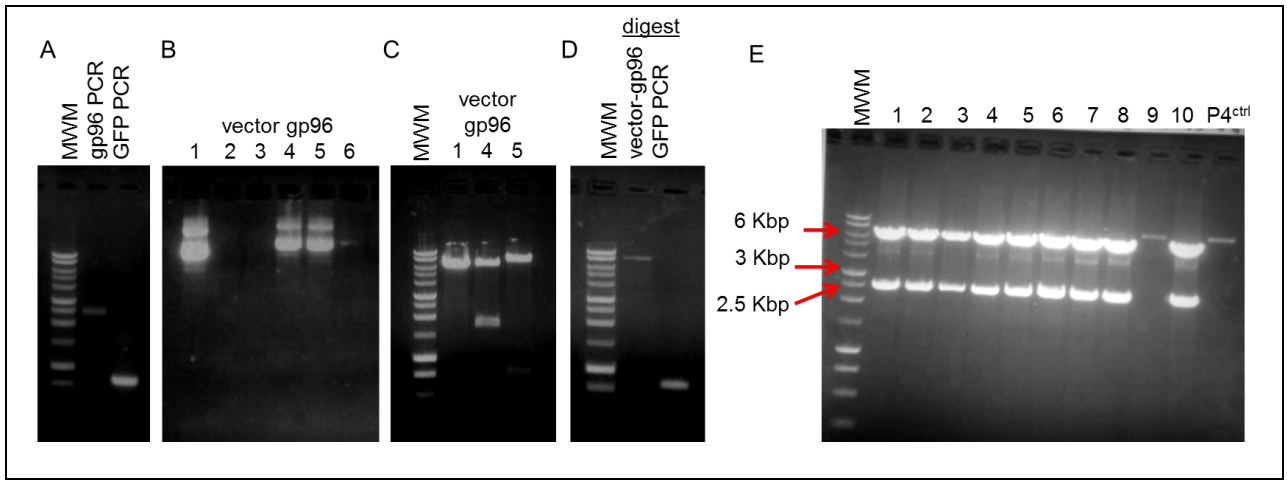

Figure 7-7. Stepwise results for gp96$_{EGFP}$ construct process.
Results of each step in the gp96$_{EGFP}$ construction process. (A) gp96 and EGFP were PCR amplified from mouse cDNA or EGFP containing vector, respectively, by step-wise PCR using the primers in Table 7-4 according to the scheme in Figure 7-5, steps 1-4. The gp96 PCR product was inserted into the pEF6/V5-His-TOPO vector (Figure 7-6) and cloned into E.coli. Plasmids were purified (B) and restriction enzyme-digested (C) to determine correct orientation (ex. plasmid 4). (D) vector-gp96 and EGFP PCR products were both digested with NotI and NdeI to linearize the vector and provide the sticky ends on EGFP for ligation. Ligated product was then cloned into E.coli, plasmids were purified, and then digested with EcoRI with cut sites in gp96 and EGFP but no sites within the vector. (E) Plasmids containing EGFP and gp96 have a 2.3 Kbp insert, while plasmids lacking EGFP are just linearized (ex. plasmid 9). Performed by MNM.

was inserted into the pEF6/V5-His-TOPO vector and orientation was confirmed by restriction enzyme digestion and sequencing analysis (Figure 7-6, Figure 7-7B,C). The final EGFP construct was ligated into the gp96 containing vector and the final product (Figure 7-7E) was fully sequenced to confirm the sequences were in frame and that no mutations occurred during assembly of this construct.

7.3.7 Analysis of HSPs draining from tumor

For HSP transfer experiments *in vivo*, $5x10^6$ CMS5 cells co-transfected with RAP and $gp96_{EGFP}$, or CMS5 co-transfected with control vector and $gp96_{EGFP}$, were injected in one footpad of wild type BALB/c or CD91 KO mice. Two days later, the draining and contra lateral (non-draining) popliteal lymph nodes were harvested. EGFP signal in $CD45^+$ cells in the lymph nodes were compared as described in the text (Aim 2, pg. 53).

7.3.8 CD91 independent T cell priming

CD91 KO mice and Cre^- littermates were immunized subcutaneously with 20μg OVA 8 peptide emulsified in Freund's adjuvant at an interval of one week. One week after the last vaccination, $5x10^6$ splenocytes were harvested from OVA 8 peptide immunized mice and cultured *ex vivo* for 5 days in the presence of OVA 8 peptide. Specific T cell responses were monitored by IL-2 ELISA.

7.3.9 Tumor growth assays in CD91 KO mice

$8x10^5$ D122 or $1x10^6$ SVB6 tumor cells were injected intradermally in CD91 KO or control mice, with or without CD8 depletion. Tumor growth was measured on two axes thereafter. CD8 T cells were depleted with anti-CD8 antibody one day before tumor challenge as previously described [215].

7.4 STATISTICAL ANALYSIS

Differences between the means of experimental groups were analyzed using the two tailed Student's *t*-test. Differences were considered significant when $p \leq 0.05$. Error bars were calculated as standard error of the mean (SEM).

APPENDIX A

PUBLICATIONS

Y.J. Zhou, **M.N. Messmer**, R.J. Binder. 2013. "Tumor-derived Heat Shock Proteins prime specific concomitant immunity through CD91." *Submitted*.

M.N. Messmer, J. Pasmowitz, L.E.Kropp, S.C. Watkins, R.J. Binder. 2013. "Identification of the cellular sentinels for immunogenic Heat Shock Proteins in vivo." *Journal of Immunology.* 191(8):4456-4465.

Binder, RJ., Y. Zhou, **M.N. Messmer**, S. Pawaria. 2012. "CD91-dependent modulation of immune responses by heat shock proteins; a role in autoimmunity." *Autoimmune Dis*. 2012: 863041.

Blalock, LT., J. Landsberg, **M. Messmer**, J. Shi, AD. Pardee, R. Haskell, L. Vujanovic, JM. Kirkwood, LH. Butterfield. 2012. "Human Dendritic Cells Adenovirally-Engineered to Express Three Defined Tumor Antigens Promote Broad Adaptive and Innate Immunity." *Oncoimmunology*. 1(3):287-297.

Pawaria, S., **M.N. Messmer**, Y. Zhou, R.J. Binder. 2011. "A role for the Heat Shock Protein-CD91 axis in initiation of immune responses to tumors." *Immunologic Research* 50(2-3):255-60.

Slight, SR., Lin, Y., **Messmer, M.**, Khader, S. 2011. "Francisella tularensis LVS-induced Interleukin-12 p40 cytokine production mediates Dendritic cell migration through IL-12 Receptor b1" *Cytokine.* 55(3):372-9.

Lin, Y., S. Ritchea, A. Logar, S. Slight, **M. Messmer**, J. Rangel-Moreno, L. Guglani, J.F. Alcorn, H. Strawbridge, S.M. Park, R. Onishi, N. Nyugen, M.J. Walter, D. Pociask, T.D. Randall, S.L. Gaffen, Y. Iwakura, J.K. Kolls, and S.A. Khader. 2009. "Interleukin-17 is required for T helper 1 cell immunity and host resistance to the intracellular pathogen Francisella tularensis." *Immunity.* 31:799-810.

BIBLIOGRAPHY

1. Lindquist S, Craig EA (1988) The heat-shock proteins. Annu Rev Genet 22: 631-677.
2. Lindquist S (1986) The heat-shock response. Annu Rev Biochem 55: 1151-1191.
3. Gross L (1943) Intradermal Immunization of C3H Mice against a Sarcoma That Originated in an Animal of the Same Line. Cancer Res 3: 326-333.
4. Foley EJ (1953) Antigenic properties of methylcholanthrene-induced tumors in mice of the strain of origin. Cancer Res 13: 835-837.
5. Prehn RT, Main JM (1957) Immunity to methylcholanthrene-induced sarcomas. J Natl Cancer Inst 18: 769-778.
6. Old LJ, Boyse EA, Clarke DA, Carswell EA (1962) ANTIGENIC PROPERTIES OF CHEMICALLY INDUCED TUMORS*. Annals of the New York Academy of Sciences 101: 80-106.
7. Srivastava PK, DeLeo AB, Old LJ (1986) Tumor rejection antigens of chemically induced sarcomas of inbred mice. Proc Natl Acad Sci U S A 83: 3407-3411.
8. Welch WJ, Garrels JI, Thomas GP, Lin JJ, Feramisco JR (1983) Biochemical characterization of the mammalian stress proteins and identification of two stress proteins as glucose- and Ca2+-ionophore-regulated proteins. J Biol Chem 258: 7102-7111.
9. Maki RG, Old LJ, Srivastava PK (1990) Human homologue of murine tumor rejection antigen gp96: 5'-regulatory and coding regions and relationship to stress-induced proteins. Proc Natl Acad Sci U S A 87: 5658-5662.
10. Mazzarella RA, Green M (1987) ERp99, an abundant, conserved glycoprotein of the endoplasmic reticulum, is homologous to the 90-kDa heat shock protein (hsp90) and the 94-kDa glucose regulated protein (GRP94). J Biol Chem 262: 8875-8883.
11. Srivastava PK, Maki RG (1991) Stress-induced proteins in immune response to cancer. Curr Top Microbiol Immunol 167: 109-123.
12. Srivastava PK, Chen YT, Old LJ (1987) 5'-structural analysis of genes encoding polymorphic antigens of chemically induced tumors. Proc Natl Acad Sci U S A 84: 3807-3811.
13. Maki RG, Eddy RL, Jr., Byers M, Shows TB, Srivastava PK (1993) Mapping of the genes for human endoplasmic reticular heat shock protein gp96/grp94. Somat Cell Mol Genet 19: 73-81.
14. Srivastava PK, Old LJ (1989) Identification of a human homologue of the murine tumor rejection antigen GP96. Cancer Res 49: 1341-1343.
15. Ullrich SJ, Robinson EA, Law LW, Willingham M, Appella E (1986) A mouse tumor-specific transplantation antigen is a heat shock-related protein. Proc Natl Acad Sci U S A 83: 3121-3125.
16. Udono H, Srivastava PK (1994) Comparison of tumor-specific immunogenicities of stress-induced proteins gp96, hsp90, and hsp70. J Immunol 152: 5398-5403.

17. Udono H, Srivastava PK (1993) Heat shock protein 70-associated peptides elicit specific cancer immunity. J Exp Med 178: 1391-1396.
18. Tamura Y, Peng P, Liu K, Daou M, Srivastava PK (1997) Immunotherapy of tumors with autologous tumor-derived heat shock protein preparations. Science 278: 117-120.
19. Basu S, Srivastava PK (1999) Calreticulin, a peptide-binding chaperone of the endoplasmic reticulum, elicits tumor- and peptide-specific immunity. J Exp Med 189: 797-802.
20. Wang XY, Kazim L, Repasky EA, Subjeck JR (2001) Characterization of heat shock protein 110 and glucose-regulated protein 170 as cancer vaccines and the effect of fever-range hyperthermia on vaccine activity. J Immunol 166: 490-497.
21. De Leo AB, Becker M, Lu L, Law LW (1993) Properties of a M(r) 110,000 tumor rejection antigen of the chemically induced BALB/c Meth A sarcoma. Cancer Res 53: 1602-1607.
22. Basu S, Binder RJ, Ramalingam T, Srivastava PK (2001) CD91 is a common receptor for heat shock proteins gp96, hsp90, hsp70, and calreticulin. Immunity 14: 303-313.
23. Binder RJ, Zhou YJ, Messmer MN, Pawaria S (2012) CD91-Dependent Modulation of Immune Responses by Heat Shock Proteins: A Role in Autoimmunity. Autoimmune Dis 2012: 863041.
24. Pawaria S, Binder RJ (2011) CD91-dependent programming of T-helper cell responses following heat shock protein immunization. Nat Commun 2: 521.
25. Flynn GC, Chappell TG, Rothman JE (1989) Peptide binding and release by proteins implicated as catalysts of protein assembly. Science 245: 385-390.
26. Li Z, Srivastava PK (1993) Tumor rejection antigen gp96/grp94 is an ATPase: implications for protein folding and antigen presentation. EMBO J 12: 3143-3151.
27. Menoret A, Peng P, Srivastava PK (1999) Association of peptides with heat shock protein gp96 occurs in vivo and not after cell lysis. Biochem Biophys Res Commun 262: 813-818.
28. Blachere NE, Li Z, Chandawarkar RY, Suto R, Jaikaria NS, et al. (1997) Heat shock protein-peptide complexes, reconstituted in vitro, elicit peptide-specific cytotoxic T lymphocyte response and tumor immunity. J Exp Med 186: 1315-1322.
29. Binder RJ (2006) Heat shock protein vaccines: from bench to bedside. Int Rev Immunol 25: 353-375.
30. Gidalevitz T, Biswas C, Ding H, Schneidman-Duhovny D, Wolfson HJ, et al. (2004) Identification of the N-terminal peptide binding site of glucose-regulated protein 94. J Biol Chem 279: 16543-16552.
31. Spee P, Neefjes J (1997) TAP-translocated peptides specifically bind proteins in the endoplasmic reticulum, including gp96, protein disulfide isomerase and calreticulin. Eur J Immunol 27: 2441-2449.
32. Stocki P, Morris NJ, Preisinger C, Wang XN, Kolch W, et al. (2010) Identification of potential HLA class I and class II epitope precursors associated with heat shock protein 70 (HSPA). Cell Stress Chaperones 15: 729-741.
33. Grossmann ME, Madden BJ, Gao F, Pang YP, Carpenter JE, et al. (2004) Proteomics shows Hsp70 does not bind peptide sequences indiscriminately in vivo. Exp Cell Res 297: 108-117.
34. Demine R, Walden P (2005) Testing the role of gp96 as peptide chaperone in antigen processing. J Biol Chem 280: 17573-17578.

35. Li HZ, Li CW, Li CY, Zhang BF, Li LT, et al. (2013) Isolation and Identification of Renal Cell Carcinoma-derived Peptides Associated with GP96. Technol Cancer Res Treat 12: 285-293.
36. Ishii T, Udono H, Yamano T, Ohta H, Uenaka A, et al. (1999) Isolation of MHC class I-restricted tumor antigen peptide and its precursors associated with heat shock proteins hsp70, hsp90, and gp96. J Immunol 162: 1303-1309.
37. Kropp LE, Garg M, Binder RJ (2010) Ovalbumin-derived precursor peptides are transferred sequentially from gp96 and calreticulin to MHC class I in the endoplasmic reticulum. J Immunol 184: 5619-5627.
38. Srivastava PK, Udono H, Blachere NE, Li Z (1994) Heat shock proteins transfer peptides during antigen processing and CTL priming. Immunogenetics 39: 93-98.
39. Zhu X, Zhao X, Burkholder WF, Gragerov A, Ogata CM, et al. (1996) Structural analysis of substrate binding by the molecular chaperone DnaK. Science 272: 1606-1614.
40. Gelebart P, Opas M, Michalak M (2005) Calreticulin, a Ca2+-binding chaperone of the endoplasmic reticulum. Int J Biochem Cell Biol 37: 260-266.
41. Stirling PC, Bakhoum SF, Feigl AB, Leroux MR (2006) Convergent evolution of clamp-like binding sites in diverse chaperones. Nat Struct Mol Biol 13: 865-870.
42. Dollins DE, Warren JJ, Immormino RM, Gewirth DT (2007) Structures of GRP94-nucleotide complexes reveal mechanistic differences between the hsp90 chaperones. Mol Cell 28: 41-56.
43. Biswas C, Ostrovsky O, Makarewich CA, Wanderling S, Gidalevitz T, et al. (2007) The peptide-binding activity of GRP94 is regulated by calcium. Biochem J 405: 233-241.
44. Vogen S, Gidalevitz T, Biswas C, Simen BB, Stein E, et al. (2002) Radicicol-sensitive peptide binding to the N-terminal portion of GRP94. J Biol Chem 277: 40742-40750.
45. Biswas C, Sriram U, Ciric B, Ostrovsky O, Gallucci S, et al. (2006) The N-terminal fragment of GRP94 is sufficient for peptide presentation via professional antigen-presenting cells. Int Immunol 18: 1147-1157.
46. Ostrovsky O, Ahmed NT, Argon Y (2009) The chaperone activity of GRP94 toward insulin-like growth factor II is necessary for the stress response to serum deprivation. Mol Biol Cell 20: 1855-1864.
47. Linderoth NA, Popowicz A, Sastry S (2000) Identification of the peptide-binding site in the heat shock chaperone/tumor rejection antigen gp96 (Grp94). J Biol Chem 275: 5472-5477.
48. Wu S, Hong F, Gewirth D, Guo B, Liu B, et al. (2012) The Molecular Chaperone gp96/GRP94 Interacts With Toll-Like Receptors And Integrins Via Its C-Terminal Hydrophobic Domain. J Biol Chem.
49. Castelli C, Ciupitu AM, Rini F, Rivoltini L, Mazzocchi A, et al. (2001) Human heat shock protein 70 peptide complexes specifically activate antimelanoma T cells. Cancer Res 61: 222-227.
50. Ren F, Xu Y, Mao L, Ou R, Ding Z, et al. (2010) Heat shock protein 110 improves the antitumor effects of the cytotoxic T lymphocyte epitope E7(49-57) in mice. Cancer Biol Ther 9: 134-141.
51. Ding Z, Ou R, Ni B, Tang J, Xu Y (2013) Cytolytic activity of the human papillomavirus type 16 E711-20 epitope-specific cytotoxic T lymphocyte is enhanced by heat shock protein 110 in HLA-A*0201 transgenic mice. Clin Vaccine Immunol 20: 1027-1033.

52. Yuan B, Xian R, Wu X, Jing J, Chen K, et al. (2012) Endoplasmic reticulum chaperone glucose regulated protein 170-Pokemon complexes elicit a robust antitumor immune response in vivo. Immunobiology 217: 738-742.
53. Suto R, Srivastava PK (1995) A mechanism for the specific immunogenicity of heat shock protein-chaperoned peptides. Science 269: 1585-1588.
54. Nieland TJ, Tan MC, Monne-van Muijen M, Koning F, Kruisbeek AM, et al. (1996) Isolation of an immunodominant viral peptide that is endogenously bound to the stress protein GP96/GRP94. Proc Natl Acad Sci U S A 93: 6135-6139.
55. Blachere NE, Udono H, Janetzki S, Li Z, Heike M, et al. (1993) Heat shock protein vaccines against cancer. J Immunother Emphasis Tumor Immunol 14: 352-356.
56. Heikema A, Agsteribbe E, Wilschut J, Huckriede A (1997) Generation of heat shock protein-based vaccines by intracellular loading of gp96 with antigenic peptides. Immunol Lett 57: 69-74.
57. Navaratnam M, Deshpande MS, Hariharan MJ, Zatechka DS, Jr., Srikumaran S (2001) Heat shock protein-peptide complexes elicit cytotoxic T-lymphocyte and antibody responses specific for bovine herpesvirus 1. Vaccine 19: 1425-1434.
58. Mo A, Musselli C, Chen H, Pappas J, Leclair K, et al. (2011) A heat shock protein based polyvalent vaccine targeting HSV-2: CD4(+) and CD8(+) cellular immunity and protective efficacy. Vaccine 29: 8530-8541.
59. Meng SD, Gao T, Gao GF, Tien P (2001) HBV-specific peptide associated with heat-shock protein gp96. Lancet 357: 528-529.
60. Zugel U, Sponaas AM, Neckermann J, Schoel B, Kaufmann SH (2001) gp96-peptide vaccination of mice against intracellular bacteria. Infect Immun 69: 4164-4167.
61. Sponaas AM, Zuegel U, Weber S, Hurwitz R, Winter R, et al. (2001) Immunization with gp96 from Listeria monocytogenes-infected mice is due to N-formylated listerial peptides. J Immunol 167: 6480-6486.
62. Breloer M, Marti T, Fleischer B, von Bonin A (1998) Isolation of processed, H-2Kb-binding ovalbumin-derived peptides associated with the stress proteins HSP70 and gp96. Eur J Immunol 28: 1016-1021.
63. Arnold D, Faath S, Rammensee H, Schild H (1995) Cross-priming of minor histocompatibility antigen-specific cytotoxic T cells upon immunization with the heat shock protein gp96. J Exp Med 182: 885-889.
64. Arnold D, Wahl C, Faath S, Rammensee HG, Schild H (1997) Influences of transporter associated with antigen processing (TAP) on the repertoire of peptides associated with the endoplasmic reticulum-resident stress protein gp96. J Exp Med 186: 461-466.
65. Binder RJ, Kelly JB, 3rd, Vatner RE, Srivastava PK (2007) Specific immunogenicity of heat shock protein gp96 derives from chaperoned antigenic peptides and not from contaminating proteins. J Immunol 179: 7254-7261.
66. Udono H, Levey DL, Srivastava PK (1994) Cellular requirements for tumor-specific immunity elicited by heat shock proteins: tumor rejection antigen gp96 primes CD8+ T cells in vivo. Proc Natl Acad Sci U S A 91: 3077-3081.
67. Kurts C, Robinson BW, Knolle PA (2010) Cross-priming in health and disease. Nat Rev Immunol 10: 403-414.
68. Basu S, Binder RJ, Suto R, Anderson KM, Srivastava PK (2000) Necrotic but not apoptotic cell death releases heat shock proteins, which deliver a partial maturation signal to dendritic cells and activate the NF-kappa B pathway. Int Immunol 12: 1539-1546.

69. Somersan S, Larsson M, Fonteneau JF, Basu S, Srivastava P, et al. (2001) Primary tumor tissue lysates are enriched in heat shock proteins and induce the maturation of human dendritic cells. J Immunol 167: 4844-4852.
70. Panjwani NN, Popova L, Srivastava PK (2002) Heat shock proteins gp96 and hsp70 activate the release of nitric oxide by APCs. J Immunol 168: 2997-3003.
71. Singh-Jasuja H, Scherer HU, Hilf N, Arnold-Schild D, Rammensee HG, et al. (2000) The heat shock protein gp96 induces maturation of dendritic cells and down-regulation of its receptor. Eur J Immunol 30: 2211-2215.
72. Binder RJ, Anderson KM, Basu S, Srivastava PK (2000) Cutting edge: heat shock protein gp96 induces maturation and migration of CD11c+ cells in vivo. J Immunol 165: 6029-6035.
73. Radsak MP, Hilf N, Singh-Jasuja H, Braedel S, Brossart P, et al. (2003) The heat shock protein Gp96 binds to human neutrophils and monocytes and stimulates effector functions. Blood 101: 2810-2815.
74. Vabulas RM, Braedel S, Hilf N, Singh-Jasuja H, Herter S, et al. (2002) The endoplasmic reticulum-resident heat shock protein Gp96 activates dendritic cells via the Toll-like receptor 2/4 pathway. J Biol Chem 277: 20847-20853.
75. Huang QQ, Sobkoviak R, Jockheck-Clark AR, Shi B, Mandelin AM, 2nd, et al. (2009) Heat shock protein 96 is elevated in rheumatoid arthritis and activates macrophages primarily via TLR2 signaling. J Immunol 182: 4965-4973.
76. Asea A, Kabingu E, Stevenson MA, Calderwood SK (2000) HSP70 peptide-bearing and peptide-negative preparations act as chaperokines. Cell Stress Chaperones 5: 425-431.
77. Moroi Y, Mayhew M, Trcka J, Hoe MH, Takechi Y, et al. (2000) Induction of cellular immunity by immunization with novel hybrid peptides complexed to heat shock protein 70. Proc Natl Acad Sci U S A 97: 3485-3490.
78. Chen T, Guo J, Han C, Yang M, Cao X (2009) Heat shock protein 70, released from heat-stressed tumor cells, initiates antitumor immunity by inducing tumor cell chemokine production and activating dendritic cells via TLR4 pathway. J Immunol 182: 1449-1459.
79. Asea A, Kraeft SK, Kurt-Jones EA, Stevenson MA, Chen LB, et al. (2000) HSP70 stimulates cytokine production through a CD14-dependant pathway, demonstrating its dual role as a chaperone and cytokine. Nat Med 6: 435-442.
80. Vabulas RM, Ahmad-Nejad P, Ghose S, Kirschning CJ, Issels RD, et al. (2002) HSP70 as endogenous stimulus of the Toll/interleukin-1 receptor signal pathway. J Biol Chem 277: 15107-15112.
81. Kuppner MC, Gastpar R, Gelwer S, Nossner E, Ochmann O, et al. (2001) The role of heat shock protein (hsp70) in dendritic cell maturation: hsp70 induces the maturation of immature dendritic cells but reduces DC differentiation from monocyte precursors. Eur J Immunol 31: 1602-1609.
82. Millar DG, Garza KM, Odermatt B, Elford AR, Ono N, et al. (2003) Hsp70 promotes antigen-presenting cell function and converts T-cell tolerance to autoimmunity in vivo. Nat Med 9: 1469-1476.
83. Wang Y, Kelly CG, Karttunen JT, Whittall T, Lehner PJ, et al. (2001) CD40 is a cellular receptor mediating mycobacterial heat shock protein 70 stimulation of CC-chemokines. Immunity 15: 971-983.
84. Wang Y, Kelly CG, Singh M, McGowan EG, Carrara AS, et al. (2002) Stimulation of Th1-polarizing cytokines, C-C chemokines, maturation of dendritic cells, and adjuvant

function by the peptide binding fragment of heat shock protein 70. J Immunol 169: 2422-2429.
85. Campisi J, Leem TH, Fleshner M (2003) Stress-induced extracellular Hsp72 is a functionally significant danger signal to the immune system. Cell Stress Chaperones 8: 272-286.
86. Wan T, Zhou X, Chen G, An H, Chen T, et al. (2004) Novel heat shock protein Hsp70L1 activates dendritic cells and acts as a Th1 polarizing adjuvant. Blood 103: 1747-1754.
87. Skeen MJ, Miller MA, Shinnick TM, Ziegler HK (1996) Regulation of murine macrophage IL-12 production. Activation of macrophages in vivo, restimulation in vitro, and modulation by other cytokines. J Immunol 156: 1196-1206.
88. De Filippo A, Binder RJ, Camisaschi C, Beretta V, Arienti F, et al. (2008) Human plasmacytoid dendritic cells interact with gp96 via CD91 and regulate inflammatory responses. J Immunol 181: 6525-6535.
89. Hilf N, Singh-Jasuja H, Schwarzmaier P, Gouttefangeas C, Rammensee HG, et al. (2002) Human platelets express heat shock protein receptors and regulate dendritic cell maturation. Blood 99: 3676-3682.
90. Banerjee PP, Vinay DS, Mathew A, Raje M, Parekh V, et al. (2002) Evidence that glycoprotein 96 (B2), a stress protein, functions as a Th2-specific costimulatory molecule. J Immunol 169: 3507-3518.
91. Li SS, Liu Z, Uzunel M, Sundqvist KG (2006) Endogenous thrombospondin-1 is a cell-surface ligand for regulation of integrin-dependent T-lymphocyte adhesion. Blood 108: 3112-3120.
92. Liu Z, Christensson M, Forslow A, De Meester I, Sundqvist KG (2009) A CD26-controlled cell surface cascade for regulation of T cell motility and chemokine signals. J Immunol 183: 3616-3624.
93. Eriksson C, Rantapaa-Dahlqvist S, Sundqvist KG (2010) T-cell expression of CD91 - a marker of unresponsiveness to anti-TNF therapy in rheumatoid arthritis. APMIS 118: 837-845.
94. Arnold-Schild D, Hanau D, Spehner D, Schmid C, Rammensee HG, et al. (1999) Cutting edge: receptor-mediated endocytosis of heat shock proteins by professional antigen-presenting cells. J Immunol 162: 3757-3760.
95. Wassenberg JJ, Dezfulian C, Nicchitta CV (1999) Receptor mediated and fluid phase pathways for internalization of the ER Hsp90 chaperone GRP94 in murine macrophages. J Cell Sci 112 (Pt 13): 2167-2175.
96. Binder RJ, Harris ML, Menoret A, Srivastava PK (2000) Saturation, competition, and specificity in interaction of heat shock proteins (hsp) gp96, hsp90, and hsp70 with CD11b+ cells. J Immunol 165: 2582-2587.
97. Singh-Jasuja H, Toes RE, Spee P, Munz C, Hilf N, et al. (2000) Cross-presentation of glycoprotein 96-associated antigens on major histocompatibility complex class I molecules requires receptor-mediated endocytosis. J Exp Med 191: 1965-1974.
98. Binder RJ, Han DK, Srivastava PK (2000) CD91: a receptor for heat shock protein gp96. Nat Immunol 1: 151-155.
99. Binder RJ, Srivastava PK (2004) Essential role of CD91 in re-presentation of gp96-chaperoned peptides. Proc Natl Acad Sci U S A 101: 6128-6133.
100. Robert J, Ramanayake T, Maniero GD, Morales H, Chida AS (2008) Phylogenetic conservation of glycoprotein 96 ability to interact with CD91 and facilitate antigen cross-presentation. J Immunol 180: 3176-3182.

101. Binder RJ (2009) Hsp receptors: the cases of identity and mistaken identity. Curr Opin Mol Ther 11: 62-71.
102. McLaughlin K, Seago J, Robinson L, Kelly C, Charleston B (2010) Hsp70 enhances presentation of FMDV antigen to bovine CD4+ T cells in vitro. Vet Res 41: 36.
103. Bendz H, Ruhland SC, Pandya MJ, Hainzl O, Riegelsberger S, et al. (2007) Human heat shock protein 70 enhances tumor antigen presentation through complex formation and intracellular antigen delivery without innate immune signaling. J Biol Chem 282: 31688-31702.
104. Huang Y, Biswas C, Klos Dehring DA, Sriram U, Williamson EK, et al. (2011) The Actin Regulatory Protein HS1 Is Required for Antigen Uptake and Presentation by Dendritic Cells. J Immunol.
105. Zitzler S, Hellwig A, Hartl FU, Wieland F, Diestelkotter-Bachert P (2008) Distinct binding sites for the ATPase and substrate-binding domain of human Hsp70 on the cell surface of antigen presenting cells. Mol Immunol 45: 3974-3983.
106. Noessner E, Gastpar R, Milani V, Brandl A, Hutzler PJ, et al. (2002) Tumor-derived heat shock protein 70 peptide complexes are cross-presented by human dendritic cells. J Immunol 169: 5424-5432.
107. Castellino F, Boucher PE, Eichelberg K, Mayhew M, Rothman JE, et al. (2000) Receptor-mediated uptake of antigen/heat shock protein complexes results in major histocompatibility complex class I antigen presentation via two distinct processing pathways. J Exp Med 191: 1957-1964.
108. SenGupta D, Norris PJ, Suscovich TJ, Hassan-Zahraee M, Moffett HF, et al. (2004) Heat shock protein-mediated cross-presentation of exogenous HIV antigen on HLA class I and class II. J Immunol 173: 1987-1993.
109. Tobian AA, Canaday DH, Boom WH, Harding CV (2004) Bacterial heat shock proteins promote CD91-dependent class I MHC cross-presentation of chaperoned peptide to CD8+ T cells by cytosolic mechanisms in dendritic cells versus vacuolar mechanisms in macrophages. J Immunol 172: 5277-5286.
110. Hart JP, Gunn MD, Pizzo SV (2004) A CD91-positive subset of CD11c+ blood dendritic cells: characterization of the APC that functions to enhance adaptive immune responses against CD91-targeted antigens. J Immunol 172: 70-78.
111. Tischer S, Basila M, Maecker-Kolhoff B, Immenschuh S, Oelke M, et al. (2011) Heat shock protein 70/peptide complexes: potent mediators for the generation of antiviral T cells particularly with regard to low precursor frequencies. J Transl Med 9: 175.
112. Lipsker D, Ziylan U, Spehner D, Proamer F, Bausinger H, et al. (2002) Heat shock proteins 70 and 60 share common receptors which are expressed on human monocyte-derived but not epidermal dendritic cells. Eur J Immunol 32: 322-332.
113. Langelaar MF, Hope JC, Rutten VP, Noordhuizen JP, van Eden W, et al. (2005) Mycobacterium avium ssp. paratuberculosis recombinant heat shock protein 70 interaction with different bovine antigen-presenting cells. Scand J Immunol 61: 242-250.
114. Matsutake T, Sawamura T, Srivastava PK (2010) High efficiency CD91- and LOX-1-mediated re-presentation of gp96-chaperoned peptides by MHC II molecules. Cancer Immun 10: 7.
115. Fischer N, Haug M, Kwok WW, Kalbacher H, Wernet D, et al. (2010) Involvement of CD91 and scavenger receptors in Hsp70-facilitated activation of human antigen-specific CD4(+) memory T cells. Eur J Immunol 40: 986-997.

116. Berwin B, Hart JP, Pizzo SV, Nicchitta CV (2002) Cutting edge: CD91-independent cross-presentation of GRP94(gp96)-associated peptides. J Immunol 168: 4282-4286.
117. Jockheck-Clark AR, Bowers EV, Totonchy MB, Neubauer J, Pizzo SV, et al. (2010) Re-Examination of CD91 Function in GRP94 (Glycoprotein 96) Surface Binding, Uptake, and Peptide Cross-Presentation. J Immunol.
118. Berwin B, Rosser MF, Brinker KG, Nicchitta CV (2002) Transfer of GRP94(Gp96)-associated peptides onto endosomal MHC class I molecules. Traffic 3: 358-366.
119. Kurotaki T, Tamura Y, Ueda G, Oura J, Kutomi G, et al. (2007) Efficient cross-presentation by heat shock protein 90-peptide complex-loaded dendritic cells via an endosomal pathway. J Immunol 179: 1803-1813.
120. Walters JJ, Berwin B (2005) Differential CD91 dependence for calreticulin and Pseudomonas exotoxin-A endocytosis. Traffic 6: 1173-1182.
121. Berwin B, Delneste Y, Lovingood RV, Post SR, Pizzo SV (2004) SREC-I, a type F scavenger receptor, is an endocytic receptor for calreticulin. J Biol Chem 279: 51250-51257.
122. Delneste Y, Magistrelli G, Gauchat J, Haeuw J, Aubry J, et al. (2002) Involvement of LOX-1 in dendritic cell-mediated antigen cross-presentation. Immunity 17: 353-362.
123. Murshid A, Gong J, Calderwood SK (2010) Heat Shock Protein 90 Mediates Efficient Antigen Cross Presentation through the Scavenger Receptor Expressed by Endothelial Cells-I. J Immunol.
124. Berwin B, Hart JP, Rice S, Gass C, Pizzo SV, et al. (2003) Scavenger receptor-A mediates gp96/GRP94 and calreticulin internalization by antigen-presenting cells. EMBO J 22: 6127-6136.
125. Tewalt EF, Maynard JC, Walters JJ, Schell AM, Berwin BL, et al. (2008) Redundancy renders the glycoprotein 96 receptor scavenger receptor A dispensable for cross priming in vivo. Immunology 125: 480-491.
126. Facciponte JG, Wang XY, Subjeck JR (2007) Hsp110 and Grp170, members of the Hsp70 superfamily, bind to scavenger receptor-A and scavenger receptor expressed by endothelial cells-I. Eur J Immunol 37: 2268-2279.
127. Randazzo M, Terness P, Opelz G, Kleist C (2011) Active-specific immunotherapy of human cancers with the heat shock protein Gp96-revisited. Int J Cancer.
128. Janetzki S, Palla D, Rosenhauer V, Lochs H, Lewis JJ, et al. (2000) Immunization of cancer patients with autologous cancer-derived heat shock protein gp96 preparations: a pilot study. Int J Cancer 88: 232-238.
129. Mazzaferro V, Coppa J, Carrabba MG, Rivoltini L, Schiavo M, et al. (2003) Vaccination with autologous tumor-derived heat-shock protein gp96 after liver resection for metastatic colorectal cancer. Clin Cancer Res 9: 3235-3245.
130. Belli F, Testori A, Rivoltini L, Maio M, Andreola G, et al. (2002) Vaccination of metastatic melanoma patients with autologous tumor-derived heat shock protein gp96-peptide complexes: clinical and immunologic findings. J Clin Oncol 20: 4169-4180.
131. Pilla L, Patuzzo R, Rivoltini L, Maio M, Pennacchioli E, et al. (2006) A phase II trial of vaccination with autologous, tumor-derived heat-shock protein peptide complexes Gp96, in combination with GM-CSF and interferon-alpha in metastatic melanoma patients. Cancer Immunol Immunother 55: 958-968.
132. Testori A, Richards J, Whitman E, Mann GB, Lutzky J, et al. (2008) Phase III comparison of vitespen, an autologous tumor-derived heat shock protein gp96 peptide complex

vaccine, with physician's choice of treatment for stage IV melanoma: the C-100-21 Study Group. J Clin Oncol 26: 955-962.
133. Eton O, Ross MI, East MJ, Mansfield PF, Papadopoulos N, et al. (2010) Autologous tumor-derived heat-shock protein peptide complex-96 (HSPPC-96) in patients with metastatic melanoma. J Transl Med 8: 9.
134. Younes A (2003) A phase II study of heat shock protein-peptide complex-96 vaccine therapy in patients with indolent non-Hodgkin's lymphoma. Clin Lymphoma 4: 183-185.
135. Oki Y, McLaughlin P, Fayad LE, Pro B, Mansfield PF, et al. (2007) Experience with heat shock protein-peptide complex 96 vaccine therapy in patients with indolent non-Hodgkin lymphoma. Cancer 109: 77-83.
136. Maki RG, Livingston PO, Lewis JJ, Janetzki S, Klimstra D, et al. (2007) A phase I pilot study of autologous heat shock protein vaccine HSPPC-96 in patients with resected pancreatic adenocarcinoma. Dig Dis Sci 52: 1964-1972.
137. Jonasch E, Wood C, Tamboli P, Pagliaro LC, Tu SM, et al. (2008) Vaccination of metastatic renal cell carcinoma patients with autologous tumour-derived vitespen vaccine: clinical findings. Br J Cancer 98: 1336-1341.
138. Wood C, Srivastava P, Bukowski R, Lacombe L, Gorelov AI, et al. (2008) An adjuvant autologous therapeutic vaccine (HSPPC-96; vitespen) versus observation alone for patients at high risk of recurrence after nephrectomy for renal cell carcinoma: a multicentre, open-label, randomised phase III trial. Lancet 372: 145-154.
139. Crane CA, Han SJ, Ahn BJ, Oehlke J, Kivett V, et al. (2012) Individual patient-specific immunity against high-grade glioma after vaccination with autologous tumor derived peptides bound to the 96 KD chaperone protein. Clin Cancer Res.
140. Messmer MN, Pasmowitz J, Kropp LE, Watkins SC, Binder RJ (2013) Identification of the Cellular Sentinels for Native Immunogenic Heat Shock Proteins In Vivo. J Immunol.
141. Houlihan JL, Metzler JJ, Blum JS (2009) HSP90alpha and HSP90beta isoforms selectively modulate MHC class II antigen presentation in B cells. J Immunol 182: 7451-7458.
142. Ichiyanagi T, Imai T, Kajiwara C, Mizukami S, Nakai A, et al. (2010) Essential Role of Endogenous Heat Shock Protein 90 of Dendritic Cells in Antigen Cross-Presentation. J Immunol.
143. Heath WR, Belz GT, Behrens GM, Smith CM, Forehan SP, et al. (2004) Cross-presentation, dendritic cell subsets, and the generation of immunity to cellular antigens. Immunological Reviews 199: 9-26.
144. Liu K, Nussenzweig MC (2010) Origin and development of dendritic cells. Immunol Rev 234: 45-54.
145. Strbo N, Pahwa S, Kolber MA, Gonzalez L, Fisher E, et al. (2010) Cell-secreted Gp96-Ig-peptide complexes induce lamina propria and intraepithelial CD8+ cytotoxic T lymphocytes in the intestinal mucosa. Mucosal Immunol 3: 182-192.
146. Wang S, Qiu L, Liu G, Li Y, Zhang X, et al. (2011) Heat shock protein gp96 enhances humoral and T cell responses, decreases Treg frequency and potentiates the anti-HBV activity in BALB/c and transgenic mice. Vaccine 29: 6342-6351.
147. Chandawarkar RY, Wagh MS, Srivastava PK (1999) The dual nature of specific immunological activity of tumor-derived gp96 preparations. J Exp Med 189: 1437-1442.
148. Chandawarkar RY, Wagh MS, Kovalchin JT, Srivastava P (2004) Immune modulation with high-dose heat-shock protein gp96: therapy of murine autoimmune diabetes and encephalomyelitis. Int Immunol 16: 615-624.

149. Slack LK, Muthana M, Hopkinson K, Suvarna SK, Espigares E, et al. (2007) Administration of the stress protein gp96 prolongs rat cardiac allograft survival, modifies rejection-associated inflammatory events, and induces a state of peripheral T-cell hyporesponsiveness. Cell Stress Chaperones 12: 71-82.
150. Liu Z, Li X, Qiu L, Zhang X, Chen L, et al. (2009) Treg suppress CTL responses upon immunization with HSP gp96. Eur J Immunol 39: 3110-3120.
151. Hanson HL, Donermeyer DL, Ikeda H, White JM, Shankaran V, et al. (2000) Eradication of established tumors by CD8+ T cell adoptive immunotherapy. Immunity 13: 265-276.
152. Binder RJ, Blachere NE, Srivastava PK (2001) Heat shock protein-chaperoned peptides but not free peptides introduced into the cytosol are presented efficiently by major histocompatibility complex I molecules. J Biol Chem 276: 17163-17171.
153. Villadangos JA, Heath WR (2005) Life cycle, migration and antigen presenting functions of spleen and lymph node dendritic cells: limitations of the Langerhans cells paradigm. Semin Immunol 17: 262-272.
154. Romani N, Clausen BE, Stoitzner P (2010) Langerhans cells and more: langerin-expressing dendritic cell subsets in the skin. Immunol Rev 234: 120-141.
155. Gray EE, Cyster JG (2012) Lymph node macrophages. J Innate Immun 4: 424-436.
156. Watkins SC, Salter RD (2005) Functional connectivity between immune cells mediated by tunneling nanotubules. Immunity 23: 309-318.
157. Pawaria S, Messmer MN, Zhou YJ, Binder RJ (2011) A role for the heat shock protein-CD91 axis in the initiation of immune responses to tumors. Immunol Res 50: 255-260.
158. Blachere NE, Darnell RB, Albert ML (2005) Apoptotic cells deliver processed antigen to dendritic cells for cross-presentation. PLoS Biol 3: e185.
159. Asano K, Nabeyama A, Miyake Y, Qiu CH, Kurita A, et al. (2011) CD169-positive macrophages dominate antitumor immunity by crosspresenting dead cell-associated antigens. Immunity 34: 85-95.
160. Delamarre L, Pack M, Chang H, Mellman I, Trombetta ES (2005) Differential lysosomal proteolysis in antigen-presenting cells determines antigen fate. Science 307: 1630-1634.
161. Lutz MB, Kukutsch N, Ogilvie AL, Rossner S, Koch F, et al. (1999) An advanced culture method for generating large quantities of highly pure dendritic cells from mouse bone marrow. J Immunol Methods 223: 77-92.
162. North RJ, Kirstein DP (1977) T-cell-mediated concomitant immunity to syngeneic tumors. I. Activated macrophages as the expressors of nonspecific immunity to unrelated tumors and bacterial parasites. J Exp Med 145: 275-292.
163. Shankaran V, Ikeda H, Bruce AT, White JM, Swanson PE, et al. (2001) IFNgamma and lymphocytes prevent primary tumour development and shape tumour immunogenicity. Nature 410: 1107-1111.
164. Schreiber RD, Old LJ, Smyth MJ (2011) Cancer immunoediting: integrating immunity's roles in cancer suppression and promotion. Science 331: 1565-1570.
165. Li M, Davey GM, Sutherland RM, Kurts C, Lew AM, et al. (2001) Cell-associated ovalbumin is cross-presented much more efficiently than soluble ovalbumin in vivo. J Immunol 166: 6099-6103.
166. Binder RJ, Srivastava PK (2005) Peptides chaperoned by heat-shock proteins are a necessary and sufficient source of antigen in the cross-priming of CD8+ T cells. Nat Immunol 6: 593-599.

167. Chen W, Syldath U, Bellmann K, Burkart V, Kolb H (1999) Human 60-kDa heat-shock protein: a danger signal to the innate immune system. J Immunol 162: 3212-3219.
168. Herz J, Clouthier DE, Hammer RE (1992) LDL receptor-related protein internalizes and degrades uPA-PAI-1 complexes and is essential for embryo implantation. Cell 71: 411-421.
169. Han JM, Park SG, Liu B, Park BJ, Kim JY, et al. (2007) Aminoacyl-tRNA synthetase-interacting multifunctional protein 1/p43 controls endoplasmic reticulum retention of heat shock protein gp96: its pathological implications in lupus-like autoimmune diseases. Am J Pathol 170: 2042-2054.
170. Yewdell JW, Norbury CC, Bennink JR (1999) Mechanisms of exogenous antigen presentation by MHC class I molecules in vitro and in vivo: implications for generating CD8+ T cell responses to infectious agents, tumors, transplants, and vaccines. Adv Immunol 73: 1-77.
171. Norbury CC, Basta S, Donohue KB, Tscharke DC, Princiotta MF, et al. (2004) CD8+ T cell cross-priming via transfer of proteasome substrates. Science 304: 1318-1321.
172. Srivastava N, Srivastava PK (2009) Modeling the repertoire of true tumor-specific MHC I epitopes in a human tumor. PLoS One 4: e6094.
173. Neefjes J, Jongsma ML, Paul P, Bakke O (2011) Towards a systems understanding of MHC class I and MHC class II antigen presentation. Nat Rev Immunol 11: 823-836.
174. Tobian AA, Canaday DH, Harding CV (2004) Bacterial heat shock proteins enhance class II MHC antigen processing and presentation of chaperoned peptides to CD4+ T cells. J Immunol 173: 5130-5137.
175. Doody AD, Kovalchin JT, Mihalyo MA, Hagymasi AT, Drake CG, et al. (2004) Glycoprotein 96 can chaperone both MHC class I- and class II-restricted epitopes for in vivo presentation, but selectively primes CD8+ T cell effector function. J Immunol 172: 6087-6092.
176. Kovacsovics-Bankowski M, Rock KL (1995) A phagosome-to-cytosol pathway for exogenous antigens presented on MHC class I molecules. Science 267: 243-246.
177. Pathak SS, Blum JS (2000) Endocytic recycling is required for the presentation of an exogenous peptide via MHC class II molecules. Traffic 1: 561-569.
178. Frauwirth K, Shastri N (2001) Introducing endogenous antigens into the major histocompatibility complex (MHC) class II presentation pathway. Both Ii mediated inhibition and enhancement of endogenous peptide/MHC class II presentation require the same Ii domains. Immunology 102: 405-415.
179. Guermonprez P, Saveanu L, Kleijmeer M, Davoust J, Van Endert P, et al. (2003) ER-phagosome fusion defines an MHC class I cross-presentation compartment in dendritic cells. Nature 425: 397-402.
180. Schmid D, Pypaert M, Munz C (2007) Antigen-loading compartments for major histocompatibility complex class II molecules continuously receive input from autophagosomes. Immunity 26: 79-92.
181. Ackerman AL, Kyritsis C, Tampe R, Cresswell P (2003) Early phagosomes in dendritic cells form a cellular compartment sufficient for cross presentation of exogenous antigens. Proc Natl Acad Sci U S A 100: 12889-12894.
182. Shinagawa N, Yamazaki K, Tamura Y, Imai A, Kikuchi E, et al. (2008) Immunotherapy with dendritic cells pulsed with tumor-derived gp96 against murine lung cancer is

effective through immune response of CD8+ cytotoxic T lymphocytes and natural killer cells. Cancer Immunol Immunother 57: 165-174.
183. Singh-Jasuja H, Hilf N, Scherer HU, Arnold-Schild D, Rammensee HG, et al. (2000) The heat shock protein gp96: a receptor-targeted cross-priming carrier and activator of dendritic cells. Cell Stress Chaperones 5: 462-470.
184. Kutomi G, Tamura Y, Okuya K, Yamamoto T, Hirohashi Y, et al. (2009) Targeting to static endosome is required for efficient cross-presentation of endoplasmic reticulum-resident oxygen-regulated protein 150-peptide complexes. J Immunol 183: 5861-5869.
185. Oura J, Tamura Y, Kamiguchi K, Kutomi G, Sahara H, et al. (2011) Extracellular heat shock protein 90 plays a role in translocating chaperoned antigen from endosome to proteasome for generating antigenic peptide to be cross-presented by dendritic cells. Int Immunol 23: 223-237.
186. Wilson NS, El-Sukkari D, Villadangos JA (2004) Dendritic cells constitutively present self antigens in their immature state in vivo and regulate antigen presentation by controlling the rates of MHC class II synthesis and endocytosis. Blood 103: 2187-2195.
187. Kato Y, Kajiwara C, Ishige I, Mizukami S, Yamazaki C, et al. (2012) HSP70 and HSP90 Differentially Regulate Translocation of Extracellular Antigen to the Cytosol for Cross-Presentation. Autoimmune Dis 2012: 745962.
188. Watts C (1997) Capture and processing of exogenous antigens for presentation on MHC molecules. Annu Rev Immunol 15: 821-850.
189. Li C, Buckwalter MR, Basu S, Garg M, Chang J, et al. (2012) Dendritic cells sequester antigenic epitopes for prolonged periods in the absence of antigen-encoding genetic information. Proc Natl Acad Sci U S A.
190. Inaba K, Turley S, Iyoda T, Yamaide F, Shimoyama S, et al. (2000) The formation of immunogenic major histocompatibility complex class II-peptide ligands in lysosomal compartments of dendritic cells is regulated by inflammatory stimuli. J Exp Med 191: 927-936.
191. Turley SJ, Inaba K, Garrett WS, Ebersold M, Unternaehrer J, et al. (2000) Transport of peptide-MHC class II complexes in developing dendritic cells. Science 288: 522-527.
192. Corbi AL, Lopez-Rodriguez C (1997) CD11c integrin gene promoter activity during myeloid differentiation. Leuk Lymphoma 25: 415-425.
193. Becker L, Liu NC, Averill MM, Yuan W, Pamir N, et al. (2012) Unique proteomic signatures distinguish macrophages and dendritic cells. PLoS One 7: e33297.
194. LaMarre J, Wolf BB, Kittler EL, Quesenberry PJ, Gonias SL (1993) Regulation of macrophage alpha 2-macroglobulin receptor/low density lipoprotein receptor-related protein by lipopolysaccharide and interferon-gamma. J Clin Invest 91: 1219-1224.
195. Costales P, Castellano J, Revuelta-Lopez E, Cal R, Aledo R, et al. (2013) Lipopolysaccharide downregulates CD91/low-density lipoprotein receptor-related protein 1 expression through SREBP-1 overexpression in human macrophages. Atherosclerosis 227: 79-88.
196. Delamarre L, Holcombe H, Mellman I (2003) Presentation of exogenous antigens on major histocompatibility complex (MHC) class I and MHC class II molecules is differentially regulated during dendritic cell maturation. J Exp Med 198: 111-122.
197. Zanetti-Domingues LC, Tynan CJ, Rolfe DJ, Clarke DT, Martin-Fernandez M (2013) Hydrophobic fluorescent probes introduce artifacts into single molecule tracking experiments due to non-specific binding. PLoS One 8: e74200.

198. Panchuk-Voloshina N, Haugland RP, Bishop-Stewart J, Bhalgat MK, Millard PJ, et al. (1999) Alexa dyes, a series of new fluorescent dyes that yield exceptionally bright, photostable conjugates. J Histochem Cytochem 47: 1179-1188.
199. Chen H, Ahsan SS, Santiago-Berrios MB, Abruna HD, Webb WW (2010) Mechanisms of quenching of Alexa fluorophores by natural amino acids. J Am Chem Soc 132: 7244-7245.
200. Stepanenko OV, Verkhusha VV, Kazakov VI, Shavlovsky MM, Kuznetsova IM, et al. (2004) Comparative studies on the structure and stability of fluorescent proteins EGFP, zFP506, mRFP1, "dimer2", and DsRed1. Biochemistry 43: 14913-14923.
201. Verkhusha VV, Kuznetsova IM, Stepanenko OV, Zaraisky AG, Shavlovsky MM, et al. (2003) High stability of Discosoma DsRed as compared to Aequorea EGFP. Biochemistry 42: 7879-7884.
202. Corish P, Tyler-Smith C (1999) Attenuation of green fluorescent protein half-life in mammalian cells. Protein Eng 12: 1035-1040.
203. Dudziak D, Kamphorst AO, Heidkamp GF, Buchholz VR, Trumpfheller C, et al. (2007) Differential antigen processing by dendritic cell subsets in vivo. Science 315: 107-111.
204. Kamphorst AO, Guermonprez P, Dudziak D, Nussenzweig MC (2010) Route of antigen uptake differentially impacts presentation by dendritic cells and activated monocytes. J Immunol 185: 3426-3435.
205. Hildner K, Edelson BT, Purtha WE, Diamond M, Matsushita H, et al. (2008) Batf3 deficiency reveals a critical role for CD8alpha+ dendritic cells in cytotoxic T cell immunity. Science 322: 1097-1100.
206. Li L, Kim S, Herndon JM, Goedegebuure P, Belt BA, et al. (2012) Cross-dressed CD8alpha+/CD103+ dendritic cells prime CD8+ T cells following vaccination. Proc Natl Acad Sci U S A 109: 12716-12721.
207. Henri S, Poulin LF, Tamoutounour S, Ardouin L, Guilliams M, et al. (2010) CD207+ CD103+ dermal dendritic cells cross-present keratinocyte-derived antigens irrespective of the presence of Langerhans cells. J Exp Med 207: 189-206, S181-186.
208. Wilson NS, El-Sukkari D, Belz GT, Smith CM, Steptoe RJ, et al. (2003) Most lymphoid organ dendritic cell types are phenotypically and functionally immature. Blood 102: 2187-2194.
209. Rohlmann A, Gotthardt M, Willnow TE, Hammer RE, Herz J (1996) Sustained somatic gene inactivation by viral transfer of Cre recombinase. Nat Biotechnol 14: 1562-1565.
210. Myers NB, Harris MR, Connolly JM, Lybarger L, Yu YY, et al. (2000) Kb, Kd, and Ld molecules share common tapasin dependencies as determined using a novel epitope tag. J Immunol 165: 5656-5663.
211. Paglia P, Girolomoni G, Robbiati F, Granucci F, Ricciardi-Castagnoli P (1993) Immortalized dendritic cell line fully competent in antigen presentation initiates primary T cell responses in vivo. J Exp Med 178: 1893-1901.
212. Srivastava PK (1997) Purification of heat shock protein-peptide complexes for use in vaccination against cancers and intracellular pathogens. Methods 12: 165-171.
213. Shastri N, Gonzalez F (1993) Endogenous generation and presentation of the ovalbumin peptide/Kb complex to T cells. J Immunol 150: 2724-2736.
214. Wei BY, Gervois N, Mer G, Adorini L, Benoist C, et al. (1991) Local structure of a peptide contact site on Ak alpha. Int Immunol 3: 833-837.

215. Sayles PC, Johnson LL (1996) Intact immune defenses are required for mice to resist the ts-4 vaccine strain of Toxoplasma gondii. Infect Immunol 64: 3088-3092